Precambrian Research 429 (2025) 107891

Contents lists available at ScienceDirect

Precambrian Research

journal homepage: www.elsevier.com/locate/precamres

Review Article

Paired metamorphic belts in the Usagaran Orogen of Tanzania: evidence for one-sided oceanic subduction in the Palaeoproterozoic

V. Schenk [a,*], T. Sarkar [b], D. Wiemer [c]

[a] Institute of Earth Sciences, Heidelberg University, 69120 Heidelberg, Germany
[b] Department of Earth Sciences, IISER Kolkata, Mohanpur 741246 West Bengal, India
[c] Economic Geology Research Centre, James Cook University, Douglas QLD 4811, Australia

ARTICLE INFO

Keywords:
Eclogites
Eclogite mylonites
Plate tectonics
Lomagundi isotope excursion
Paired metamorphic belts
Wilson cycle

ABSTRACT

Paired metamorphic belts (PMB) are the tectono-metamorphic expression of the one-sided subduction of oceanic lithosphere beneath continental margins and island arcs, which represents a key characteristic of terrestrial plate tectonics. PMB that are spatially and timely paired are mainly known from Phanerozoic orogenic belts, although the metamorphic rock record points to a duality of thermal regimes since the Palaeoproterozoic. Here we describe the tectono-metamorphic evolution of the Usagaran Orogen at the SE-margin of the Tanzania Craton, which includes PMB of Palaeoproterozoic age. The orogen's lithological inventory reflects a Wilson cycle: (1) The passive margin sequence (Konse Group) was deposited during the Lomagundi carbon isotope excursion (2.22–2.06 Ga) and metamorphosed at 2.03 Ga during the Usagaran orogeny. (2) The precursors of most eclogites were ocean-floor basalts, but those of the Ky- and Opx-eclogites of boninite chemistry were related to subduction-initiation. Peak eclogite metamorphism at mantle depths (850–880 °C/18–19 kbar) was followed by transient granulite-facies conditions during exhumation (750–800 °C/6–10 kbar). High-*T*-*P* shear zones in Opx-eclogites and felsic mylonites formed at P < 15 > 10 kbar are related to exhumation. (3) High-P amphibolite-facies metamorphism of metasediments enveloping the eclogite belt (770 °C/13.2 kbar at 2.0 Ga) is attributed to an accretionary wedge setting. The concurrent evolutions and the preserved growth zonations in garnet of both units point to a shared short-lived metamorphism. (4) Low-P Grt-Crd-Sil-granulites, which overlie the accretionary wedge metasediments as a nappe, experienced a counter-clockwise *P*-*T* path at ca. 2.06 Ga (peak 820 °C/7.2 kbar) in an arc setting that predates the orogeny for 50–60 Myr. We attribute their protomylonitic texture to post-peak NW-thrusting towards the orogenic foreland during collision. Late-stage *P*-*T* paths of all units in the nappe stack (isobaric cooling at 20 km depth) are interrelated. Other Palaeoproterozoic PMB in orogens around the Congo Craton and in the Yangtze Craton, in addition to subduction-related eclogites in the Trans-North China Orogen, indicate that subduction of oceanic lithosphere and its partial exhumation after slab breakoff at mantle depths were already viable tectonic processes. Pre-Neoproterozoic eclogites representing exhumed oceanic crust are dominantly known from a short time interval (2.1–1.8 Ga), during which warm (12–14 °C/km) and cold (<11 °C/km) subduction zones existed, which both show the tectono-metamorphic characteristics akin to modern asymmetric one-sided oceanic subduction.

1. Introduction

A key characteristic of terrestrial plate tectonics is the self-sustained one-sided oceanic subduction at convergent plate margins. Major factors that control this style of subduction process are a high plate strength and the presence of a weakened subduction slab interface, the formation of which is attributed to metamorphic dehydration of the subducting slab and the migration of water to form this hydrated interface (Gerya et al., 2008; van Hunen and van den Berg, 2008). Whether this style of subduction tectonics was viable in a hotter early Earth is still debated, as exhumed, deeply subducted oceanic lithosphere (subduction-related eclogites and blueschists) is scarce in the pre-Neoproterozoic rock record. This rarity has been attributed to compositional buoyancy of the early oceanic lithosphere (e.g., Davies, 1992) or, alternatively, to lithospheric weakness that did not provide a mechanism for exhumation, such as slab breakoff at mantle depths (van Hunen and van den

* Corresponding author.
E-mail addresses: volker.schenk@geow.uni-heidelberg.de (V. Schenk), tapabrato@iiserkol.ac.in (T. Sarkar), daniel.wiemer@jcu.edu.au (D. Wiemer).

https://doi.org/10.1016/j.precamres.2025.107891
Received 14 August 2024; Received in revised form 7 August 2025; Accepted 8 August 2025
Available online 9 September 2025

Berg, 2008). One of the tectono-metamorphic expressions of a former self-sustained one-sided oceanic subduction is provided by paired metamorphic belts (PMB) in the sense of Miyashiro (1961, 1973), i.e. a high-P/low-T belt spatially and timely associated with a low-P/high-T belt. The formation of such paired belts is related to the partial exhumation of a deeply subducted cold and dense oceanic lithosphere (high-P/low-T belt) and, landward, to a coeval low-P/high-T metamorphic belt in a magmatic arc environment (Miyashiro, 1961; Ernst, 2010).

Such PMB with the lithological (eclogites or blueschists), geochemical (ocean-floor basalts) and metamorphic characteristics (subduction to mantle depths) have been described predominantly from Phanerozoic orogens, although the metamorphic rock record points to the existence of a duality of thermal regimes (as a proxy for subduction processes on Earth) at least since the Palaeoproterozoic era (Holder et al., 2019; Brown et al., 2024). This observation relates to the highly debated question, when the plate-tectonic mode with deep subduction of oceanic lithosphere began.

In relation to the evolving thermal state of the mantle, the Earth is thought to have experienced different tectonic modes. The primary proposed modes include a mantle plume dominated stagnant lid (after solidification of the last magma ocean), a stagnant-deformable (squishy) lid (during part of the Archaean) and the active mobile lid of the modern global-scale plate tectonics (e. g., Lenardic, 2018; Stern, 2018; Gerya et al., 2021; Cawood et al., 2022; Brown et al., 2024). However, there is no consensus about possible gradual transitions between these tectonic modes or their possible simultaneous operations at different tectonic settings. Suggestions for the start of the modern plate tectonic mode span the time from the early Archaean to the Neoproterozoic. They depend largely on the interpretation and selective emphasis on specific observations and how we define plate tectonics (e. g., Stern, 2005, 2018; Brown, 2006; Hopkins et al., 2010; Sizova et al., 2010; Brown and Johnson, 2018; Bédard, 2018; Condie, 2018; Brown et al., 2024; Windley et al., 2021; Kusky et al., 2021; Arndt, 2023; Cawood et al., 2022; Condie and Stern, 2023). In the present study we put emphasis on the metamorphic record of early deep subduction of oceanic lithosphere to mantle depths and the related evolution of PMB in the sense of Miyashiro (1961, 1973).

In this paper we describe Palaeoproterozoic PMB in the Usagaran Orogen at the SE border of the Archaean Tanzania Craton, which are connected to a plate-tectonic 'Wilson cycle'. They reflect the asymmetric one-sided subduction of the oceanic plate to mantle depths, which represents the hallmark for the terrestrial plate tectonic regime (Gerya et al., 2008). We present metamorphic *P-T* paths, geochemical data and U-Th-total Pb monazite ages from the Yalumba Hill low T/P belt and the paired Igula high T/P granulites. These data underpin their related evolutions at an eastward-directed Palaeoproterozoic subduction zone (present day coordinates) of oceanic lithosphere below an obscured Archaean block that was reworked during the Kuunga orogenic event (at ca. 550 Ma) in the Mozambique Belt of Tanzania (Fig. 1a). Our data allow a relatively detailed reconstruction of a full-fledged Wilson cycle between ca. 2.15 and 2.0 Ga related to the Usagaran orogeny and document key pieces of evidence for at least the local operation of modern plate-tectonic processes in the Palaeoproterozoic.

The Usagaran Wilson cycle is recorded in a passive margin succession on the Tanzania Craton, high-P amphibolite-facies accretionary wedge metasediments, an eclogite-facies oceanic crust subducted to mantle depths, associated minor orthopyroxene-eclogites of low-Si boninite chemistry (which have magmatic precursors related to subduction initiation), high-T/high-P shear zones that formed during exhumation of the subducted oceanic slab and finally a nappe of low-P/high-T granulites emplaced on top of the high-P units during the Usagaran orogeny.

The Usagaran PMB may represent one of the so far oldest examples (ca. 2.0 Ga) for the development of PMB in the sense of Miyashiro with cold subduction of oceanic crust to mantle depths (<ca. 14 °C/km or 500 °C/GPa as redefined with the Phanerozoic metamorphic data set by Holder et al., 2019). These paired belts testify that subduction of rigid oceanic lithosphere to mantle depths and its partial exhumation after slab-detachment – characteristic features of modern subduction zones – were already viable tectonic processes during Nuna/Columbia formation.

2. Geological setting of Palaeoproterozoic belts of Tanzania

Palaeoproterozoic orogenic belts of Tanzania surround the Archaean Tanzania Craton on its southwestern (Ubendian Belt) and southeastern (Usagaran Belt) margins (Fig. 1a). The crust of the Tanzania Craton has mainly grown during the Neoarchaean (ca. 2.72–2.61 Ga) but older rocks revealing formation ages of >2.82 Ga and ca. 3.2 Ga have also been reported (Thomas et al., 2013, 2016; Kabete et al., 2012). Both Palaeoproterozoic belts contain eclogites that formed from ocean floor basalts during subduction metamorphism dated at 2.0 Ga in the Usagaran Orogen (Möller et al., 1995; Collins et al. 2004; Tamblyn et al., 2021) and at 1.88–1.86 Ga in the Ubendian Orogen (Boniface et al., 2012). These eclogites are spatially associated with coeval belts containing garnet-cordierite-sillimanite gneisses (Meinhold, 1970; Kazimoto et al., 2014, Loose and Schenk, 2018). Both belts experienced several tectono-metamorphic events in the Palaeoproterozoic (between 2.1 and 1.82 Ga; Kazimoto et al., 2014; Möller et al., 1995; Reddy et al., 2003; Tamblyn et al., 2021) pointing to similar evolutions, even if the dated eclogite-facies events of the two belts differ in age by about 140 Ma. The recognized tectono-metamorphic events in the Usagaran and Ubendian belts were associated with different generations of calc-alkaline magmatism between ca. 2.1 and 1.8 Ga reflecting different phases of Palaeoproterozoic crustal growth at the craton margins (Fig. 1; Wendt et al., 1972; Gabert and Wendt, 1974; Möller et al., 1998, 2000; Reddy et al., 2003; Thomas et al., 2013; Kazimoto et al. 2014; Tulibonywa et al., 2015; Sommer and Kröner, 2019). However, both Palaeoproterozoic belts also contain considerable amounts of reworked Archaean crust from the craton margins (Fig. 1; Möller et al., 1998; Johnson et al., 2003; Collins et al., 2004; Kazimoto et al. 2015). Kazimoto et al. (2015) and Loose and Schenk (2018) proposed on the basis of the PMB concept that the Palaeoproterozoic subduction in the Ubendian Belt was directed towards the northeast below the Tanzania Craton, whereas the subduction in the Usagaran Belt was east-directed below an Archaean crustal block to the east (Fig. 1, 'Mozambique Belt Meta-Craton'; reworked during the Neoproterozoic orogenies; Möller et al., 1995; Loose and Schenk, 2018). Other studies (Brown D.A. et al., 2020b; Tamblyn et al., 2021) not aware of the existence and the position of the low-P belt in the Usagaran (Meinhold, 1970; Meinhold and Frisch, 1970) and misinterpreting the Konse Group metasediments as a post-orogenic instead of a passive margin succession of the Usagaran Wilson cycle, left the direction of subduction open and discussed both possibilities.

The Ubendian Belt, bracketing the Archaean Tanzania and Bangweulu cratons, shares many similarities with its Palaeoproterozoic Usagaran twin orogen on the SE side of the Tanzania craton. However, in contrast to the Usagaran Orogen, it experienced several reworking events during Mesoproterozoic and Neoproterozoic orogenic cycles (Boniface et al., 2012; Boniface and Schenk, 2012; Boniface et al., 2014). Its Palaeoproterozoic evolution seems to be more complicated than that of the Usagaran Belt, as monazite and zircon ages show evidence for several Palaeoproterozoic tectono-metamorphic events (e. g., Kazimoto et al., 2015). Recent evolutionary models of the Ubendian Belt are critically reviewed in the supplementary material (S1). Therein we point out that some aspects of these models, in particular the two Palaeoproterozoic 'oceanic corridors' (Boniface & Tsujimori, 2021), are incompatible with the available petrological and age data.

3. Geology of the Usagaran Belt

In the Usagaran Belt, the best-preserved Palaeoproterozoic metamorphic rocks occur in a narrow wedge-shaped area along the border of the Tanzania Craton (Figs. 1, 2a). A compilation map showing the

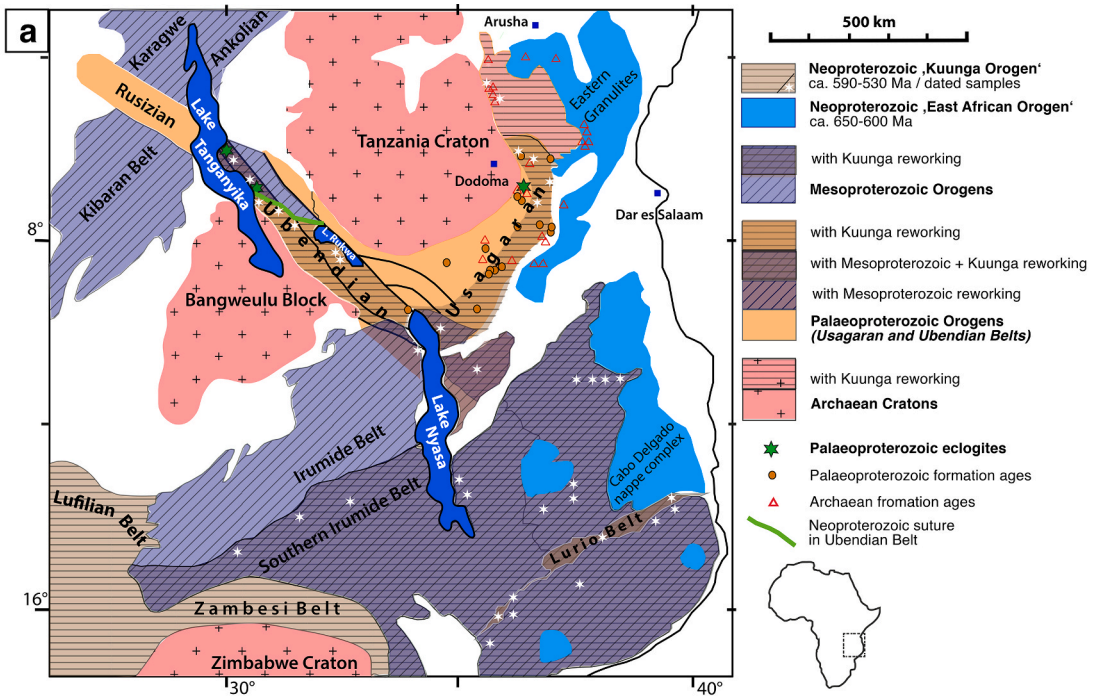

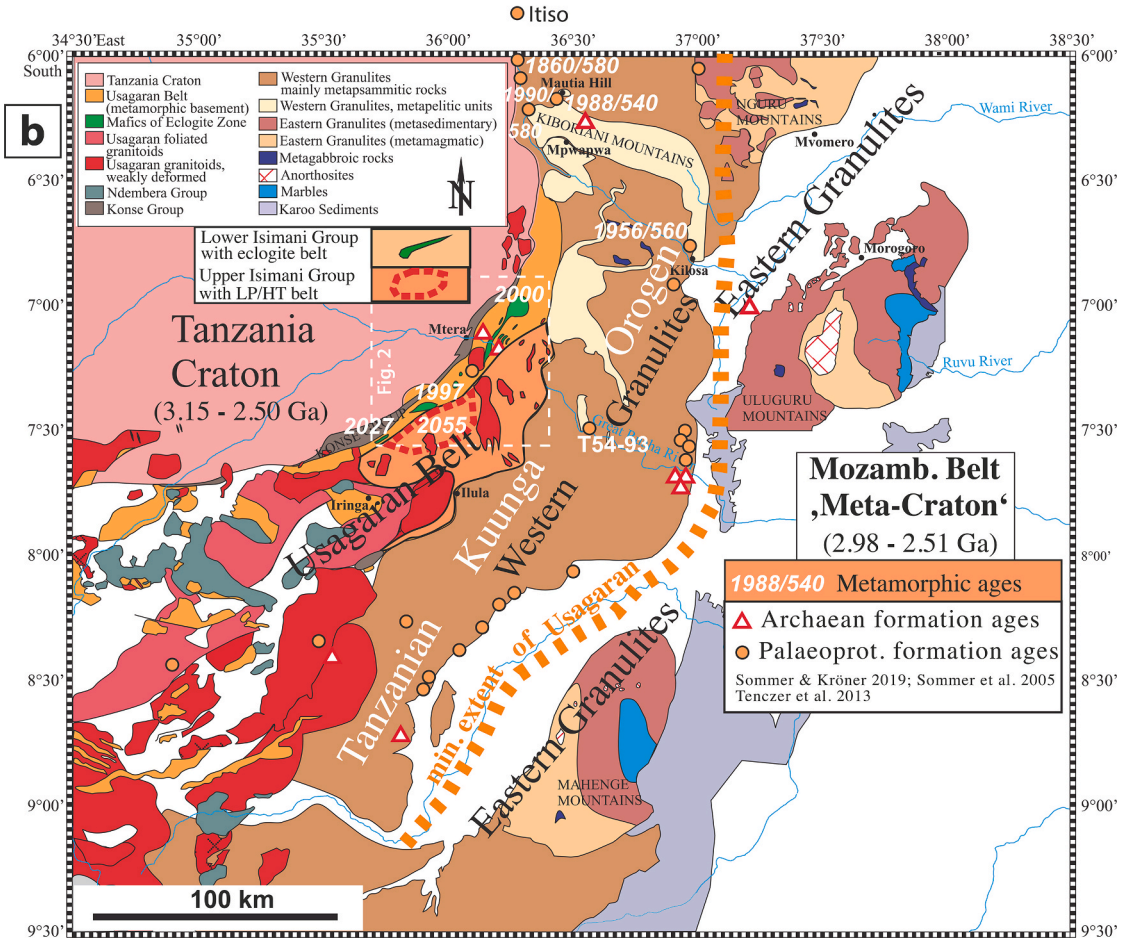

(caption on next page)

Fig. 1. Precambrian orogenic belts around the Tanzania Craton. The formation ages make clear that the suture of the Palaeoproterozoic Usagaran Belt (eclogite belt) separates two Archaean blocks of similar age: the Tanzania Craton and the ‚Mozambique Belt Meta-Craton'. (a) The Archaean and Palaeoproterozoic formation ages are only given for the Tanzanian part of the Mozambique Belt (zircon: Sommer et al., 2005, Thomas et al., 2013; Tenczer et al., 2013, Sommer and Kröner, 2019). Orogenic events overprinting older basement are marked by hatching: In central Tanzania, when the ‚Eastern Granulites' (ca. 650-600 Ma) where thrust towards west, the Archaean and Palaeoproterozoic rocks of the lower plate were overprinted by an amphibolite-facies metamorphism during the Kuunga orogeny (ca. 540 Ma). The Palaeoproterozoic Usagaran belt mostly evaded this overprinting only in a wedge shaped area close to the craton. (b) Geological map of the Usagaran Belt and adjoining areas, modified after the compilation map of Fritz et al. (2005). The Palaeoproterozoic paired metamorphic belts are at the SE border of the Tanzania Craton. The Neoproterozoic Mozambique Belt contains Neoarchaean and Palaeoproterozoic basement ('Mozambique Belt Meta-Craton'), implying that the Palaeoproterozoic suture separates two Archaean terrains. The Neoproterozoic Mozambique Belt consists of two orogenic belts: ‚Eastern Granulites' (ca. 0.64 Ga) and, near the craton, the Tanzanian Kuunga Belt (ca. 0.55 Ga). The Kuunga collisional event led to an amphibolite-facies reworking of the so-called ‚Western Granulites'. The so far undated Itiso ophiolite (just outside the map area) is thought to mark the northern termination of the Palaeoproterozoic Usagaran belt. The areal extent of the Usagaran Belt in the compilation map of Fritz et al. (2005) is not correct. New age data show a much wider area with Palaeoproterozoic formation and metamorphic ages ('minimum extent of Usagaran').

assumed extent of Usagaran rocks along the SE corner of the Tanzania Craton (Fritz et al., 2005, 2013; Fig. 1b) is based on 56 Quarter Degree Sheets (QDS) published by the Tanzanian Geological Survey (mapped by German Geological Mission 1963–1969; Temperley et al. (1953) and Whittingham (1959)). However, the assumed regional extent of the wedge-shaped Usagaran Belt is biased by a systematic increase of mica cooling ages towards the craton (from 430 to 1960 Ma), pointing to a gradually decreasing influence of the Neoproterozoic orogenies (Wendt et al., 1972; Gabert and Wendt, 1974; Coolen et al., 1982). The true extent of the belt with dated Palaeoproterozoic magmatism and metamorphism is much wider towards north and east (cf. discussion in 3.1). The Palaeoproterozoic Usagaran Belt is bordered in the NW by the Archaean Craton and in the SE by two Neoproterozoic belts, which were grouped together under the umbrella of the Mozambique Belt (Fig. 1; Holmes, 1951; Hepworth, 1972) or East African Orogen (EAO; Stern, 1994), not discriminating between the two different Neoproterozoic events and belts that have been recognized later. These are the 'Eastern Granulites' (Fig. 1), which are characterized by a counter-clockwise *P-T* evolution at ca. 650–600 Ma (Appel et al., 1998; Möller et al., 2000) and the Kuunga collisional event at ca. 540 Ma, which is characterized by a clockwise *P-T* evolution (Jöns and Schenk, 2004). The thrusting of the Eastern Granulites nappe may have caused the Kuunga age metamorphism in the underlying 'Western Granulites' (Jöns and Schenk, 2004; Cutten et al., 2006; Fritz et al., 2013). The eastern boundary of the Palaeoproterozoic Usagaran Belt within the Neoproterozoic Mozambique Belt is obscured (and thus not known) due to this strong Neoproterozoic reworking. However, the presence of this older crust within the Mozambique Belt is reflected by the occurrence of Archaean and Palaeoproterozoic formation ages (Fig. 1).

3.1. *Estimating the regional extent of the Usagaran Orogen*

Taking the distribution of published Palaeoproterozoic formation ages as evidence for traces of a Palaeoproterozoic orogeny in the Neoproterozoic Mozambique Belt and adding new texturally controlled metamorphic monazite ages (Fig. S2 and S3), we can considerably expand the hitherto assumed regional extent of the Usagaran Orogen (Fig. 1b) towards east and towards north (up to Itiso, Ikawla (T44-93); SW of Mautia Hill (T37-93), NW Kiboriani Mountains). We propose that the Itiso ophiolite, exposed just outside the map area of Fig. 1b (80 km NNW of Mautia), marks the northernmost point of the wedge shaped Usagaran Orogen. For this Itiso ophiolite a Neoproterozoic age has been assumed so far (Shackleton, 1986; Berhe, 1990). However, monazite ages (U-Th-total Pb dating) from staurolite-kyanite-garnet 2-mica schist at the nearby Ikawla location clearly point to two metamorphic events (at ca. 1860 and 560 Ma) that affected these rocks (T44-93; Fig. 1b; Fig. S3k), making the Palaeoproterozoic age of the ophiolite likely. Furthermore, at Kilosa (Fig. 1b, T46-93) and at Mbuyuni (T54-93), which are locations far outside the assumed area of the Usagaran Orogen (Fig. 1b), two metamorphic events are evident. Monazite grains included in garnet porphyroblasts (T46-93; Kilosa) revealed Palaeoproterozoic ages (1956 ± 13 Ma), whereas ages of monazite matrix grains reflect the Neoproterozoic reworking (583 ± 10 Ma; Fig. S3a-j). Thus, the main metamorphism, which resulted in the growth of garnet porphyroblasts, is of Palaeoproterozoic age, whereas the later reworking was of minor importance in the Kiboriani Mountains. Petrographic evidence for two orogenic events have also been found at Mbuyuni, further south at the Great Ruaha river (T54-93: Grt-Ky-Bt gneiss; Fig. 1b). During the first event garnet porphyroblasts were formed, which subsequently were partially replaced by Bt-Ky symplectites (Fig. S2). These retrograde textures were overgrown by a second garnet generation. The textures indicate two orogenic-metamorphic events, which are separated by a phase of retrogression. This is in accordance with the Palaeo- and Neoproterozoic monazite ages further north.

The new Palaeoproterozoic monazite ages from Ikawla and Kilosa are in agreement with zircon data obtained from metasediments mapped by Temperley et al. (1953) along the eastern craton margin. These metasediments are known as the Mpwapwa Group (Thomas et al., 2013) and crop out in the Kiboriani Mountains as well as along and south of the Dodoma-Dar es Salaam road (Fig. 1). The Mpwapwa Group displays a lithological W-E zonation. Quartzites, metapelites with some intercalated marbles, which occur near the craton, may correspond to those of the Konse group. The felsic gneisses with mafic intercalations, in the eastern part, resemble those of the Lower Isimani Group, occurring further south. These metasediments experienced their main metamorphism (amphibolite facies) during the Palaeoproterozoic (Zrc and Ttn: 1993/1999 Ma; Thomas et al., 2013) and were only weakly affected by the Neoproterozoic reworking (ca. 550 Ma; Thomas et al., 2013). In contrast, at Mautia Hill, only ca. 20 km away from the craton border, the Neoproterozoic reworking is clearly the dominant metamorphic event as all monazite ages (LA-ICPS; Apen pers. com.), Sm-Nd garnet ages (Möller in Jöns and Schenk, 2004) and U-Pb zircon ages (Cutten et al., 2006) are Neoproterozoic (ca. 550–540 Ma). The *P-T* path of the Mautia whiteschists points to a strong Neoproterozoic crustal thickening (720 °C/10–11 kbar at ca. 550 Ma; Jöns and Schenk, 2004). Palaeoproterozoic monazite ages (ca. 2000 Ma) were only found in one spessartine-kyanite sample collected ca. 5 km SW of Mautia Hill towards the Kiboriani Mountains (T37-93).

The new metamorphic ages from Ikawla, Mbuyuni, the Mautia Hill and the Kiboriani Mountains (Mpwapwa Group) demand a new view for the regional extent of the Usagaran Orogen, which affected the southern part of the so-called ‚Western Granulites'. The Usagaran Orogen reaches further north and further east (Fig. 1b) than indicated in the compilation map of Fritz et al. (2005). The basement in the northern part of the Tanzanian Kuunga Orogen, which is also part of the ‚Western Granulites', seems to consist only of Archaean precursors. Correspondingly, we assume a northern limit of the Palaeoproterozoic Usagaran Belt (Fig. 1a). We conclude that the southern part of the so-called ‚Western Granulites' was affected by an upper amphibolite-facies metamorphism of Palaeoproterozoic age (2000–1960 Ma), which we detected by texturally controlled monazite dating in metapelites. This demonstrates that metamorphic traces of the Palaeoproterozoic Usagaran orogeny can be found in the Neoproterozoic Mozambique Belt.

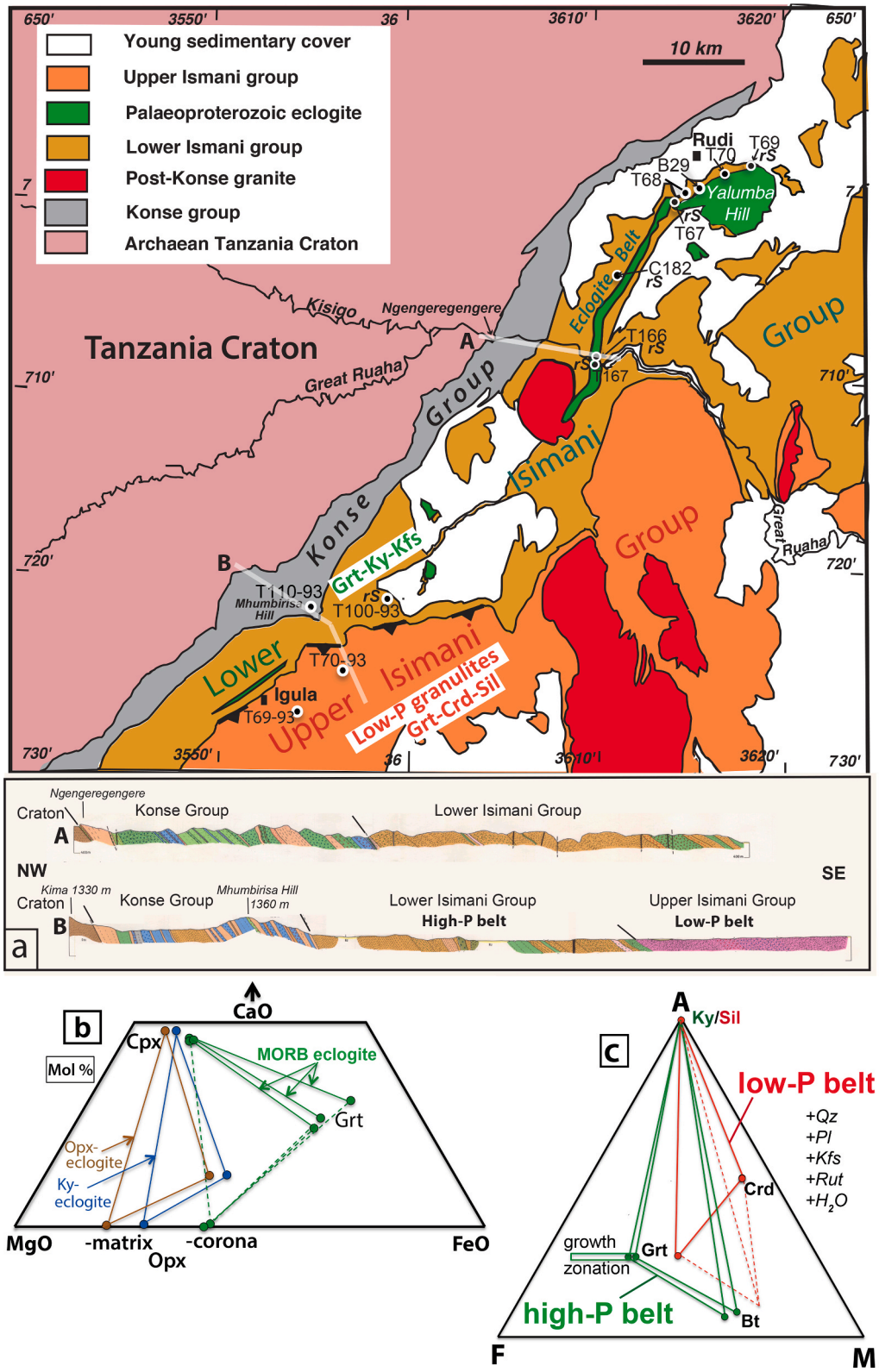

Fig. 2. (a) Geological map with sample locations (map area marked in Fig. 1b) and two NW–SE geological cross-sections (white lines A and B) through the PMB of the Usagaran Orogen at the SE border of the Tanzania Craton. Color-coding of cross-sections as in Fig. 3 (modified after Meinhold, 1970 and QDS 198). Mineral abbreviations after Whitney and Evans (2010). The Lower Isimani Group envelops the eclogite belt. Late-stage sillimanite rims around kyanite (*rS*) are characteristic for the Lower Isimani Group. The high T/P granulite metamorphism (nappe of Upper Isimani Group) is ca. 55 Ma older than the eclogite metamorphism. The boundary of the granulite nappe is not well constrained, except in the SW. (b) The Usagaran eclogites comprise rare Mg-rich Opx-eclogites and Ky-eclogites in addition to common Fe-rich eclogites of MORB chemistry. (c) AFM (Thompson) projection of metapelites of the Lower Isimani Group (Grt-Ky-Bt, with preserved growth zoning in Grt) and of the Upper Isimani Group (Grt-Crd-Sil), emphasizing their contrasting phase relations.

3.2. Geology of paired metamorphic belts in the Usagaran Orogen

The Palaeoproterozoic Usagaran rocks in the wedge-shaped area at the SE corner of the Tanzania Craton (Fig. 1b) experienced only mild Neoproterozoic reworking (Wendt et al., 1972). This area was mapped and lithologically subdivided by earlier authors (Fig. 2; Meinhold, 1968, 1970; Whittingham, 1959; Temperley et al., 1953; Fritz et al., 2005 and references therein). Meinhold (1970) distinguished the high-grade Isimani Group (‚Usagaran highly metamorphic rocks' of Whittingham, 1959) and the lower-grade Konse Group metasediments, which discordantly overlie migmatitic gneisses of the Archaean Tanzania Craton (map and profiles in Figs. 2 and 3 modified after Meinhold, 1970). According to Meinhold (1970), the Konse Group is overlain by the Lower Isimani Group, which consists of various types of metasediments (including Grt-Ky metapelites) and intercalated metabasites (amphibolites and eclogites), in addition to some tectonic slivers of felsic Archaean basement (Möller et al., 1998; Collins et al., 2004). The Upper Isimani Group consists mainly of granulites (Grt-Crd-Sil) and rests on top

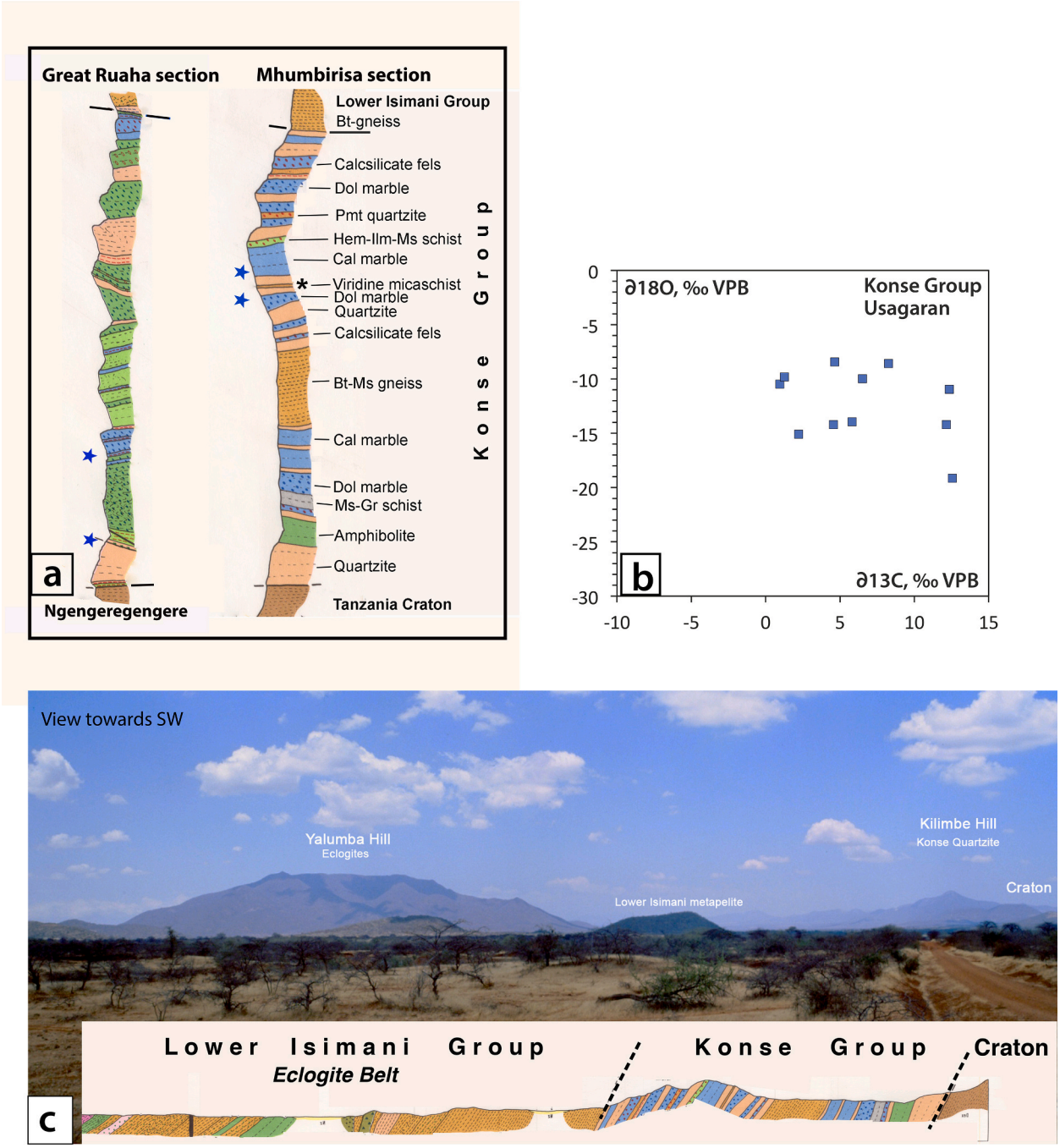

Fig. 3. (a) Stratigraphic columns of the Konse Group (passive margin sequence, ca. 2–3 km thick) as mapped by Meinhold (1970) at the Mhumbirisa Hill and along the Great Ruaha River. Columns correspond to the two cross-sections A and B shown in Fig. 2 (blue stars: carbon isotope samples; black star: Mn-andalusite-spessartine micaschist; its metamorphism is dated at 2028 ± 15 Ma). (b) Plot of $\delta^{18}O_{carb}$ vs. $\delta^{13}C_{carb}$ in ‰ VPDB for Konse Group marbles (modified after Schenk et al., 2025). The high positive $\delta^{13}C_{carb}$ values (up to +12.6 ‰ VPDB) point to deposition during the Lomagundi C-isotopic excursion at 2.22–2.06 Ga. (c) Landscape view towards SW at Yalumba Hill, the prominent outcrop of eclogites. The Konse Group (passive margin sequence) overlies the Tanzania Craton. Inserted schematic cross-section at craton margin as in Fig. 2; modified from Meinhold (1970).

of the Lower Isimani Group (Meinhold, 1970). The occurrence of these granulites is restricted to the southern part of the belt (ca. 30 km in length, near Igula; Fig. 2).

The Konse Group is a 2–3 km thick volcano-sedimentary succession, metamorphosed to upper greenschist to lower amphibolite facies (Meinhold, 1970; Meinhold and Frisch, 1970) with increasing grade towards east, which follows the margin of the craton for more than 200 km. It is composed of quartzites, metaconglomerates, greenschists, amphibolites, micaschists, graphite-muscovite schists, iron-rich quartzites, some minor oxidized Mn^{3+}-silicate bearing micaschists and Mn-rich quartzites, which are associated with some dolomite and calcite marbles (Fig. 3; Meinhold, 1970; Mruma, 1995). The succession is regarded as a single sedimentary group. It pinches out north of Yalumba Hill (Fig. 2) and varies in composition along strike, as quartzite units and metavolcanic intercalations vary in thickness. A strong late-stage greenschist-facies overprint increases towards the craton, i.e. towards the deeper stratigraphic members of the group (profiles in Fig. 2a). This overprinting is attributed to the Neoproterozoic NW-thrusting of the Konse Group metasediments towards the craton.

The stratigraphic age of the Konse Group has been controversially discussed for a long time. Because Grantham (1927), Whittingham (1959) and Mruma (1989, 1995) have assumed that the Konse sediments unconformably overlie the folded Lower Isimani Group, most authors regard the Konse Group as a succession deposited in an epicontinental basin after the Usagaran orogeny. In contrast, Meinhold (1968, 1970) and Meinhold and Ott (1993, unpubl. BGR report) regard the well-preserved Konse succession as a temporal equivalent to the Lower Isimani Group, which was deposited as continental margin sediments along the craton border. The tectonically overlying Lower Isimani Group is regarded by Meinhold (1970) as the deeper part of the same basin. Recent monazite dating of the lower amphibolite-facies metamorphism of a Mn-andalusite-spessartine micaschist, which represents a characteristic rock type of the Konse Group (Fig. 3; at Mhumbirisa Hill), revealed an age of 2028 ± 15 Ma (SIMS; Schenk et al., 2025). This metamorphic age is related to the Usagaran orogeny and excludes a post-orogenic depositional age. Thus, the Konse Group has been re-interpreted as a passive margin succession of the Usagaran Wilson cycle. Carbon isotope studies of the Konse Group marbles revealed distinctly high $\delta^{13}C_{carb}$ values (of up to + 12.6 ‰ VPDB) like those of marine carbonates deposited during the 'Lomagundi event' (Schenk et al., 2025). This carbon isotope excursion is a worldwide chemostratigraphic marker, which indicates carbonate depositional ages between 2.22 and 2.06 Ga (Schidlowski et al., 1976; Karhu and Holland, 1996; Bekker et al., 2006). Carbon isotope studies of the Mpwapwa Group marbles, which represent the sedimentary cover of the 'Western Granulites' in the Neoproterozoic Mozambique Belt, revealed similar high $\delta^{13}C_{carb}$ values characteristic of the Lomagundi event (Schenk et al., 2025). The Konse and Mwapwa groups are thus regarded as members of the same Palaeoproterozoic sedimentary succession, which stretches for about 300 km along the eastern border of the Tanzania Craton. The new stratigraphic ages for the Konse and Mpwapwa groups (Schenk et al., 2025) indicate that both groups are correlative with passive margin successions at other Archaean cratons of southern Africa: e.g., the Lomagundi Group (Magondi Belt, NW of Zimbabwe Craton; Schidlowski et al., 1976; Master et al., 2010), the Buganda Group (Ruwenzori Fold Belt, N of Tanzania Craton; Master et al., 2013) and the Gumbu Group (Limpopo Belt, S of Zimbabwe Craton; Buick et al., 2003).

The Lower Isimani Group (or 'Amphibolite-bearing Gneiss Group' of Meinhold, 1970) mainly consists of kyanite-garnet ± K-feldspar bearing metapelites and other metasedimentary rocks, which are associated with some reworked felsic gneisses of Neoarchaean age (ca. 2.7 Ga; Möller et al., 1998; Reddy et al., 2003; Collins et al., 2004). Carbonatic rocks, quartzites and Mn-bearing schists, which are common in the Konse Group, are missing or are rare. The Lower Isimani Group envelops the eclogite belt, which stretches along the craton border (Fig. 2). The general tectono-stratigraphic relationship between craton, Konse Group passive margin sediments and the Lower Isimani Group with its included eclogite belt is nicely exposed near the northern end of the high-P belt at Yalumba Hill (Fig. 3c).

The granulite nappe of the Upper Isimani Group (or 'Amphibolite-free Gneiss Group' of Meinhold, 1970) consists mainly of garnet-cordierite-sillimanite bearing metapelites apart from some rare mafic 2-pyroxene granulites in an area NNE of Iringa (near Igula; Fig. 1b, Fig. 2). The outcrop situation of this group is very poor, mainly along dry riverbeds in a flat area. The high-grade character is hardly recognizable in the field due to a late-stage tectonic overprint after peak metamorphism (section 5.5). Meinhold (1970) recognized in the Upper Isimani Group an 'Abukuma-type' of metamorphism, which contrasts to the 'Barrow-type' metamorphism of the Grt-Ky gneisses of the Lower Isimani Group. The contrasting metamorphic styles, which affected the two Isimani groups have been confirmed in the present study by mineral chemical data and are demonstrated by the contrasting phase relations of metapelites in AFM-projections (Fig. 2c). The granulites must be regarded as a nappe, because of their differing *P-T* path and age of metamorphism, as discussed in the present study (Fig. 2; Sections 5.5, 6 and 7). Meinhold (1970) mapped a horizon of peculiar, fine-grained platy, banded gneisses, which contain different porphyroclasts (feldspars, garnet, orthopyroxene; Plate 5, Figs. 1 and 2 in Meinhold, 1970). These gneisses define the base of the Upper Isimani Group and are likely mylonites, which supports our nappe interpretation of the Upper Isimani Group granulites.

Whittingham (1959) described the eclogites at Yalumba Hill of ‚apparently Archaean age' embedded in the Ky-Grt metapelites of the Lower Isimani Group. However, the eclogite-facies metamorphism was dated by Möller et al. (1995) at 2000 ± 2 Ma (U-Pb monazite age of the Lower Isimani Group) and 1996 ± 2 Ma (titanite cooling age for eclogite). These precise TIMS ages were confirmed by a zircon SHRIMP age of 1972 ± 39 Ma for an eclogite and 1989 ± 10 Ma for a metapelite (Collins et al., 2004). Recently, Tamblyn et al. (2021) re-analyzed zircon of two eclogite samples of Collins et al. (2004) adding further support for the age of the high-P metamorphism at ca. 2.0 Ga (2023.4 ± 9.3 Ma and 2010 ± 7.2 Ma) using a laser ablation split stream system. The authors also presented new Lu-Hf ages for eclogite garnet (1994 ± 9 Ma, with a range of ca. 1960–2140 Ma). Subsequent to the exhumation of the subduction-related units, the two Isimani Groups and the Konse Group were thrust together during the Usagaran orogeny in a sinistral transpressive regime towards NW onto the craton (Whittingham, 1959; Meinhold, 1970; Reddy et al., 2003), like the Mpwapwa group further north (Temperley et al., 1953; Thomas et al., 2013). This NW directed thrusting was associated with a post-eclogite-facies, amphibolite-facies deformation (D2 of Reddy et al., 2003), which was dated with zircon from a pegmatoid vein crosscutting the foliation (1991 ± 2 Ma; Collins et al., 2004). This age indicates fast cooling and exhumation of the eclogites, in accordance with the 1996 ± 2 Ma U-Pb titanite cooling age of Möller et al. (1995; 20–25 °C/Ma cooling rate).

U-Pb rutile ages of eclogites (Möller et al., 1995; Tamblyn et al., 2021), Ar-Ar ages of white mica (Reddy et al., 2004), as well as systematically decreasing Rb-Sr biotite ages from the craton border eastwards (Wendt et al., 1972) revealed a weak Neoproterozoic overprint on all rocks of the Usagaran (at ca. 540 Ma). This is likely related to the local greenschist-facies overprint at the base of the Konse Group and to the Neoproterozoic thrusting of the Konse and Isimani Groups northwestwards onto the craton (Meinhold, 1970; Reddy et al., 2004). Structural studies in the area north of Yalumba Hill, up to the ophiolite of Itiso (Fig. 1b), revealed the same NW directed tectonic transport of the Mpwapwa Group towards the Tanzania Craton (Temperley et al., 1953; Thomas et al., 2013), as for the Isimani groups. As the new stratigraphic classification of the Mpwapwa Group (Lomagundi event) is also the same as for the Konse Group, the two areas (the northern Mpwapwa area and the southern Yalumba-Konse area) seem to have experienced very similar evolutions. The main differences are the missing eclogite belt and the missing nappe of Grt-Crd-Sil granulites (Upper Isimani Group) in

the northern area, in which, at Itiso, an ophiolite is outcropping (Fig. 1b).

3.3. Previous P-T estimates for Usagaran eclogites and associated metasediments

The knowledge of the thermal conditions during subduction and exhumation of the exposed oceanic crust and of their tectono-metamorphic relation to the associated metasediments are most valuable for the understanding of tectonic processes at Palaeoproterozoic subduction zones. The first petrological attempts to gain such information were based on conventional Grt-Cpx/-Opx thermobarometry (Möller et al., 1995). They resulted in peak-metamorphic conditions for the eclogites of about 18 kbar/750–800 °C, after which the rocks were isothermally exhumed to transient granulite-facies conditions. A high-P metamorphism (GASP equilibrium estimates) was also deduced for the associated metapelites of the Lower Isimani Group. However, peak pressures of the metasediments seemed to be less than those of the eclogites. Uncertainties arose mainly from poor temperature constraints (Grt-Bt thermometry) for the high-grade Grt-Ky-Bt schist. Because of the coeval metamorphic evolutions of eclogites and metapelites, the authors assumed a subduction metamorphism for both lithological units. All subsequent studies followed this interpretation.

Recently, Brown D. A. et al., 2020 and Tamblyn et al. (2021) attempted to improve the petrological constraints for the *P-T* evolution of the eclogites and metapelites of the Lower Isimani Group by pseudosection modeling and Zr-in-rutile thermometry on a small number of samples of Collins et al. (2004). Generally, the results are in good agreement with the *P-T* path of Möller et al. (1995) but show some distinct features (S3). The most recent attempt to determine the *P-T* conditions of the subduction metamorphism at Yalumba Hill stems from Herms et al. (2023). The authors observed carbonate-bearing polymineralic inclusions in garnet porphyroblasts of one 'restitic metapelite' sample (T70 in Fig. 2a), which they interpreted as melt inclusions of peraluminous rhyolitic compositions. Reheating experiments at high pressures (25 kbar) on these inclusions revealed complete homogenization only at $T > 950$ °C.

In summary, so far, all studies that aimed at characterizing the metamorphic history of the eclogites and the associated metasediments (Lower Isimani Group) have considered only a restricted number of samples (1–4), collected from a very restricted area (mainly from Yalumba Hill). In addition, the applied methods had some flaws. Some *P-T* estimates were either based on data obtained without textural control and/or were based on unproven assumptions. A critical evaluation of the methods and results of these previous *P-T* estimates is provided in the supplementary material (S3). For a better understanding of the tectonic processes, which operated at the Palaeoproterozoic subduction zone of the Usagaran Orogen, it is necessary to investigate more samples from different rock types with better preserved metamorphic reaction histories, collected from a larger area of the belt. This approach is presented in section 5.

4. Geochemistry of eclogites

The most prominent occurrence of Usagaran eclogites is at the Yalumba Hill, where they form an impressive elevation above the peneplain near the village of Rudi (Fig. 3c). At this hill, the rocks were first recognized as eclogites (by Harpum in 1952 in an unpublished report; cf. Whittingham, 1959) and were regarded as of 'apparently Archaean age' (Geolog. Map of Tanganyika 1: 2 000 000; Geol. Survey, 1959; Whittingham, 1959). Two whole-rock eclogite analyses published by Möller et al. (1995) revealed that the precursor melts were derived from a depleted mantle source (MORB). Here we present further whole rock geochemical data of eclogites from Yalumba Hill and its SW extent along the craton border to prove the validity of the restricted published data. Despite possible element mobility during high-grade metamorphism, we attempt to deduce tectonic settings for the magmatic precursors of the recognized eclogite types.

Based on our new data set (Table S1), we can distinguish three groups of eclogites of subalkaline chemistry plotting mainly in the basalt field of the TAS diagram with two samples in the picrite basalt field (Fig. S4). 1. MORB-type1 eclogites reveal similarities to N-MOR basalts with flat chondrite-normalised REE pattern (ca. 12-20x enriched relative to chondrite) showing some depletion of LREE (mainly La, Ce; Fig. 4a) and no Eu anomaly, excluding major crustal contamination. The patterns of MORB-normalized trace element concentrations are also flat, slightly below the normalization values (Hofmann, 1988) and show weak negative Zr-Hf anomalies, but lack Nb-Ta anomalies (Fig. 4c). The fluid mobile elements (Sr, K, Rb, Ba) are either enriched or depleted, which we attribute to fluid-rock interaction during metamorphism. The precursor melts of these N-MORB eclogites were derived from a depleted mantle source reflected by their high Zr/Nb and Nb/Th ratios (Fig. 4g). The Mg numbers (52–48; assuming $Fe_2O_3 = 0.1\ Fe_2O_3tot$) point to some degree of fractionation from primary mantle melts. 2. MORB-type2 eclogites represent a second (subordinate) group showing REE patterns that are characterized by a slope due to enrichments of LREE relative to HREE (Fig. 4b). The MORB-normalized trace element patterns of this group (Fig. 4d) also show a slope increasing towards elements of increasing incompatibility and display negative Zr-Hf anomalies. Some samples are also depleted in Ti. The fluid mobile elements of this group are also either enriched or depleted due to metamorphic fluid-rock interaction. These eclogites of MORB chemistry derive from melts produced in an E-MORB environment as reflected by their low Zr/Nb at high Nb/Th ratios (Fig. 4g). Most eclogite samples of the two groups of MORB chemistry plot along the MORB-OIB array in the Th/Yb vs. Nb/Yb plot (Pearce, 2008) between typical N-MORB and E-MORB but some samples with higher Th/Yb suggest an influence of subduction fluids (Fig. 4h) that is also indicated by samples with Zr-Hf and Ti depletion.

The third group of eclogites, which contain prograde matrix-orthopyroxene, has high Mg numbers (76) and high SiO_2 contents (Table S1). Their minerals (Grt-Opx-Cpx) are also more Mg-rich than those of the two groups of MORB chemistry (Fig. 2b). The latter group contains orthopyroxene only in late-stage coronas around garnet but never in the matrix. The MgO- and SiO_2-rich rocks fall into the field of basalts of the TAS diagram (Fig. S4), but can be classified (after normalization according to the Ti8-Si8 nomenclature of Pearce and Reagan, 2019) as low-Si boninites with high MgO contents (18.14; 19.46 wt %; Mg-numbers of 78 and 79) and Si8 values of 53–54 and low Ti8 of 0.3–0.4 (Fig. S5). The REE display upward concave patterns typical for boninites, high Zr and Hf relative to the middle REEs, pronounced Nb-Ta troughs and negative Zr-Hf-Ti anomalies indicating a subduction environment for the formation of their precursor melts (Fig. 4e,f). This is in agreement with the very low Nb/Th at relatively high Zr/Nb that points to a hydrated mantle source (Fig. 4g). This type of low-Si boninites is interpreted as the product of shallow wet melting and strongly indicative of subduction initiation (Pearce and Reagan, 2019). A magmatic subduction environment is also indicated by one further eclogite sample displaying a flat REE pattern, a pronounced Nb-Ta trough and negative Zr-Hf-Ti anomalies (T69-26; Fig. 4e–h). Their magmatic formation may be attributed to a forearc environment.

In summary, the different types of eclogites of the Yalumba Hill high-P belt contain geochemical signatures characteristic of ocean-floor basalts of which some derived from a depleted and others from an enriched MORB mantle source. The latter group is more commonly formed during the early stages of ocean basin formation. The eclogites of ocean-floor basalt chemistry are associated with eclogites of low-Si boninite affinity and forearc basalt chemistry, the magmatic precursors of which may have formed during subduction initiation in the forearc region and became subsequently involved in the subduction process.

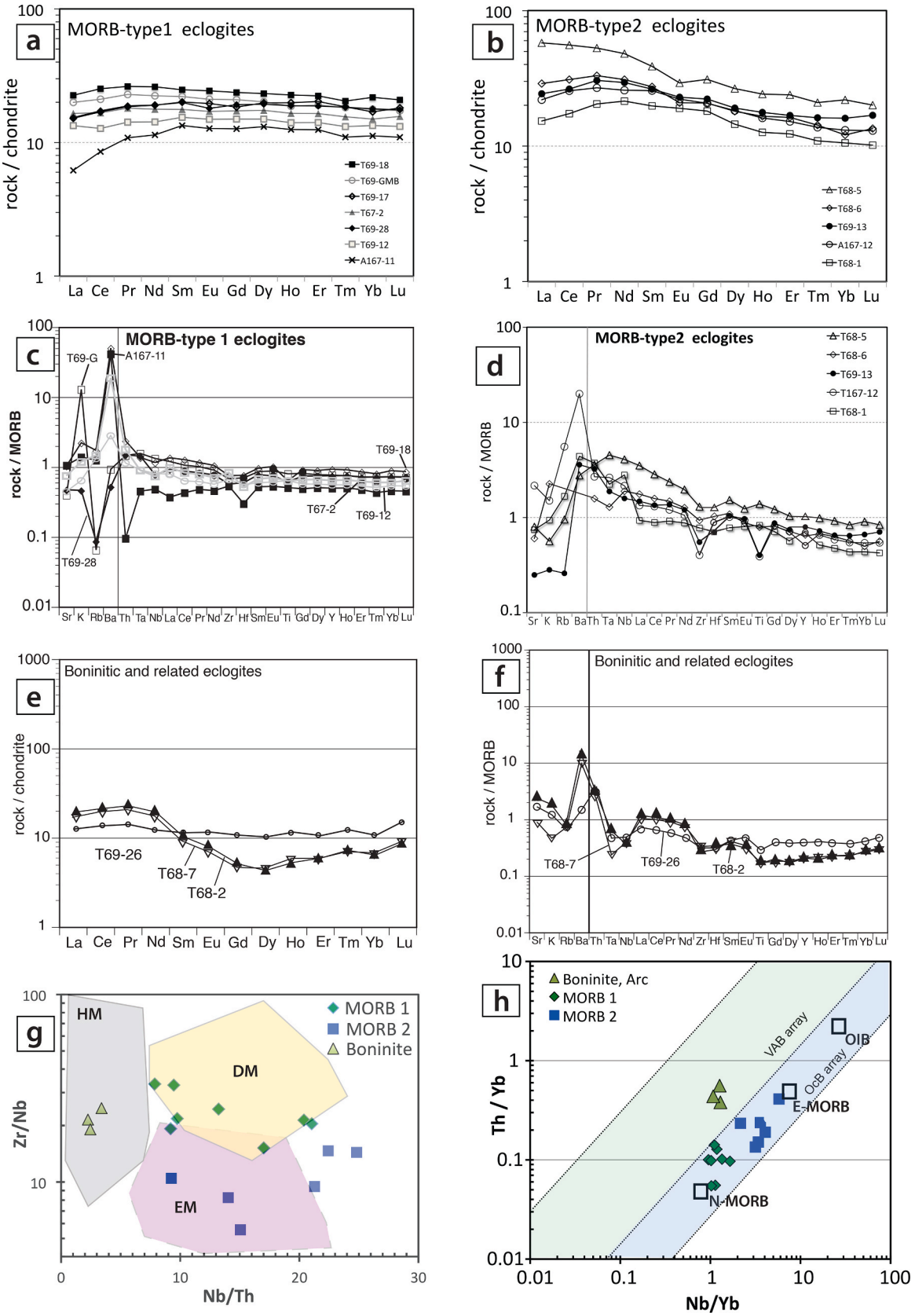

Fig. 4. (a-f) REE and trace element patterns of eclogites with affinity to ocean floor basalts can be subdivided in two groups (N-MORB (a, c) and E-MORB (b, d). The N-MORB1 patterns indicate the derivation of the melts from a depleted MORB source (DM in g); the MORB2 group derives from an enriched MORB mantle source (EM in g). The Mg-rich Opx-eclogites are of low-Si boninite chemistry (e, f) and derive form a hydrated mantle (HM in g) with high Th/Yb ratios (h) and exhibit negative Nb-Ta anomalies like Izu-Bonin boninites. The third eclogite pattern (T69-26) in (e) and (f) reflect an influence of subduction fluids. Fields of HM, EM and DM in (g) after Condie (2015), discrimination diagram (h) after Pearce (2008).

5. Petrology of the paired metamorphic belts

Because of the diverse nature and character of the different tectono-metamorphic units that constitute the Usagaran Orogen, the mineral chemistry and petrology of the diverse litho-tectonic units will be treated in separate sections: (1) The two eclogite-groups that formed from ocean floor basalts (N-MORB and E-MORB) are petrographically quite distinct from the boninitic Opx-eclogites as they are much more Fe- and Ca-rich and contain no prograde orthopyroxene (Fig. 2b). (2) The Mg-rich Opx-eclogites that display a chemical affinity to subduction-initiation related low-Si boninites. These Opx-eclogites were only found in a restricted area on the western side of Yalumba Hill (T68-93; Fig. 2a,b). One Ky-eclogite sample (B29) has similar Mg-rich minerals. (3) The exhumation-related high-T mylonites that developed locally from these Opx-eclogites are associated with felsic mylonites. (4) The Grt-Ky bearing metapelites of the Lower Isimani Group, which are interpreted to have been formed from accretionary wedge sediments and envelope the eclogites of the Yalumba Hill high-P belt. (5) High T/P Grt-Sil-Crd granulites of the Upper Isimani Group, which form a nappe on top of the Lower Isimani Group.

5.1. Petrology of eclogites formed from ocean floor basalts

The eclogites of MORB chemistry represent by far the most common rock type in the Yalumba Hill high-P belt and mainly consist of poikilitic garnet porphyroblasts (ca. 2–4 mm, rarely 2 cm in diameter) in a medium grained matrix (1–2 mm) of omphacite, rutile and quartz. In addition, many samples contain pargasitic hornblende, plagioclase, ilmenite, titanite and clinozoisite. Where these phases occur as inclusions in garnet, they are attributed to the prograde stage. Where they are part of the matrix the timing of their crystallization is in many cases not unequivocal. Due to common strong reworking during retrogression, the prograde phases are partially replaced by granulite- to amphibolite-facies minerals (Fig. 5 and Fig. S6): In many samples, omphacite is surrounded by rims of hornblende and garnet is commonly surrounded by coronas of Cpx-Pl ± Hbl ± Opx ± Ilm (Fig. 5b, c; 6a, c). Garnet is riddled with numerous rutile needles with preferred crystallographic orientations that are interpreted as exsolutions after peak-metamorphism (Fig. 5f). Such exsolutions are known to occur mainly in rocks, which experienced extreme metamorphic conditions (Ague and Eckert, 2012). As the Ti content of garnet is pressure and temperature sensitive (Zhang et al., 2003) it can often be related to UHT or UHP metamorphic conditions. Element mapping (SEM) of such exsolved core regions in garnet (T68-6) revealed tiny zircon crystals (<1μm in diameter) that are always associated with the exsolved rutile needles (inset in Fig. 5f; Fig. S7). However, ilmenite, apatite, quartz or negative garnet crystal 'pores', as described by Ague and Eckert (2012), have not been found. Remaining TiO_2 contents in such exsolved garnet cores are in the range of 0.1–0.2 wt% TiO_2 (Table S4, T68-6). Omphacite porphyroclasts of these eclogites are in most cases strongly altered by 'exsolutions' of plagioclase, which form needles in different crystallographically preferred orientations (Fig. 5b,d,e) or blebs. This resulted in zoned omphacite grains (Fig. 5b) due to the loss of the jadeite component. The prograde composition of omphacite is therefore likely not or only rarely preserved. However, analyzed inclusions in a large garnet porphyroblast, which is heavily broken and partially replaced by hornblende (Fig. S6a), revealed ca. 32–36 mol. % jadeite component (Fig. S6a, b). The retrogression of the eclogites is not restricted to the described modification of the peak minerals but affected the whole rock fabric and mineral content. The polished hand specimen (Fig. 5a) shows such late-stage veins and small-scale shear zones that developed nearly everywhere during amphibolite-facies overprinting of the eclogites. These shear zones consist mainly of a fine-grained recrystallized plagioclase and hornblende matrix surrounding garnet and exsolved omphacite porphyroclasts (Fig. 5c,d,e). The porphyroclasts partly survived the late-stage reworking attesting to the earlier high-P stage of the retrogressed eclogites.

To decipher the prograde subduction *P-T* evolution of the eclogites, we selected a sample of N-MORB chemistry (T69-12; Fig. 6; Table S1 and S2), in which garnet shows a preserved growth zoning (Fig. 6a,b), a texturally recognizable inclusion-rich inner core (thus contrasting to the inclusion-poor outer core; Fig. 6a, c) and only minor late-stage rehydration, evidenced by local hornblende rims at omphacite grains. Some rare hornblende grains of the matrix are texturally of ambiguous nature. If these formed already during the prograde evolution, they represent only minor relicts. The inclusion assemblage in garnet cores, with common titanite in addition to Qz, Rt, Omp, Hbl, Czo (Fig. 6a,c), is absent in the matrix and thus reflects the prograde growth history. In the outer parts of the inclusion-rich core, rutile is mantled by a reaction-rim of titanite and omphacite inclusions occur outside the inclusion rich core (Fig. 6a, c). The chemical growth zoning of garnet is overprinted at the rim by a retrograde near-rim zonation due to the formation of a late-stage Di-Pl corona (Fig. 6a, b, c). The growth zonation in the core is characterized by decreasing XFe (Fe/(Fe + Mg) from 0.82 to a minimum of 0.66 and decreasing spessartine contents (from 5 to 1 mol.%) at constant Grs contents (36 mol.%). Grossular content decreases only in the outer core to 26 mol.% at the minimum XFe (0.66) and the maximum preserved pyrope content of 24 mol.% near the rim. At the outermost preserved growth zoning (at min. XFe) the pyrope content abruptly decreases, whereas the almandine content and XFe increases, which is attributed to exhumation-related corona formation that erased the peak composition at the garnet rim.

The eclogite T69-12 (chemistry in Tables S1 and S2) was modeled in the system Na_2O-CaO-FeO-MgO-Al_2O_3-SiO_2-H_2O-TiO_2-Fe_2O_3-MnO. Thermodynamic gridded free energy minimization computation was performed with Perple_X (Connolly, 2009; version 6.9.1; source update June 2021), using the internally consistent thermodynamic database of Holland and Powell (2011; update: "hp633ver.dat"). Further details on the modeling are given in the Supplementary material. By combining the prograde zoning pattern with the garnet inclusion textures, we constructed the prograde *P-T* path in the modeled phase diagram (Fig. 6d). The prograde *P-T* path touches the stability field for titanite + rutile (inclusions in garnet core) in addition to garnet and glaucophane at T < 400 °C. At 12–13 kbar a field is entered where titanite is growing at the expense of rutile, which explains the titanite rims around rutile. The path is also in accordance with omphacite inclusions in the outer core of garnet (Fig. 6a). At T > 600 °C rutile is stabilized again and the isopleths of XMg and XGrs are steeply crossed in accordance with the observed strong zoning pattern in the outer core (Fig. 6b). Information about the prograde path ends when the lowest preserved XFe of garnet is reached and both grossular and pyrope are at about 24 mol.%, which is at about 17–18 kbar and 750–800 °C as indicated by intersecting isopleths (Fig. 6d; Table S3). The original rim composition (now resorbed) likely would have pointed to even higher conditions, where the rock was possibly totally dehydrated. However, this sample is not suitable for deducing peak conditions due to retrograde corona formation. Instead, we deduce from the retrograde zoning near the garnet rim the exhumation history, assuming a slight rehydration during retrogression in accordance with textures of retrograde hornblende around omphacite. Assuming equilibrium of the retrograde garnet rims with the rock matrix, the intersecting isopleths for grossular (XGrs 0.24–0.20) and XMg (0.31–0.28) (Fig. 6e; Table S3) of the rims indicate some cooling during high temperature exhumation (800–700 °C). The late-stage corona consists only of Di + Pl and contains no orthopyroxene. This restricts the near-isothermal exhumation to 7–8 kbar, as orthopyroxene would have formed below that (Fig. 6e). The pressures during the late-stage exhumation agree with the formation of late-stage sillimanite in the enveloping metapelites of the Lower Isimani Group (Fig. 2).

5.2. Petrology of boninitic Opx-eclogites and Ky-eclogite

Boninitic Opx-eclogites were not recognized as such in the field and

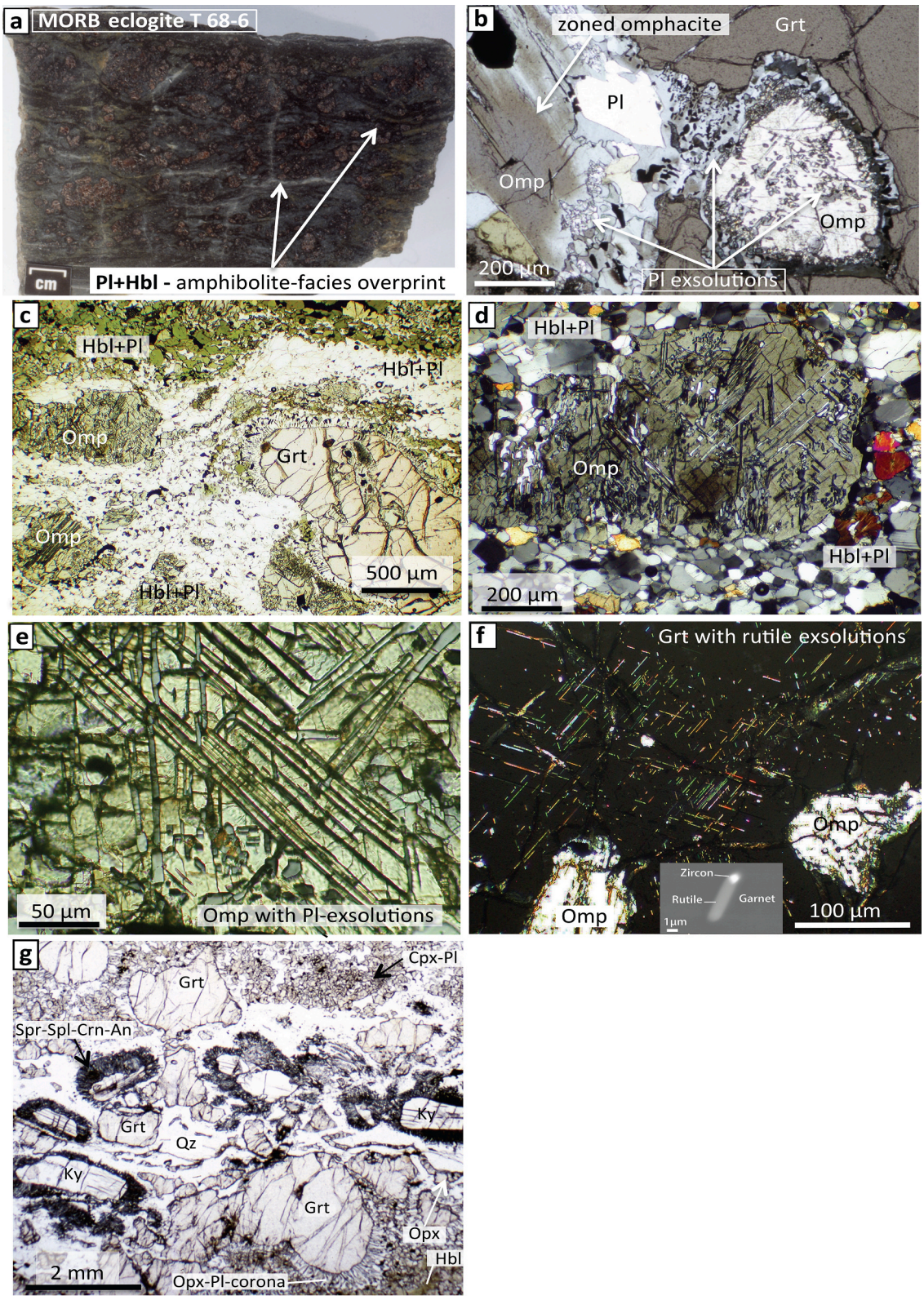

Fig. 5. Textures of eclogite with MORB chemistry (T68-6; a–f)) and Ky-eclogite (B29; g) (loc. in Fig. 2): (a) Hand specimen showing late-stage amphibolite-facies shear zones and veins containing fine-grained recrystallized plagioclase and hornblende (cf. Fig. 5c). (b) Garnet porphyroclast with inclusion of an omphacite grain, which is zoned due to plagioclase ‚exsolution' during retrogression. (c) Garnet and exsolved omphacite porphyroclasts surrounded by amphibolite-facies shear zones, which consist of recrystallized fine-grained Pl+Hbl. (d) Omphacite porphyroclast with plagioclase ‚exsolution lamellae', embedded in late-stage amphibolite-facies shear zones. (e) Omphacite with crystallographically oriented ‚exsolution lamellae' of plagioclase in four directions. (f) Garnet porphyroclast with omphacite inclusions and exsolved rutile needles, which include tiny zircon grains (inset). (g) Ky-eclogite (B29). Ky is concentrated in thin layers. Ky is surrounded by Spr-Spl-Crn-An symplectites. Garnet is always surrounded by coronas of Opx-Pl symplectites.

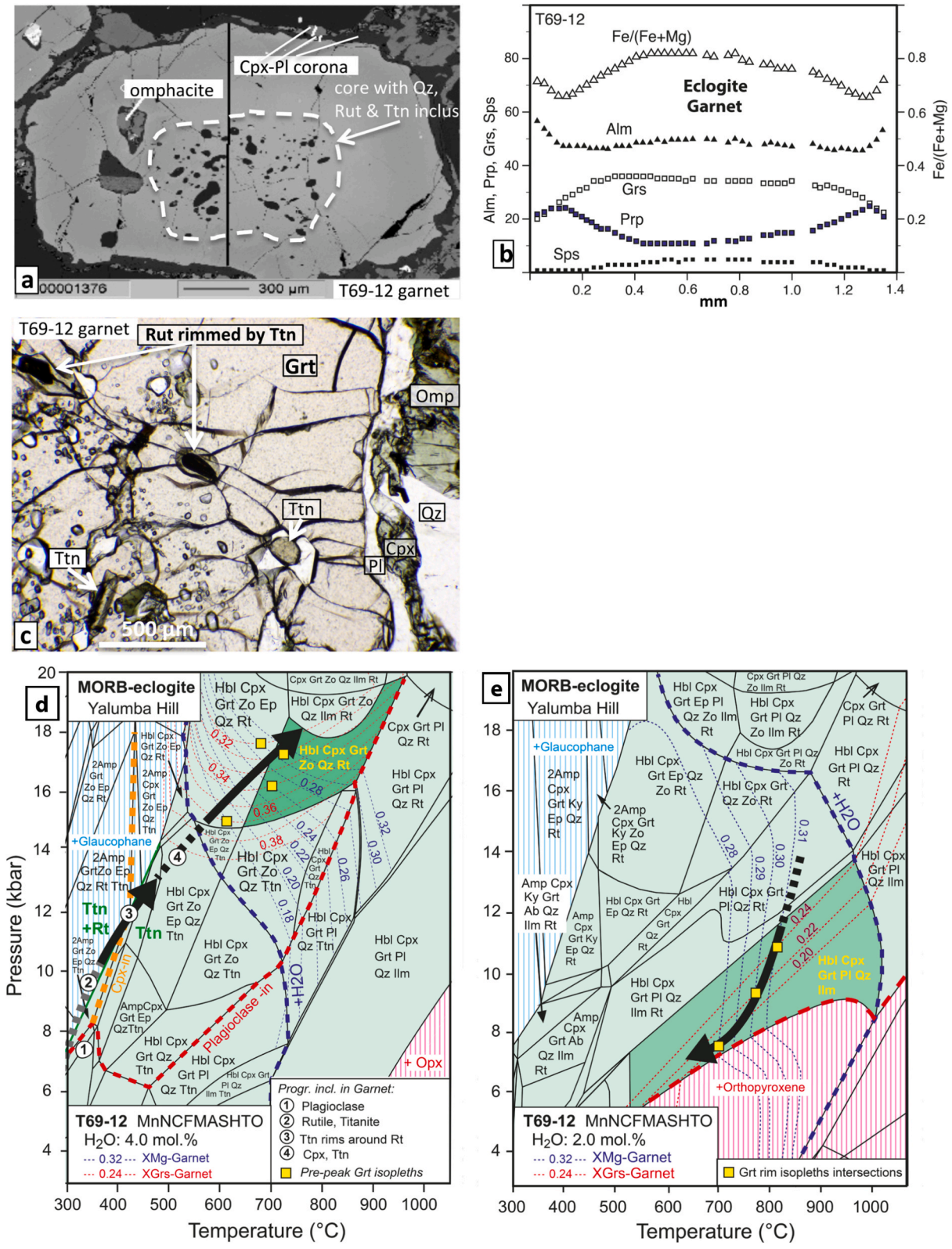

Fig. 6. (a) BSE picture of garnet in T69-12 (eclogite of MORB-chemistry). (b) The preserved growth zoning points to a short-lived metamorphism (cf. zonation in metapelite garnet of Lower Isimani Group; Fig. 11a, b). Garnet core contains numerous inclusions of prograde titanite. Ttn is absent in the matrix (not part of peak-assemblage). Near-rim zonation is due to formation of a late-stage Cpx-Pl corona. (c) Rutile inclusions in garnet core are mantled by titanite rims, which support the modeled prograde *P-T* path (in d). (d) Pseudosection for eclogite T69-12 with preserved growth zonation of garnet. Peak composition at rim is not preserved due to the formation of the late-stage corona. The early prograde path enters the eclogite stability field at about 12 kbar, when Ttn is overgrowing Rt (cf. c). The late-stage prograde path crosses perpendicular the Grs- and XMg-isopleths (cf. strong zonation of outer core in b). (e) The retrograde path of eclogite T69-12 is modeled with the near-rim compositions (cf. b). The path is in accordance with the formation of Cpx-Pl-Hbl-Ilm coronas around Grt and the lack of Opx in these coronas.

were found only at the western side of Yalumba Hill (Fig. 2a at T68). The samples were collected mainly because several of them showed lithological banding and a mylonitic fabric on the weathered surface but are otherwise fine-grained black rocks, in which minerals are hardly recognizable. As the boninitic rocks are poor in Na_2O (0.9–1.0 wt%; Table S1), omphacite with high jadeite contents could not form during eclogite-facies metamorphism (10–16 mol.% jadeite; Table S4-Cpx). They are thus not eclogites sensu stricto. Nevertheless, clinopyroxene in these rocks shows exsolutions of plagioclase lamellae that are crystallographically preferred oriented (Fig. 7e,f) and garnet shows exsolution of rutile needles and is surrounded by late-stage coronas consisting of Opx-Pl ± Hbl (Fig. 7e,f). Garnet contains inclusions of orthopyroxene,

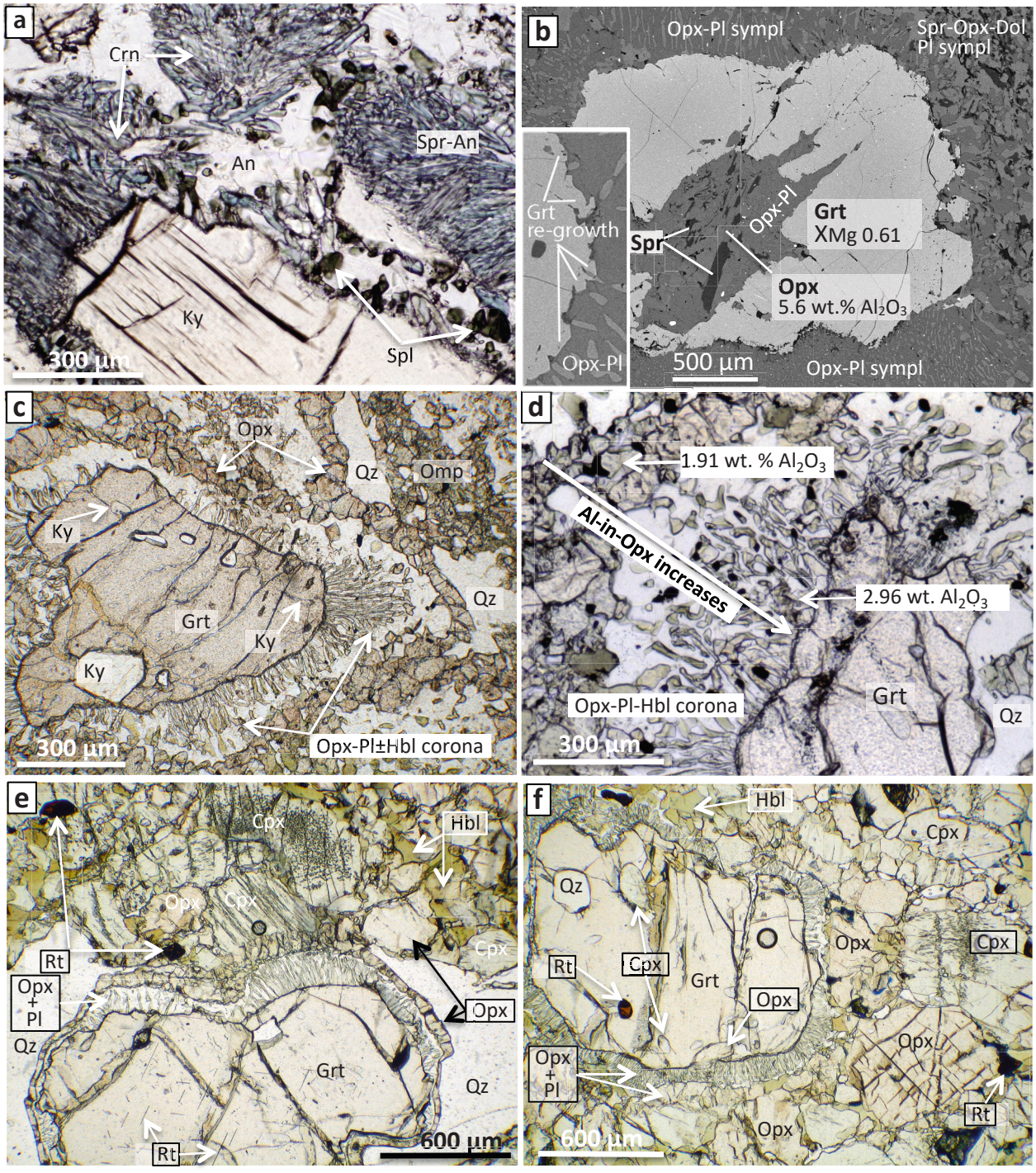

Fig. 7. Textures of Ky-eclogite B29 (a, c, d), Opx-eclogites T68-7 (e, f) and T69-3 (b), which underpin the high-T during exhumation of the eclogites. (a) Corona minerals around Ky are Spr, Crn, Spl and An. (b) Magnesian garnet (Pyrop 52) is replaced by symplectites of sapphirine, aluminous orthopyroxene and plagioclase ±dolomite. Inset shows late-stage Grt re-growth at the expense of exhumation-related Opx-Pl symplectites (cf. Fig. S7). (c) Garnet with rounded kyanite inclusions (B29) is surrounded by a concentrically layered corona of orthopyroxene (outward) and Opx-Pl±Hbl symplectite (inward). (d) Symplectitic corona (Opx-Pl-Hbl) around Grt (B29), in which Al in Opx of the corona increases towards the relict garnet. (e) Garnet in Opx-eclogite T68-7 is surrounded by an Opx-Pl corona and contains exsolved rutile needles. Late-stage Hbl occurs only in interstices between pyroxenes. Qz forms irregular lenses. (f) Garnet porphyroblast with Opx, Omp and Rt inclusions is surrounded by an Opx-Pl corona. The matrix consists of in Opx-Cpx-Rt, Hbl occurs in interstices.

clinopyroxene and rutile, whereas hornblende and quartz occurs only in the matrix (Fig. 7e,f). Some hornblende forms rims at clinopyroxene grains and occurs in late-stage coronas around garnet and is then obviously a retrograde formation. However, the textures are not unequivocal and do not allow to deduce if hornblende was stable at peak. Most orthopyroxene grains of the matrix and as inclusion in garnet are poor in alumina (about 1.6–1.9 wt% Al_2O_3; Table S4-Opx) and Mg-rich (XMg 0.80). Quartz was not found as inclusion in any other mineral

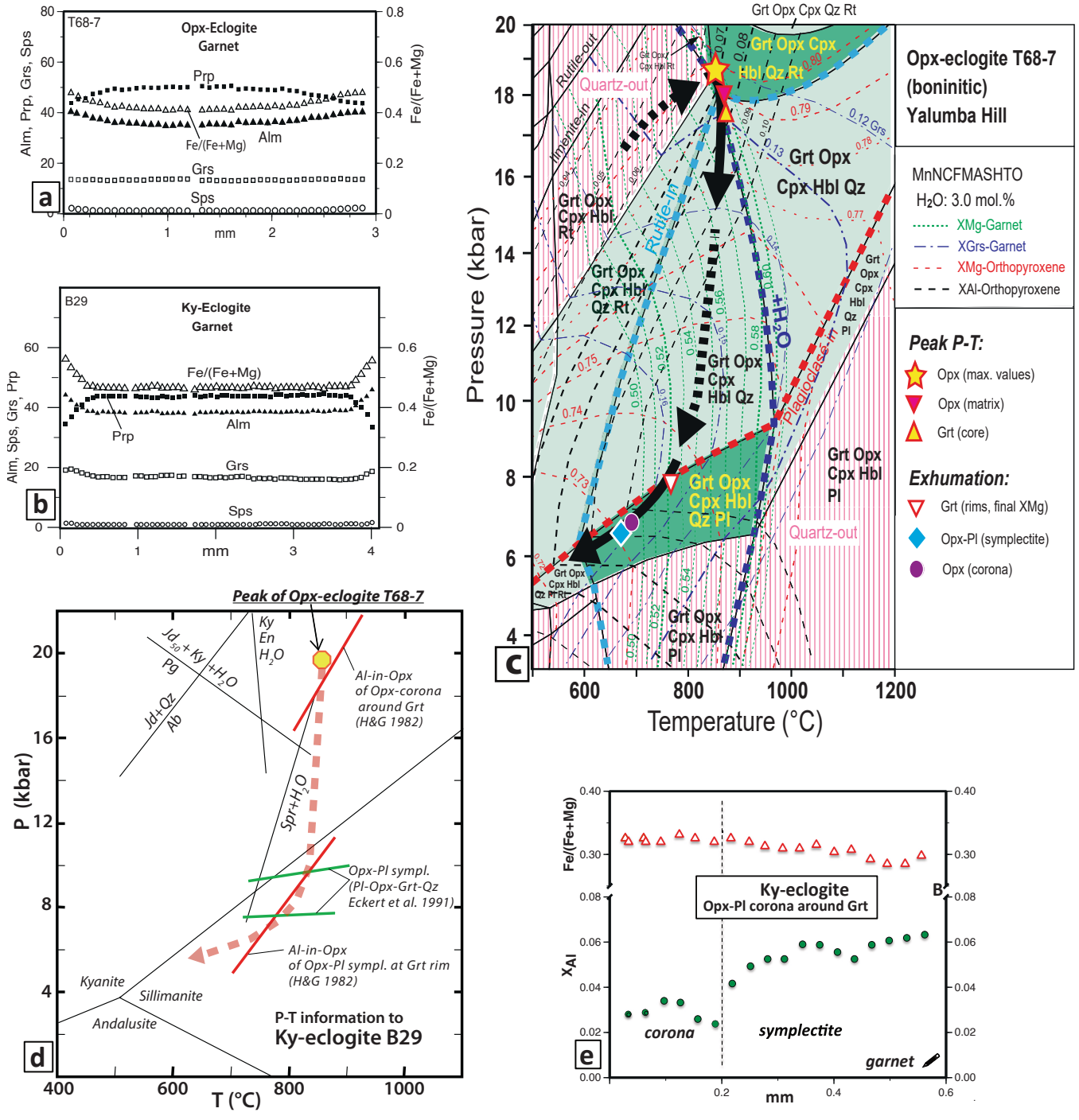

Fig. 8. (a) Garnet zonation pattern in Mg-rich and Ca-poor Opx-eclogite (T68-7) and in (b) Ky-eclogite (B29): homogenous cores and near-rim zonation, due to corona formation (Opx-Pl±Hbl). Core composition was used to deduce peak-metamorphic conditions. (c) Pseudosection for Opx-eclogite T68-7, contoured for XMg and XGrs of Grt, XMg and XAl of Opx. Peak composition of garnet (Tab. S4: XMg 0.59, XGrs 0.13) and orthopyroxene (XMg 0.80, XAl 0.07-0.08) point to 850-880 °C at about 18-19 kbar. Symplectitic Opx-Pl coronas (XMg 0.73; XAl 0.10-0.09) coexisting with Grt rim were formed at P <8 kbar at ca. 750 °C (granulite facies). (d) *P-T* diagram with conditions for different stages of the Ky-eclogite B29. Relevant mineral stability fields for reference: Jadeite and paragonite equilibria after Holland (1979, 1980), sapphirine+H_2O stability after Ackermand et al. (1975), Ky-En-H_2O stability taken from Simon & Chopin (2001). Al-poor Opx of the outer corona (cf. e and Fig. 7d) define near-peak *P-T* (Harley and Green, 1982), whereas increasing Al contents in Opx of the inner symplectites (cf. e; Fig. 8e) point to high-T exhumation. Opx-Pl symplectites and Grt rim formed at granulite-facies conditions (Grt-Opx-Pl-Qz assemblage; Eckert et al., 1991). (e) XMg and XAl (=Al/2) in late-stage Opx coronas and Opx-Pl-Hbl symplectites around garnet in Ky-eclogite B29. The increase of XAl in Opx of symplectites is attributed to high T during decompression (calculated after Harley & Green, 1982).

and is not homogenously distributed in the matrix but rather forms lenses or layers (Fig. 7e). The Opx-eclogite T68-2 with only few Qz-lenses also contains, in addition to Opx-Pl ± Hbl coronas around garnet, sapphirine (XMg 90), which coexists with late-stage orthopyroxene (XMg 0.85) that contains up to 5.6 wt% Al_2O_3. The Spr-Opx assemblage replaces the core of extreme Mg-rich garnet containing 53 mol. % pyrope (XMg 0.61; Fig. 7b; Table S4-Opx, −Grt, −Spr), reflecting the high temperature during its late-stage formation. This interpretation is in agreement with the common Opx-Pl ± Hbl coronas around garnet in Opx-eclogites (Fig. 7c–f) and Spr-Spl-Crn-An coronas around kyanite in the Ky-eclogite B29 (Fig. 5g, Fig. 7a), which are all attributed to a granulite-facies stage during exhumation. However, subsequent to the formation of granulite-facies Opx-Pl symplectites at the expense of garnet, garnet grew again, which resulted in very thin seams of new poikilitic garnet that includes the immediately adjoining symplectite phases resulting in the ragged appearance of the garnet grain bounderies (inset in Fig. 7b; Fig. S8). This re-grown garnet, which overgrows the decompression-related symplectites, is not restricted to the boninitic eclogites but also developed in the Ky-eclogite B29 (see below) and some eclogite samples of ocean floor basalt chemistry. Similar reaction textures are known from granulites (Schenk, 1984; Schenk et al., 2002; Karmakar and Schenk, 2015; Cartwright and Barnicoat, 1987) and are attributed to the reversal of the reaction Grt + Cpx + Qz ↔Opx + Pl during near-isobaric cooling that followed a first uplift of the eclogites or granulites to intermediate crustal levels.

Garnet of the modeled Opx-eclogite (T68-7) and the Ky-bearing eclogite (B29) is pyrope rich (50 and 45 mol.%; Table S4 and S5; Fig. 8a,b) but poor in grossular (13 and 16 mol.% in core) and displays unzoned cores. As growth zoning is not preserved due to homogenization at peak temperatures, the garnet contrasts with the growth-zoned grossular-rich garnet (36 mol.% Grs; Fig. 6b) of the eclogites of MORB chemistry. The ubiquitous late-stage Opx-Pl ± Hbl coronas that replace garnet rims produced a retrograde zoning in garnet, which resulted in increasing XFe and grossular content. The very low spessartine content slightly increases at the outermost rim. The erased growth zoning due to homogenization of garnet does not enable to deduce the prograde subduction history of the Opx-eclogites. Instead, the well homogenized unzoned core compositions of garnet and pyroxenes in the assemblage Opx-Cpx-Grt-Hbl-Rt-Qz are used for estimation of peak metamorphic conditions that are complementary to information obtained from eclogites with a chemical affinity to ocean-floor basalts.

Thermodynamic modeling of the non-mylonitic granoblastic Opx-eclogite T68-7 (Table S1 and S2) was performed with Perple_X in the system Na_2O-CaO-FeO-MgO-Al_2O_3-SiO_2-H_2O-TiO_2-Fe_2O_3-MnO (Fig. 8c) like the eclogite (T69-12) of MORB chemistry (modeling details in Supplementary material). In contrast, we applied conventional thermobarometry for the deduction of the metamorphic history of the Ky-eclogite (B29; Fig. 8d), as this rock contains some scapolite in several thin mm-scale layers, which we interpret as the product of metasomatism, i. e., the rock experienced a change in chemistry at some stage of its evolution.

If we assume a similar prograde *P-T* evolution for the Opx-eclogite T68-7 as for the eclogite T69-12 (MORB), the prograde stage passed through the stability field of Grt-Opx-Cpx-Hbl-Rt (without quartz). In the stability field of the Qz-bearing assemblage the isopleths of garnet (XGrs 0.13; XMg 0.59) and orthopyroxene (XMg 0.80; XAl 0.07–0.08) are intersecting, pointing to peak conditions near 850–880 °C at 18–19 kbar (Fig. 8c; Table S4-Grt-Opx). Information about the exhumation history of the Opx-eclogite (T68-7) can be obtained from the composition of the granulite-facies corona minerals, which formed below ca. 8–9 kbar, where plagioclase is stabilized. Isopleths of late-stage minerals (Grt rim: XMg 0.52, XGrs 0.14; orthopyroxene of symplectites (XAl 0.09–0.10) define the granulite-facies stage at ca. 6–7 kbar between 700 and 800 °C (Fig. 8c). However, the XMg of orthopyroxene in symplectite (0.77) at the garnet rim is too high and the 'fitting' XMg of the corona orthopyroxene (XMg 0.73; Table S4) is unlikely to be in equilibrium with the later formed garnet rim. A further isothermal decompression below 5–6 kbar would have led to the formation of clinopyroxene in the corona around garnet, which is not the case. The late-stage corona assemblage in the Opx-eclogite thus indicates that the near-isothermal exhumation did not proceed to pressures below about 5 kbar (Fig. 8c), in agreement with results for the modeled eclogite of MORB chemistry (Fig. 6e).

The metasomatized scapolite-bearing Ky-eclogite B29 preserves porphyroblastic garnet that is unzoned in the core, Ca-poor (17 mol.% Grs) and Mg rich (XMg ca. 0.53; 44 mol.% Py) pointing to its chemical similarity to the boninitic Opx-eclogites (Fig. 8a,b; Fig. 2b; Table S5-Grt). Garnet contains numerous inclusions of rounded kyanite grains in certain mm-scale layers, indicating a kyanite-consuming garnet growth (Fig. 7c). Orthopyroxene and omphacite do not occur as inclusions. It is ambiguous whether matrix-orthopyroxene, which is restricted to mm-scale Hbl-rich shear zones, is of prograde nature or formed during retrogression in these shear zones from common late-stage orthopyroxene coronas around garnet that have similar Al_2O_3 contents (ca. 2.0–2.2 wt%). Garnet of B29 is surrounded by well-developed Opx-Pl ± Hbl coronas, in which the symplectitic orthopyroxene becomes more aluminous towards the relict garnet porphyroblast (from ca. 1.3 to ca. 3.0 wt% Al_2O_3; Fig. 7d and Fig. 8e; Table S5-Opx). This textural observation in combination with mineral chemical data allow the deduction of the near-peak and the retrograde *P-T* evolution of the rock based on the changing Al-content of orthopyroxene grains that formed during different exhumation stages: At peak temperatures of ca. 850–880 °C (cf. Opx-eclogite T68-7; Fig. 8d) the low Al-content in the early formed Opx-corona (1.3 wt% Al_2O_3; Fig. 8e) point to near-peak pressures of 18 kbar (Harley and Green, 1982), whereas the higher Al-content of later formed orthopyroxene in symplectites near the relict garnet (ca. 3.0 wt% Al_2O_3) points to ca. 8 kbar at 800 °C. The pressure of the corona formation stage has been estimated with the Pl-Opx-Grt-Qz barometer (Eckert et al., 1991) to about 8–10 kbar (Fig. 8d), in agreement with thermodynamic modeling for the corona stage of the Opx-eclogite T68-7 (Fig. 8c). Kyanite porphyroblasts are surrounded by Spr-An-Spl-Crn bearing assemblages (Fig. 7a) that formed during high-T exhumation within the stability fields of sapphirine +H_2O, Opx-Ky-H_2O and Omp-Ky-H_2O, which are shown for reference in Fig. 8d. The late-stage sapphirine (XMg 0.20) is chemically similar (more aluminous than the 7:9:3 (Mg:Al:Si) composition; Table S5-Spr) to that of other reported sapphirine bearing coronas around kyanite in decompressed Ky-eclogites from the Rodope zone of the Alps or the Sweconorwegian orogen (Liati and Seidel, 1994; Möller, 1999). Subsequent to the ubiquitous granulite-facies corona formation, the reaction history of the Ky-eclogite was followed by a re-growth of garnet at the expense of the symplectitic corona minerals (Opx + Pl; inset of Fig. 7b; Fig. S8), which led to the formation of poikilitic garnet seams and rugged grain boundaries. This texture is attributed to near-isobaric cooling at depth, which again stabilized the HP granulite-facies assemblage Grt-Cpx-Qz in the sense of Green and Ringwood (1967).

5.3. *Exhumation-related mylonites of boninitic (Opx-eclogites) and of felsic compositions*

Information about the high-T exhumation history of the subducted slab that we obtained from pseudosection modeling can be complemented by petrographic observations and mineral chemical data from mylonites that formed during the exhumation process. The protomylonites described here form m-scale shear zones within the eclogite outcrops and blocks at the western side of Yalumba Hill (T68; Fig. 2). Our restricted collection of mylonites includes low-Si boninitic and felsic compositions (Fig. 9). The boninitic mylonites are banded in the cm-scale and consist of alternating Opx-dominated and Cpx-dominated layers (Fig. 9a,c; Fig. S9a). Both type of layers contain the same mineral assemblage consisting mainly of Opx-Cpx-Grt in addition to some minor Pl-Rt-Hbl and traces of late-stage kyanite and spinel in coronas

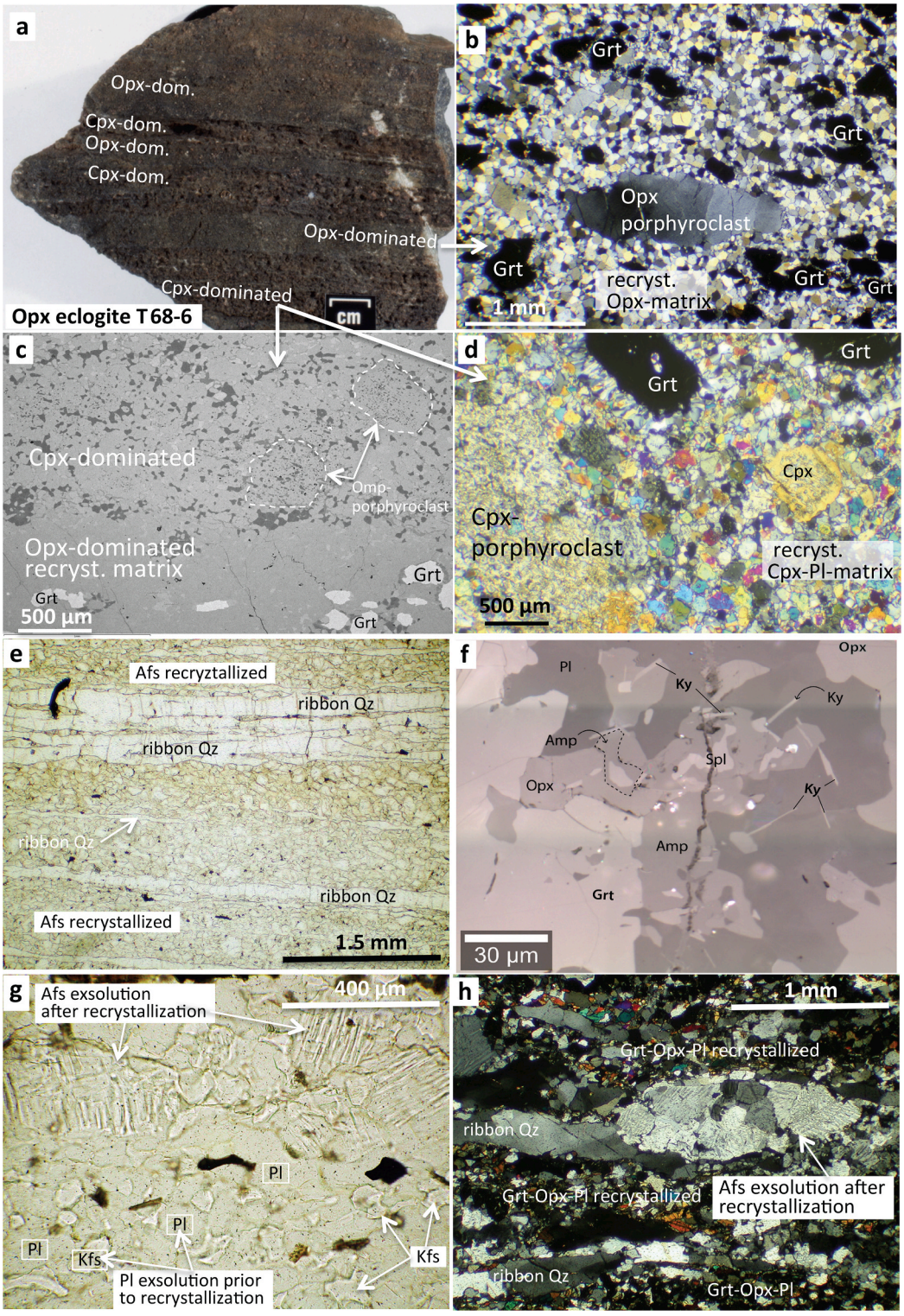

Fig. 9. Textures of mylonites of eclogitic (a–d; f) and felsic compositions (e,g,h) from Yalumba Hill, which reflect high-T deformation in shear zones during eclogite exhumation. (a) Handspecimen of layered Opx-eclogite (T68-7) with Opx-dominated and Cpx-dominated layers (cf. Fig. S8). (b) and (d) Microphotograph and (c) BSE image of layered mylonite. Porphyroclasts of Opx, Cpx and fragments of garnet in a fine-grained recrystallized matrix. The Cpx-dominated layer (d) displays former omphacite porphyroclasts sieved with exsolved plagioclase patches. The recrystallized matrix contains Cpx and Pl as separated grains pointing to deformation after exsolution, i.e. below the omphacite-diopside solvus. (e, g, h) Textures of felsic ultra-mylonites (T68-4; Grt-Cpx-Opx-Afs-Pl-Qz-Rt). (e) Ribbon quartz alternating with fine-grained feldspar layers. (f) Symplectitic corona (Opx-Pl-Ky-Spl-Hbl) between Grt porphyroclast and recrystallized Opx matrix of protomylonitic Opx-eclogite (T69-2). The newly formed Ky needles constrain the pressure during the preceding high-T mylonitization (cf. Fig. S8c–e). (g) Recrystallized grains of Afs showing exsolution after recrystallization. The finer-grained layer with separated grains of Kfs and Pl (lower part of picture) recrystallized after exsolution of antiperthite. (h) Mesoperthite porphyroclast in a band of ribbon quartz recrystallized prior to exsolution (cooling), which indicates high temperatures during deformation.

around garnet porphyroclasts (Fig. 9f). The Opx-dominated layers consist mainly of fine-grained recrystallized orthopyroxene matrix grains (60–80 μm in diameter), which surround the orthopyroxene porphyroclasts (1–2 mm) displaying wavy extinction (Fig. 9b). Some of these orthopyroxene grains are mantled porphyroclasts. Garnet commonly contains orthopyroxene inclusions and forms irregular to ellipsoidal fragments, which are embedded in a recrystallized orthopyroxene matrix (Fig. 9b,c; Fig. S9b). These garnet fragments seem to be formed from larger porphyroclasts during the dynamic recrystallization of the orthopyroxene matrix. Some of the garnet fragments are surrounded, mainly in the pressure shadows, by tiny Opx-Pl ± Hbl ± Ky-Spl coronas (Fig. 9f) indicating that decompression in the kyanite stability field was still in progress during and after the mylonitization process. The tiny kyanite needles and spinel have been determined by Raman spectrometry (S9c, d, e). The orthopyroxene composition in the recrystallized matrix is like that of the orthopyroxene porphyroclasts (XMg 0.82; ca. 1.8–2.0 wt % Al_2O_3), with a tendency to slightly higher alumina contents in the recrystallized grains (ca. 2.0–2.2 wt % Al_2O_3) at the same high XMg (0.82) as the porphyroclasts. Garnet is very rich in pyrope (XPrp 0.52 at XMg 0.60) and thus similar to garnet of the non-mylonitic Opx-eclogites. The textures indicate dynamic recrystallization of orthopyroxene at granulite-facies temperatures. In contrast, garnet at the same event displays brittle deformation, pointing to high strain rates during exhumation.

The Cpx-dominated mylonite layers (Fig. 9a,c,d) are coarser grained than the Opx-dominated layers and contain preserved larger garnet porphyroclasts, which are surrounded by Opx-Pl ± Hbl coronas (Fig. 9d; Fig. S9a). Relict clinopyroxene porphyroclasts with up to 8 mol.% preserved jadeite component are quite common and contain numerous 'exsolution' blebs of plagioclase (ca. An30). Clinopyroxene and plagioclase form separate grains in the recrystallized mylonite matrix between the porphyroclasts (Fig. 9c,d). We interpret this texture as the result of breakdown of the precursor omphacite (i.e., Omp => Di + Pl, the Pl-'exsolution' in Omp) that was already in progress during the syn-decompression mylonitization. On the other hand, the mylonitization did not destroy the well-preserved coronas around the garnet porphyroclasts, implying ongoing decompression after mylonitization (Fig. 9d, f; Fig. S9a, d).

The associated felsic mylonites are striped rocks of andesitic to rhyolitic composition (TAS diagram in Fig. S4). They consist mainly of Qz-Pl-Kfs dominated layers and intercalated thin bands enriched in mafic minerals (mainly Grt, Opx, Cpx, some Hbl and Bt). Within the felsic layers quartz forms large ribbons, which alternate with feldspar-dominated layers (Fig. 9e). Within the latter coarser grained layers and extremely fine-grained layers can be distinguished (Fig. 9g, lower part). The coarser grained layers consist of recrystallized mesoperthitic grains, which display exsolution lamellae. This points to high temperatures during recrystallization above the critical alkali solvus, as the grains exsolved (cooled) only after the recrystallization. In contrast, the finer-grained layers of this mylonite show separate grains of plagioclase and K-feldspar, pointing to exsolution of the coexisting antiperthitic plagioclase prior to recrystallization (Fig. 9g). Similar features are seen in mylonites of intermediate composition, where relict alkali feldspar porphyroclasts recrystallized prior to exsolution, indicating high temperatures during deformation (Fig. 9h).

In summary, textures and mineral chemistry of exhumation-related mylonites of mafic and felsic compositions associated with the eclogites of Yalumba Hill attest to high temperature deformation processes (granulite facies: ca. 800 °C at >10–12 kbar) during ongoing exhumation of the eclogites. Recrystallization of exsolved omphacite characterizes the mylonitization as a post peak-pressure process below the omphacite-diopside solvus. The formation of late-stage kyanite after mylonitization (in coronas between garnet porphyroclast and recrystallized Opx-matrix) represents a low-pressure bracket for the mylonitization. The high-T and high-P information obtained from the mylonites agrees with the information obtained from petrological phase diagram modeling.

5.4. Petrology of Grt-Ky-Bt gneisses of the Lower Isimani Group

The eclogite belt, which stretches from Yalumba Hill in the NE to Igula in the SW (Fig. 1b, Fig. 2a), is surrounded by gneisses of the Lower Isimani Group. Among these Grt-Ky bearing metapelites are the most common rock type. At Yalumba Hill, metapelitic gneisses are associated and intercalated with the eclogites (Meinhold and Ott, 1993). We have investigated many samples of these metapelites between Yalumba Hill and Igula (up to Loc. T100-93 in the SW; Fig. 2a). The petrographic observations suggest a common evolution as the mineral assemblages are very similar along the belt and include Grt-Bt-Ky-Pl-Qz ± Kfs ± Ms-Rt-Ilm-Zrc-Mnz-Ap. In addition, sillimanite is found as a common late-stage mineral (Fig. 2a; Fig. 10d,f) and staurolite as a rare prograde relict, mostly included in garnet or kyanite. Some samples without K-feldspar contain late-stage hornblende.

Garnet is mostly porphyroblastic reaching 2 cm in diameter in some rocks (Fig. 10a) and often includes all minerals that occur also in the matrix: Kyanite, rutile, ilmenite, biotite, feldspars and quartz. In some cases, the porphyroblasts are euhedral and confined by perfect crystal faces. The inclusions are in some samples extremely rich in layers that cross the porphyroblasts as straight bands indicating a lack of rotation during the growth of the porphyroblasts (Fig. 10a,b). This contrasts with the highly deformed and recrystallized matrix, in which kyanite, antiperthitic plagioclase, K-feldspar and biotite porphyroclasts show wavy extinction. These porphyroclasts are embedded in a fine-grained matrix of recrystallized Qz-Fsp-Bt grains, which form bands between the late-stage rotated garnet porphyroblasts (Fig. 10c). The late-stage deformation has led to partial recrystallization of kyanite porphyroblasts, in which the recrystallized smaller grains show sutured grain boundaries (Fig. 10e). This texture serves as an evidence for late-stage deformation in the kyanite stability field. Although the matrix is strongly deformed, garnet porphyroblasts are locally surrounded by a preserved thin corona of Ky-Pl-Qz-Bt, implying that retrogression started in the kyanite stability field (Fig. 10a). Several samples contain mm- to cm-sized kyanite porphyroblasts, which are partially replaced or overgrown by sillimanite (Fig. 10d,f). This texture gives important information for the late-stage *P-T* evolution of the whole Lower Isimani Group (Fig. 2a).

We have selected two coarse-grained metapelites for phase diagram modeling (T69-4; Fig. 11a,c,d and T100-1-93; Fig. 11b, e), which contain cm-sized garnet porphyroblasts with preserved growth zonations. The Grt-Ky schist T69-4, which was collected at the northern slope of Yalumba Hill (Figs. 2 and 3c), is clearly not migmatitic, whereas the Grt-Ky gneiss from Igula (T100-1-93) shows leucocratic schlieren in the outcrop indicating conditions favorable for the formation of anatectic melts. As the two samples come from distant localities, they give information about regional variations in metamorphic grade along the belt. The fact that garnet growth zoning is preserved in both samples (Fig. 11a,b) points to a relatively short duration of the tectono-metamorphic event (cf. garnet zonation in eclogite, Fig. 6b). However, only *P-T* determination can clarify if eclogites and associated metasediments experienced the same subduction history or different evolutions.

Garnet of T69-4 shows a weak bell-shaped spessartine zoning in the core (Fig. 11a) and a slight Mn-increase near the rim in accordance with the presence of a thin garnet-resorbing corona (Fig. 10a). XFe is very high (0.9) in large parts of the core and sharply decreases in the outer zones to a minimum at XFe of 0.68 (Table S6). Only in the outermost rim XFe increases again (to 0.74) due to the retrograde corona formation. The grossular content is constantly high (23 mol.%) nearly throughout the grain, and drops only at the outermost rim, which is affected by retrograde processes. The zoning pattern of garnet in two analyzed Grt-Ky-Bt gneisses from Igula (T100-1-93/ T100-4-93) is in principle the same (Fig. 11b) as described for garnet of T69-4 from Yalumba Hill. However, it is less pronounced and with lower but also constant

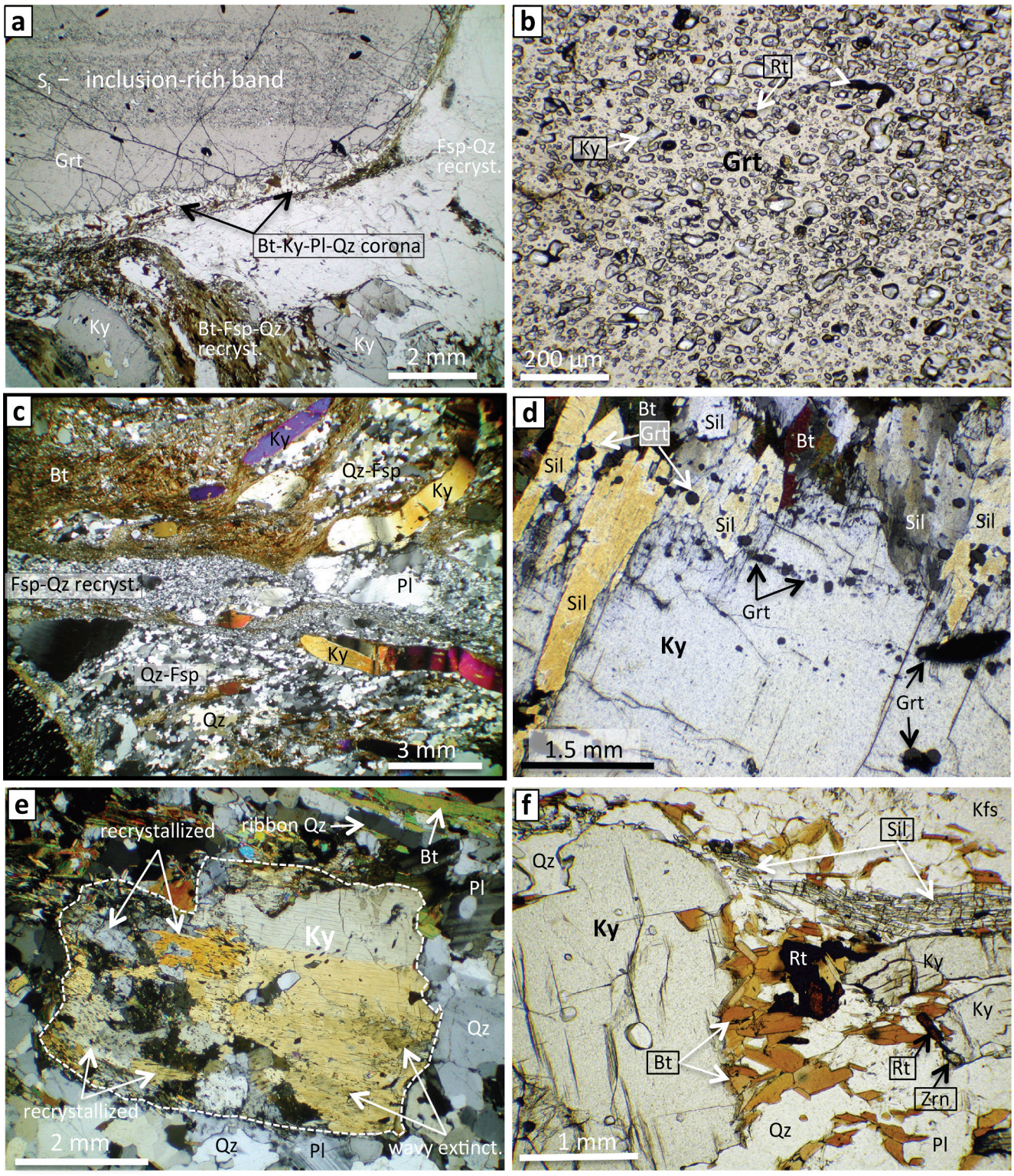

Fig. 10. Textures of high-P metapelites (Lower Isimani Group). (a) Metapelitic gneiss (T69-4, Yalumba Hill, Grt-Ky-Kfs-Bt assemblage) with 2 cm sized garnet porphyroblasts. The inclusion-rich bands (S_i) are straight throughout the whole grain. This reflects a lack of rotation during garnet growth. A thin corona of of Ky-Bt-Pl-Qz replaces the Grt rim. (c) Late-stage mylonitic deformation of the Bt-Qz-Fsp matrix points to rotation and deformation of the porphyroblasts during exhumation (T69-4). (b) Densly and homogeneously distributed fine-grained inclusions of all matrix minerals (Bt-Rut-Ilm-Ky-Kfs-Pl-Qz) within the inclusion-rich layer of (a). (c) Inhomogenous deformation of the Bt-Qz-Pl-Kfs matrix (T69-5) led to inhomogenous grain size distribution in shear zones, which surround the deformed Ky and Pl porphyroclasts. (d) Kyanite porphyroblast (T166-18) is partially replaced by late-stage coarse-grained sillimanite. Garnet inclusion trails continue into the late-stage sillimanite. (e) Kyanite porphyroclast partially recrystallized during exhumation (C182-1). (f) Kyanite porphyroclast (T100-4a-93) is surrounded by late-stage Sil and partially replaced by Bt.

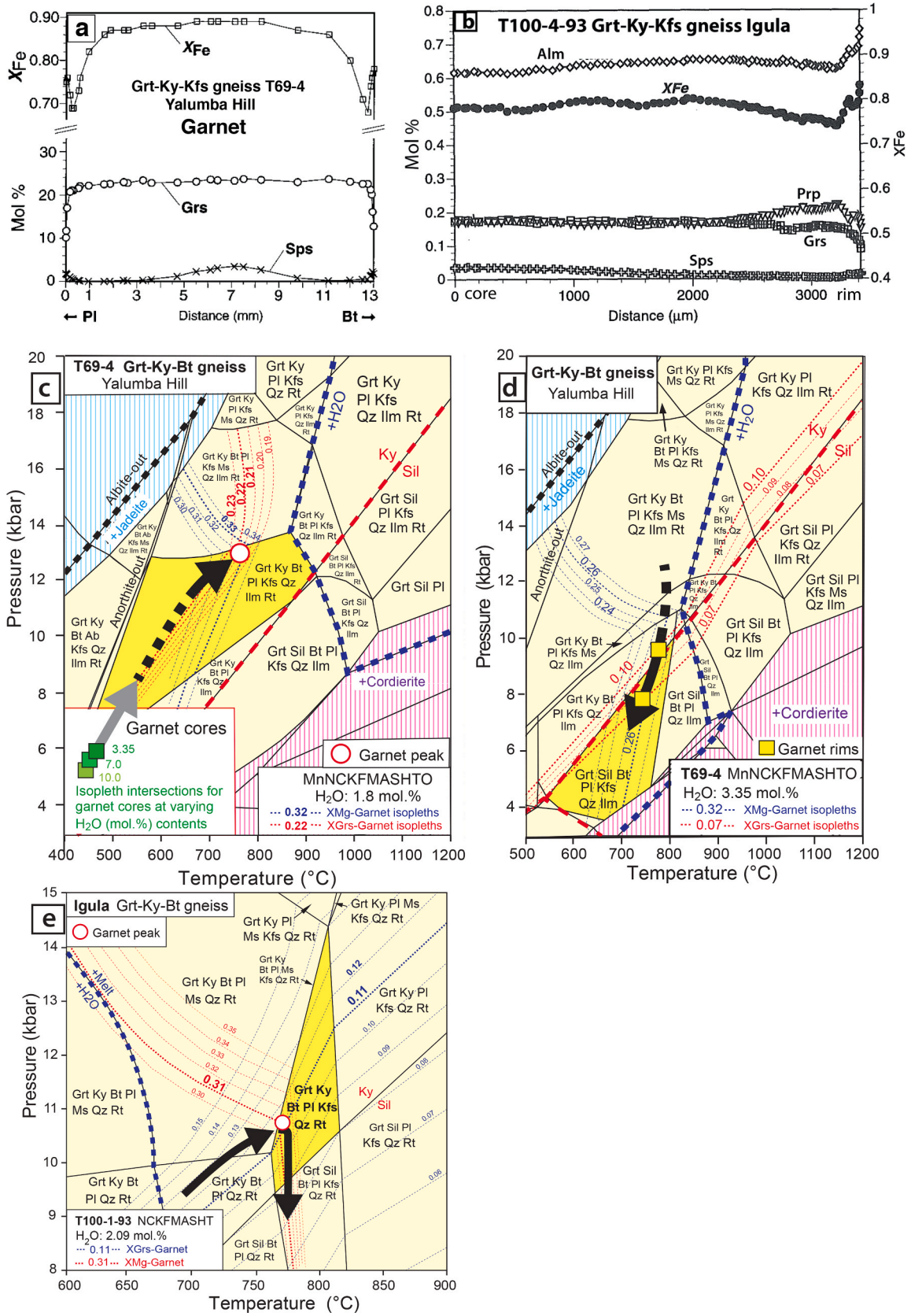

(caption on next page)

Fig. 11. Garnet zonation (a, b) and pseudosections (d, e, f) for Grt-Ky metapelites of Lower Isimani Group. (a) Preserved growth zonations in high-grade gneisses T69-4 (Yalumba Hill) and (b) T100-4-93 (Igula) point to a short-lived metamorphism. Near-rim zonation is due to the formation of a retrograde corona (cf. Fig. 10a). (c) *P-T* pseudosections for the Grt-Ky-Kfs-Bt-Pl-Kfs-Ilm-Rut bearing gneiss T69-4 (Yalumba Hill; loc. in Fig. 2), calculated in the system MnO-Na_2O-CaO-K_2O-FeO-MgO-Al_2O3-SiO_2-H_2O-TiO_2 (MnNCKFMASTO) with 1.8 mol.% H_2O. Melt is not present in this rock. The pseudosection is contoured for X_{Mg} and X_{Grs} of garnet. Inferred *P-T* path is in agreement with Ky-Bt-Rut-Ilm inclusions in Grt and the retrograde replacement of Ky by Sil (cf. Fig. 10). The decreasing XFe at near-constant XGrs constrains the late prograde path, which runs parallel to the Grs isopleths. (d) *P-T* pseudosection for T69-4 (as in c), but with 3.35 mol.% H_2O to account for retrograde biotite formation (due to water influx). The path is in agreement with textural evidence of the late-stage crossing of the Ky-Sil phase boundary and the lack of late-stage cordierite. Yellow field indicates the stability of the late-stage assemblage (Grt-Sil-Bt-Pl-Kfs-Qz-Ilm) and the yellow squares correspond to compositions of the near-rim increasing XFe in (a). (e) *P-T* pseudosection for migmatitic Grt-Ky-Kfs metapelite T100-1-93 (near Igula, loc. in Fig. 3), contured for XMg and XGrs. Bulk rock composition in Tab. S2, mineral chemical data in Tab. S6. Yellow field represents the observed peak-metamorphic assemblage. The red point marks peak-metamorphic *P-T* range inferred from mineral compositional data taken at minimum XFe values near rim.

grossular contents in the cores, which only drop near the rims (from 17 to 11 mol.%). The XFe in the core of the two samples (0.70/0.78) is much lower than in the metapelite of Yalumba Hill (0.9) and reaches minima at 0.69/0.74, before it increases again to 0.79/0.84 at the rim. Spessartine is less enriched in the core (compared to T69-4, Fig. 11a, b) and increases slightly at the rim reflecting minor garnet resorption, like in T96-4 from Yalumba Hill.

The two metapelites T69-4 and T100-1–93 were modeled with Perple_X in the system Na_2O-CaO-K_2O-FeO-MgO-Al_2O_3-SiO_2-H_2O-TiO_2-Fe_2O_3-MnO. Computed stability fields of mineral assemblages and isopleths for XGrs and XMg in garnet are plotted in Fig. 11. The peak assemblage of T69-4 (Grt-Ky-Bt-Pl-Kfs-Qz) is stable in a wide *P-T* field from 500 °C up to 900 °C. The field is restricted towards higher pressures by the stability field of a muscovite bearing assemblage, a phase that is not observed as a prograde constituent of this sample. The calculated peak conditions (red circle) require a maximum of 1.8 mol.% H_2O for equilibration at ca. 13.2 kbar and ca. 770 °C to stabilize biotite, but not muscovite, at matching XMg (0.33) and XGrs (0.22) isopleths in garnet, which is the composition of garnet at the minimum XFe that formed close to peak temperatures (Fig. 11a; Table S6). The slope of the prograde burial path is nicely constrained, as it follows the steep Grs isopleths characterizing the nearly constant grossular contents (XGrs 0.23) in the core with changing XMg. Early prograde *P-T* conditions for almandine-rich garnet cores (white rectangle in lower left of Fig. 11c) are based on intersections of XMg and XGrs isopleths for various bulk H_2O contents (green rectangles for 10, 7, and 3.35 mol.% H_2O, respectively), which reflect garnet growth during strong initial dehydration of the metasediments during greenschist-facies metamorphism. The retrograde path of T69-4 is constrained by intersecting XMg and XGrs isopleths (XMg = 0.26; XGrs = 0.10 to 0.07) in the outermost rim of garnet, which is interpreted to have equilibrated during late-stage sillimanite formation, replacing or rimming peak kyanite (Fig. 10d, f). The corresponding *P-T* path (bold black arrow in Fig. 11d) requires a bulk-system H_2O content of approximately 3.35 mol.%, i. e., some retrograde water influx in agreement with the observed growth of late-stage biotite (e.g. Fig. 10f). At lower bulk H_2O concentrations, the garnet isopleth intersections shift towards lower temperature conditions, where sillimanite is not stable. At higher bulk H_2O the garnet isopleths intersect at temperatures that would require additional retrograde heating (>800 °C) and/or plot within the stability of muscovite bearing assemblages, which are not observed.

The other modeled Grt-Ky gneiss of the Lower Isimani Group from Igula in the SW (T100-1-93 and T100-4-93: Fig. 2) has leucocratic schlieren, interpreted as anatectic melts. The XMg (0.31) and XGrs (0.11–0.12) isopleths of garnet at the minimum preserved XFe (0.69) near the rim (Table S6) point to peak metamorphism of about 770 °C at 10.7 kbar (Fig. 11e), which indicates a shallower burial depth than that for the sample from Yalumba Hill (13.2 kbar) 50 km further north. The type of *P-T* path for both samples is very similar. It starts in the kyanite stability field during garnet growth (inclusions) and follows the Grs isopleths to near peak conditions. During exhumation, the kyanite => sillimanite reaction is crossed (Fig. 10f, Fig. 11e).

5.5. Petrology of Grt-Crd-Sil granulites (nappe of high T/P belt)

Meinhold (1970) recognized the different metamorphic and lithological characters of the Upper Isimani Group compared to the adjoining Lower Isimani Group and created a new lithotectonic unit for these granulites.

All samples of our collection point to a uniform metamorphic grade and display similar textures. The peak-metamorphic mineral assemblages always include Grt-Sil-Bt-Pl-Qz, whereas cordierite and K-feldspar are missing in some samples. Additional retrograde minerals are kyanite, muscovite, chlorite and scapolite. Some garnet grains form cm-scale poikilitic porphyroblasts that are surrounded by leucocratic melt pockets, suggesting that they formed by Bt-dehydration melting. In contrast, smaller garnet porphyroblasts in the matrix contain inclusions of the surrounding matrix minerals, including sillimanite and biotite (Fig. 12b). Thus, the prograde *P-T* path with garnet growth in the sillimanite stability field contrasts to that of metapelites of the Lower Isimani Group. The most striking feature of these migmatites is their uniform protomylonitic texture, characterized by the ubiquitous presence of mantled porphyroclasts formed by plagioclase and cordierite (Fig. 12a, e), in which the recrystallized mantles of plagioclase and cordierite have similar grain sizes of about 60–80 μm (Fig. 12e). Antiperthitic plagioclase grains affected by this recrystallization show plagioclase and exsolved K-feldspar blebs as separate grains, indicating recrystallization after exsolution. Fig. 12 c and d show the same detail of a recrystallized band cutting through an antiperthitic porphyroclast under crossed polarizers (c) and with polarized light (d), to highlight the separate plagioclase and K-feldspar grains. The recrystallization temperature is constrained by the exsolution temperature of the antiperthite and by the minimum recrystallization temperatures for plagioclase (ca. 450–500 °C; Voll, 1976) pointing to a recrystallization temperature of about 550 ± 50 °C of the protomylonites. This is in accordance with the estimated minimum recrystallization temperature of cordierite, as this mineral is not stable below ca. 500–550 °C (Seifert and Schreyer, 1970).

All samples are affected by different degrees of re-hydration, evidenced by the replacements of garnet by biotite and kyanite along cracks (Fig. 13c) or by total replacements in pseudomorphs after garnet (Fig. 13d). As some pseudomorphs contain sillimanite alongside kyanite (Fig. 13d), this rehydration must have started after the peak in the sillimanite stability field and continued after the sillimanite-kyanite phase boundary had been crossed during cooling. Other garnet replacement textures also include chlorite (Fig. 13f) or scapolite next to green biotite (Fig. 13e) implying a carbonaceous component in the late-stage fluids. Similar replacement textures are also found at cordierite grains. Cordierite may be partially replaced by Sil-Bt-Qz intergrowths (Fig. 13a) and symplectites of Ky-Chl-Ms-Qz can form pseudomorphs after cordierite (Fig. 13b). The hydrous breakdown of cordierite also affected recrystallized cordierite grains, which are locally replaced by Sil-Bt intergrowths (Fig. 12e). These textures indicate that recrystallization occurred prior to the rehydration event. This interpretation is supported by hydrous replacement of recrystallized plagioclase that is overgrown by clinozoisite and white mica (Fig. 13g). The re-hydration is also observed in 2-pyroxene granulites, in which late-stage clinozoisite and calcite replace clinopyroxene and plagioclase (Fig. 13h) providing

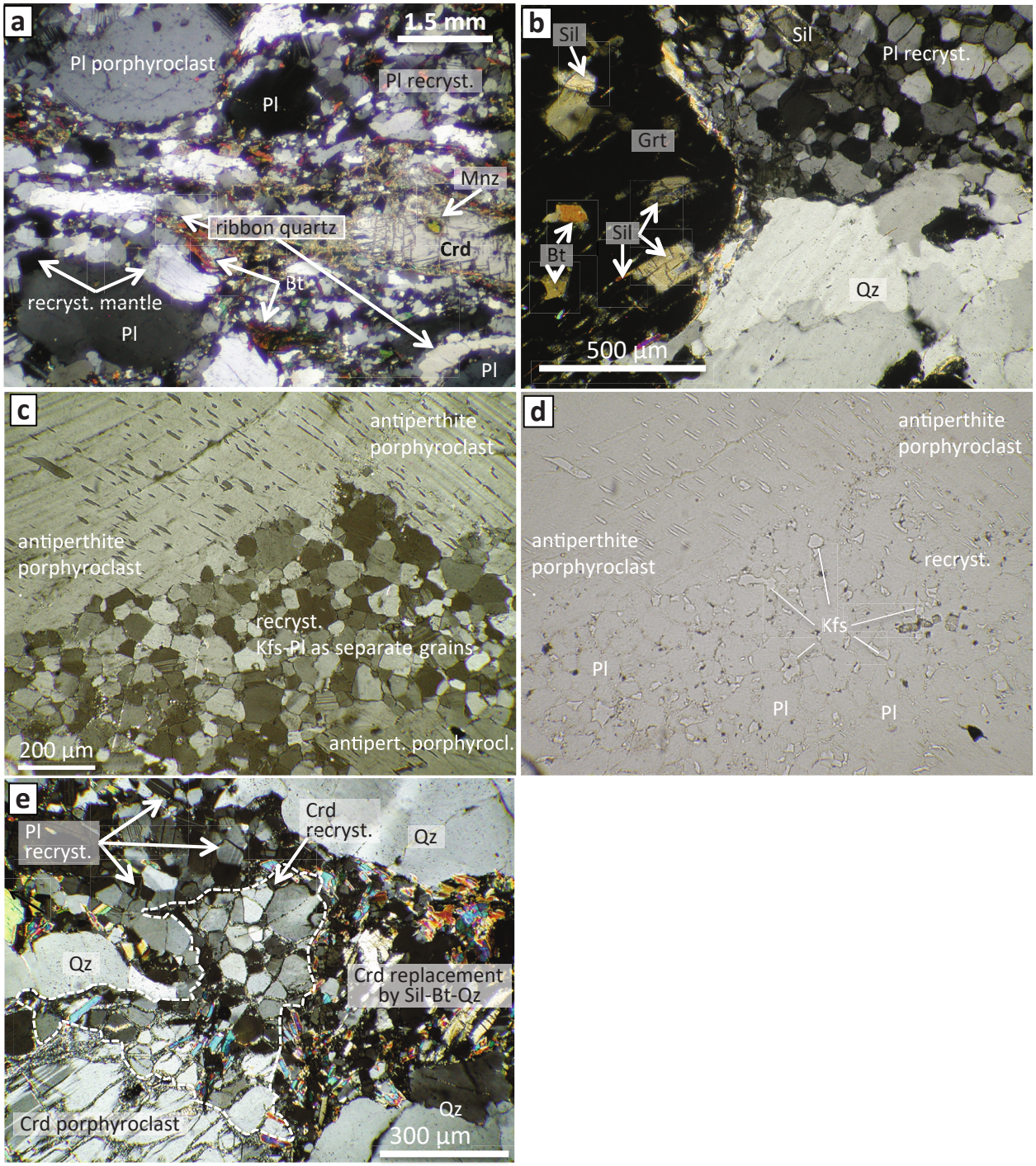

Fig. 12. Textures of protomylonitic high T/P granulites of Igula. Upper Isimani Group, T69-5b-93 and T70-5-93; Grt-Crd-Sil-Bt. (a) Plagioclase porphyroclasts surrounded by mantles of recrystallized grains and ribbon quartz; note cordierite porphyroclast with Mnz inclusion. (b) Grt porphyroblast with inclusions of Sil and Bt is surrounded by recrystallized Pl and Qz grains. Inclusions in Grt reflect contrasting conditions during prograde garnet growths in Upper and Lower Isimani Group metapelites (Sil vs. Ky). (c, d) Same detail shown under (c) crossed polarisors and (d) polarised light. The antiperthitic plagioclase porphyroclast is partially replaced by recrystallizates, in which Pl and Kfs form separate grains, pointing to recrystallization after exsolution. (e) Cordierite porphyroclast sourrounded by recrystallized matrix of Crd, Pl, Qz. Hydrous breakdown products of Crd (Sil-Bt-Qz) replace recrystallized cordierite grains.

evidence for late-stage invading fluids, which affected all rock types of the Upper Isimani Group.

Summing up the petrographic information obtained from the Upper Isimani Group metapelitic granulites, we conclude that this unit experienced a *P-T* path with prograde garnet growth in the stability field of sillimanite and a retrograde metamorphism that started in the sillimanite stability field but continued after entering the kyanite stability field. During cooling (after exsolution of antiperthite) the granulites were affected by penetrative recrystallization resulting in the omnipresent protomylonitic textures. The recrystallization event was followed by a re-hydration event, resulting in a partial or total replacement of the high-grade minerals (Grt, Crd) and the post-peak recrystallizates of cordierite and plagioclase. During the re-hydration the *P-T* path crossed the sillimanite/kyanite phase boundary during near-isobaric

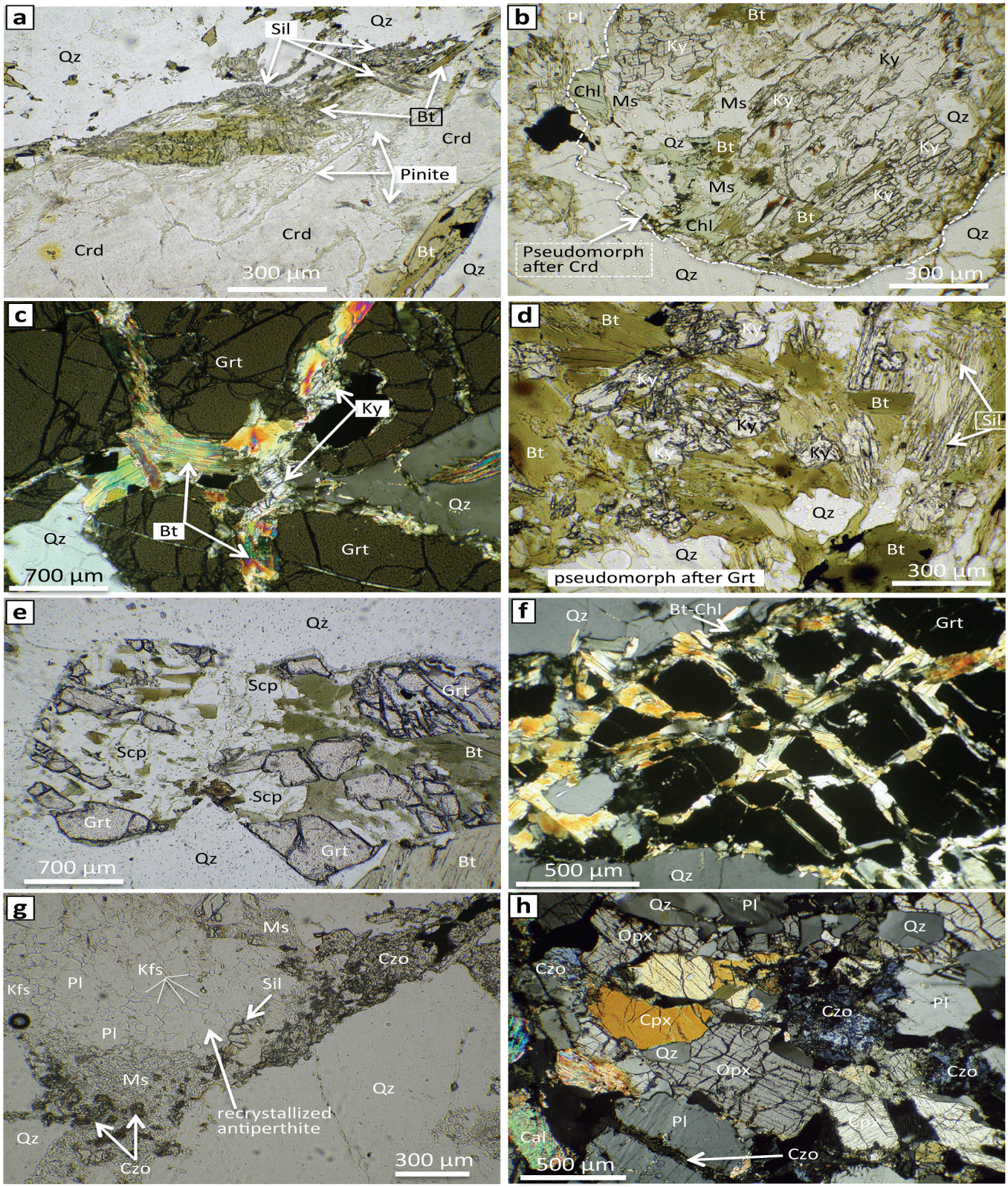

Fig. 13. Textures of hydration-retrogression in the high T/P granulites (T70-4-93, T70-8-93, T69-4-93, T69-3-93), emphasizing rehydration of the granulites after the recrystallization-deformation event. (a) Crd partially replaced by Sil-Bt-Qz and pinite. (b) Pseudomorph after Crd consisting of Ky-Ms-Bt-Chl-Qz. (c) Grt partially replaced by Ky-Bt-Qz along cracks. (d) Part of a pseudomorph after Grt, consisting of Sil-Ky-Bt-Qz formed during crossing the Ky-Sil phase boundary. (e) Grt partially replaced by scapolite and biotite due to late-stage fluid infiltration (T70-4-93). (f) Garnet replaced by Bt-Chl-Qz along a deformation pattern of cracks (T70-8-93). (g) Fine-grained recrystallized plagioclase of protomylonitic metapelite (T69-4) partially replaced by Czo and Ms (i. e., rehydration after deformation). (h) Garnet-free two-pyroxene granulite (T69-3-93) showing late-stage Czo and Carb formation due to fluid infiltration.

cooling.

The minerals of the granulites are chemically fairly homogeneous and are only affected by some retrograde changes near late-stage cracks (Fig. 14a, b), which are filled by e.g. biotite in garnet or pinite in cordierite. The chemical homogeneity of garnet porphyroblasts in the granulites contrasts with the preserved growth zoning in garnet of the Grt-Ky-Bt gneisses of the Lower Isimani Group (Fig. 11a, b) and in the eclogites (Fig. 6b). Compared to these rocks, the Grt-Crd-Sil granulites seem to have experienced a hotter and/or prolonged metamorphism, which resulted in homogenization of the garnet grains by diffusion during peak metamorphism. A *P-T* pseudosection was calculated in the system Na_2O-CaO-K_2O-FeO-MgO-Al_2O_3-SiO_2-H_2O-TiO_2 (Perple_X) for a representative sample of the low-P granulite belt (Grt-Crd-Sil-Bt gneiss T69-5–93; see Fig. 2a for location, composition given in Table S2). Mineral chemical data obtained from other samples revealed little differences (Table S7), which points to a similar metamorphic grade in the whole Upper Isimani Group. The pseudosection (Fig. 14c) is contoured for X_{Mg} of garnet and X_{Mg} of cordierite. The narrow yellow field marks the observed peak-metamorphic assemblage Grt-Crd-Sil-Bt-Pl-Kfs-Qz-Rt. The red point marks the peak-metamorphic conditions of ca. 820 °C at 7.2 kbar inferred from mineral compositional data of the unzoned minerals (XMg 0.48 for Grt; 0.83–0.84 for Crd) and lies above the solidus (bold stippled line) in agreement with field observations of leucocratic melt schlieren. The inferred prograde *P-T* path is also in agreement with the presence of sillimanite and the absence of cordierite inclusions in garnet. The assumed retrograde *P-T* path suits the observed breakdown

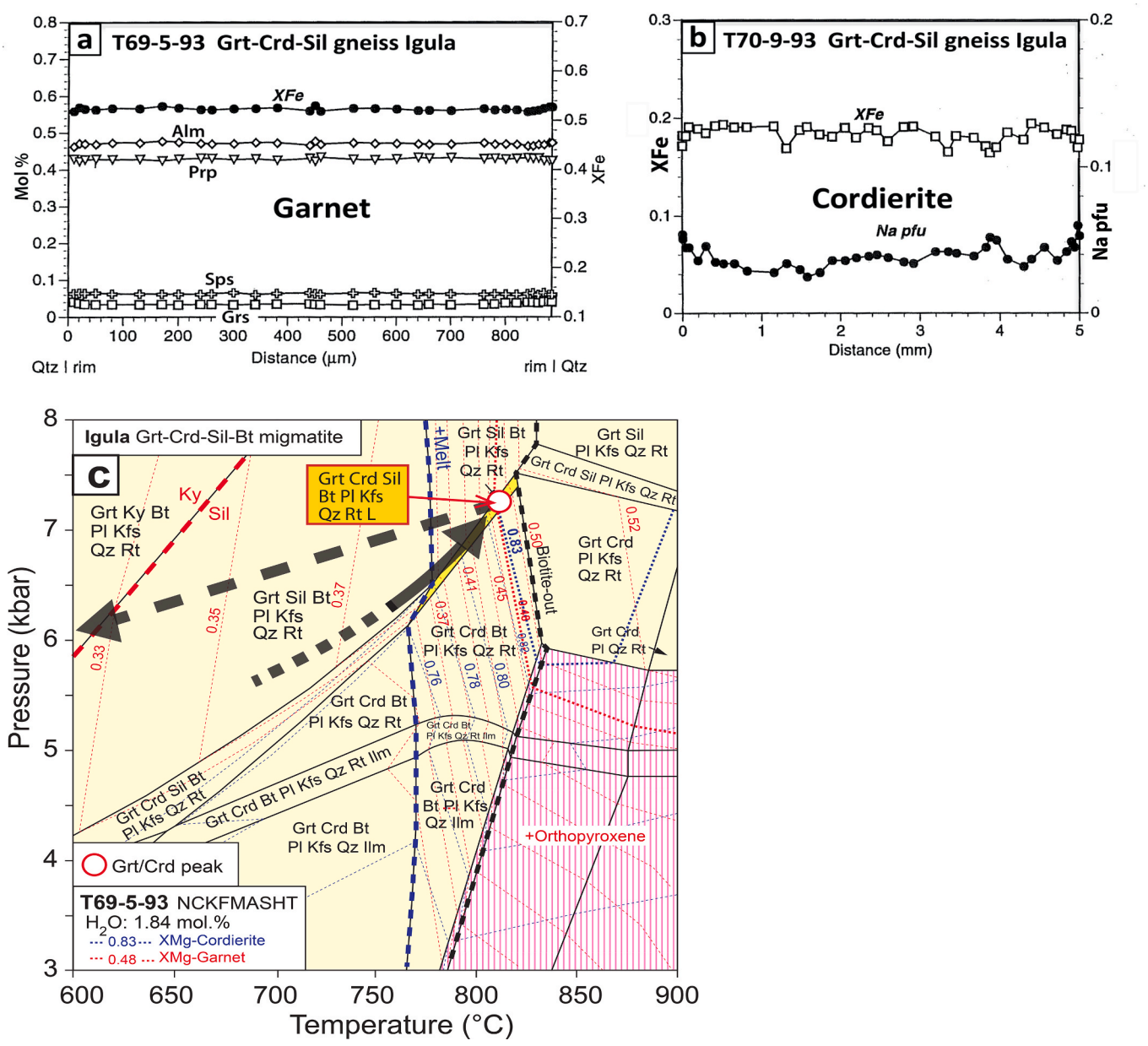

Fig. 14. (a, b) Zoning pattern of garnet and cordierite in high T/P granulites of the Upper Isimani Group. The minerals homogenized during peak metamorphism. Cordierite zonation shows some disturbance by pinitization along cracks. (c) *P-T* pseudosection in the system Na_2O-CaO-K_2O-FeO-MgO-Al_2O_3-SiO_2-H_2O-TiO_2 for Grt-Crd-Sil-Bt gneiss T69-5-93 of the high T/P granulite belt from Igula. Bulk rock data in Tab. S2, mineral chemical data in Tab. S7. Pseudosection contoured for X_{Mg} of garnet and cordierite. Yellow field represents the observed peak-metamorphic assemblage Grt-Crd-Bt-Sil-Kfs-Pl-Qz-Rt. Red point marks peak-metamorphic *P-T* inferred from mineral compositional data in unzoned cores: XMg 0.48 in Grt and XMg 0.83-0.84 in Crd. Solidus is indicated by a bold stippled line. Inferred *P-T* path is in agreement with presence of Sil and Bt inclusions in Grt and the lack of Crd inclusions. The retrograde path is constrained by the consecutive breakdown of Crd and Grt to Sil and Ky bearing assemblages (cf. Fig. 13 a-d).

textures of cordierite and garnet to late-stage sillimanite and kyanite bearing assemblages (cf. Fig. 13a–d). The deduced counter-clockwise *P-T* path agrees with the well-developed mineral reaction textures. It contrasts to the clockwise paths of the eclogites and the Grt-Ky gneisses of the Lower Isimani Group.

6. Geochronology

Until recently only the eclogites and associated metasediments of the Lower Isimani Group attracted researchers to determine the age of this unusually old eclogite metamorphism at ca. 2000 Ma. For this purpose, only samples from the eclogite locality Yalumba Hill had been selected so far (Möller et al., 1995; Reddy et al., 2003; Collins et al., 2004; Tamblyn et al., 2021). Recently, monazite dating of the amphibolite-facies metamorphism in the Konse Group revealed its relation to the Usagaran orogeny and elucidated the role of the Konse Group as a passive margin succession of the Usagaran Wilson cycle (Schenk et al., 2025).

We report new monazite ages for the Upper Isimani Group (Grt-Crd granulite) and for the Lower Isimani Group (Grt-Ky gneiss). Two samples of the latter group were dated to clarify whether the metamorphic age of the Lower Isimani Group stays the same along the whole belt, even in the far SW near Igula, where this group is overlain by the Upper Isimani granulite nappe. U-Th-total Pb EPMA dating was performed on thin sections to allow analyses of grains in different textural settings and specific domains of zoned grains. The internal textures of monazite grains of the Grt-Crd-Sil migmatite (T69-5-93; Fig. S10a-e; Fig. 2 for location) are either rather patchy with brighter and darker patches in BSE pictures (Fig. S10a, c) or are more homogeneous with concentric growth zones of different brightness (Fig. S10b, e). The different grain-internal textures cannot be assigned to different textural settings of the grains (matrix vs. inclusion). The cumulative curve of all obtained ages (n = 43) in the population have a common enveloping curve indicating a weighted mean age of 2055 ± 8.5 Ma (Fig. 15c). In contrast, the monazite grains of the two Grt-Ky samples (Lower Isimani Group; T100-1-93 and T100-5–93) do not show such patchy grains but are either homogeneous or show some concentric growth zones of different brightness, irrespective of their textural setting in the matrix or as inclusion in garnet (Fig. S10: f-o inclusion grain (g) in (r) and matrix grains (g) in (q) are both homogeneous). The weighted mean ages for monazite grains of both Grt-Ky samples (inclusions and matrix) are within error identical 1997 ± 5.1 and 1992 ± 6.1 Ma (Fig. 15a,b) and very similar to the monazite age (TIMS) obtained for a metapelite sample from Yalumba Hill (2000 ± 2 Ma; Möller et al., 1995). No Neoproterozoic ages, such as for matrix grains in Grt-Ky gneisses of the Kiboriani Mts. (T46-2-93, T44-93; Fig. 2b; Fig. S3), were found. This re-confirms that, close to the craton, only a minor thermal Neoproterozoic imprint affected the rocks of the Lower Isimani Group.

In conclusion, the different dating methods (TIMS versus U-Th-total Pb by EPMA) yield very similar results for all monazite ages of the Lower Isimani Group. The age of metamorphism is very close to 2000 Ma, similar to the age of the associated eclogites and is identical along the belt between Yalumba Hill in the NE and 60 km further SW at Igula, where the Lower Isimani Group is overlain by a nappe of Grt-Crd-Sil granulites. The SIMS monazite age received for the Konse metamorphism (2028 ± 15 Ma; Fig. 15d; Schenk et al. 2025) was obtained from actually U-free grains of a highly oxidized Mn^{3+}-rich micaschist and is thus a pure Th-Pb age. Its slightly older age may be attributed to this special analytical case. However, the high T/P metamorphism of the Grt-Crd granulites (Upper Isimani Group) is about 50–60 Ma older than that of the underlying Lower Isimani Group. This age difference, together with the contrasting *P-T* paths and phase relations of both units, underpins the allochthonous character of the low-P/high-T granulites of the Upper Isimani Group.

7. Interrelated *P-T* paths in the nappe stack and a geodynamic model

Petrographic observations, mineral chemical data, contrasting peak metamorphic conditions and contrasting *P-T* paths of the distinguished lithotectonic units of the Usagaran Belt reveal compelling evidence that the Konse Group, Lower Isimani metasediments, eclogites and Upper Isimani granulites form a stack of nappes, which came into contact during the Palaeoproterozoic orogeny. In the following section we describe their interrelated evolutions during tectonic processes of the Usagaran orogeny.

The eclogites, which formed from the basaltic oceanic crust and from subduction initiation-related boninites, experienced the deepest subduction (18–19 kbar) of all studied units. They were heated to about 850–880 °C, before they started to rise from 60-70 km mantle depths to crustal levels and became part of a nappe stack. The exhumation was likely triggered by slab breakoff or crustal extension after collision, like in Phanerozoic orogens. Phase diagram modeling of the eclogite T69-12 suggests that the subducting oceanic slab was cool ('modern-style'; ca. 10 °C/km) during the early stages of the subduction and touched the blueschist stability field (Fig. 6d). At the state of deepest subduction, the apparent thermal gradient was in the range of 13–14 °C/km indicating a warm subduction regime. The high temperatures, similar to those of the peak, remained during a significant part of the exhumation, as indicated by granulite-facies coronas around garnet porphyroblasts. Temperatures near 800 °C are calculated for corona formation that developed during exhumation at 8–10 kbar, i.e., at the likely MOHO depth. In addition, high temperature mylonites of Opx-eclogites and felsic rocks, which are associated with the eclogites, indicate that exhumation was accompanied by mylonitization at high pressures in the kyanite stability field (Ky in late-stage symplectites; Fig. 9f and Fig. S9b-e), but occurred after the breakdown of omphacite (to Di + Pl; Fig. 9c,d). Decompression continued after mylonitization as indicated by preserved late-stage Opx-Pl coronas around garnet porphyroclasts, which formed after recrystallization of the surrounding mylonitic orthopyroxene matrix (Fig. 9d,f; Fig. S9). The associated felsic mylonites also indicate recrystallization at high temperatures, as recrystallized alkali feldspar porphyroclasts exsolved after recrystallization (Fig. 9e, g, h; Fig. 17e).

The Grt-Ky-Bt gneiss T69-4 of the Lower Isimani Group at Yalumba Hill was metamorphosed at the same time as the eclogites (ca. 2000 Ma), but did not experience the high pressures and temperatures of the eclogites. The peak *P-T* conditions for the gneiss were 13.2 kbar at 770 °C, corresponding to higher apparent geothermal gradients (ca. 17 °C/km) than those obtained for the eclogites. However, the gneisses show the same type of clockwise *P-T* path, which evolved on its prograde part through the kyanite stability field. Furthermore, gneisses and eclogites both have grossular-rich garnet porphyroblasts with preserved growth zonation. This indicates that both lithologies were affected by a similar, relatively short-lived tectono-metamorphic event. This event was not of sufficient duration to allow for homogenization of garnet, despite the high metamorphic temperatures (ca. 850–880 and 770 °C). The retrograde path of the Lower Isimani Grt-Ky gneisses also resembles that of the eclogites; our phase diagram modeling indicates that high temperatures persisted during exhumation (Fig. 11d, e). This is supported by the widespread occurrence of late-stage coarse-grained sillimanite, which replaces the peak-metamorphic kyanite porphyroblasts (Fig. 10d, f). Nevertheless, the high-temperature exhumation of the eclogite and the associated Grt-Ky gneiss ran out at pressures above ca. 6 kbar (lack of late-stage cordierite in metapelites; lack of orthopyroxene in Cpx-Pl ± Hbl coronas around garnet in the modeled eclogite; Fig. 6e, Fig. 11d). The interrelated *P-T* paths for the eclogites and the embedding metapelites (Lower Isimani Group) appears to be valid for the whole belt, because retrograde replacement of kyanite by late-stage sillimanite is observed all along the belt from Yalumba Hill to Igula in the SW (Fig. 2). However, by comparing the peak pressures, a deeper burial of the Lower Isimani Group at Yalumba (13.2 kbar) compared to Igula (10.7 kbar;

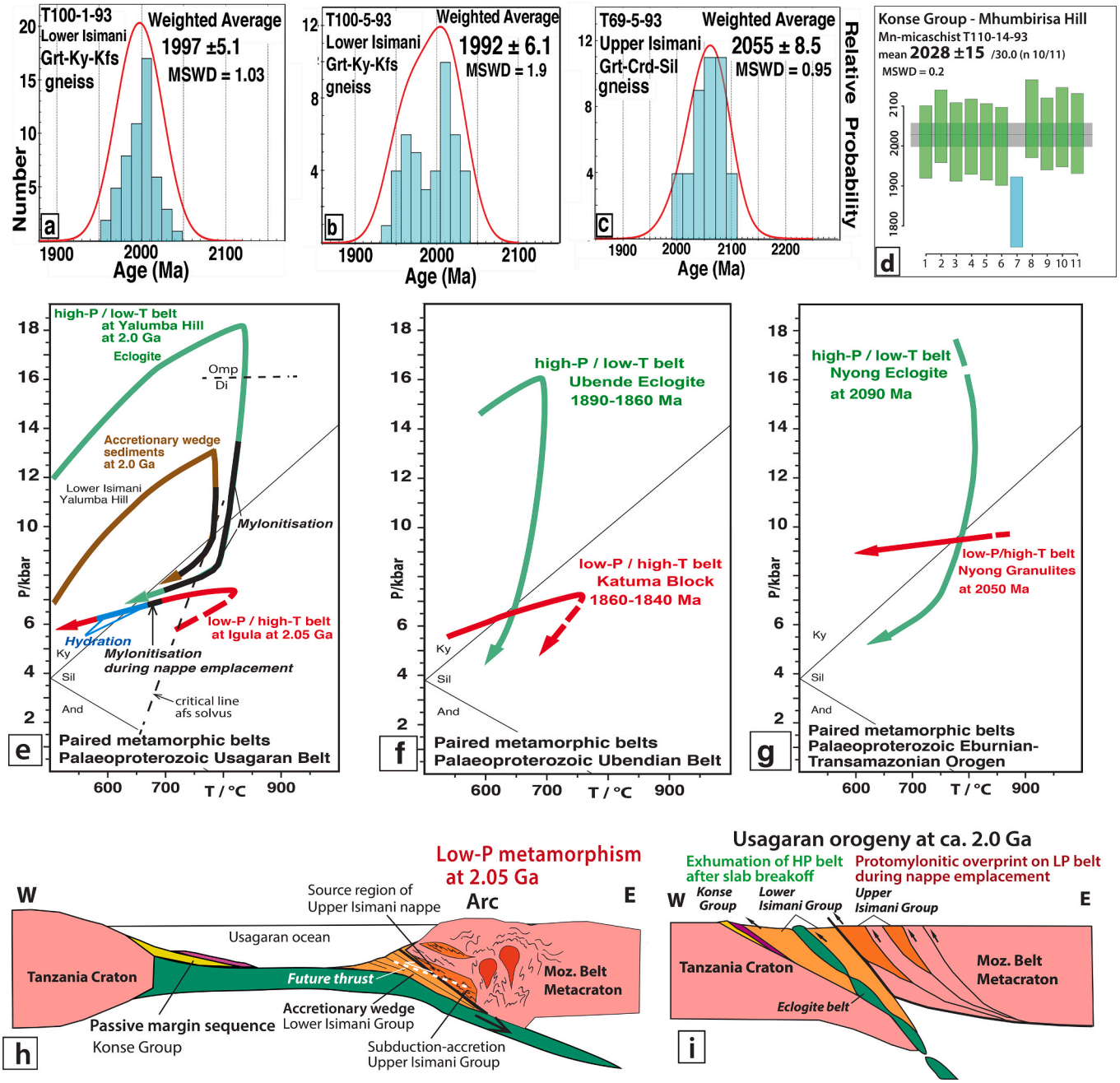

Fig. 15. (a, b) Histograms with weighted mean ages of monazite grains in the low T/P metapelites from Igula (T100-1-93 and T100-5-93; Lower Isimani Group; Grt-Ky-Kfs). (c) Histogram for high T/P granulite T69-5-93 (Grt-Crd-Sil; Igula). The enveloping curve is the cumulative curve for the age population. The bars are frequency histograms. The age of the high T/P metamorphism in the Upper Isimani Group (ca. 2055 Ma) is 50-60 Ma older than the metamorphism in the Lower Isimani Group (ca. 2000 Ma). (d) SIMS monazite age of Mn-andalusite-spessartine micaschists (T110-93) of the Konse Group from Mhumbirisi Hill (cf. Fig. 2 and 3; modified after Schenk et al., 2025). (e–g) *P-T* paths for the three known Palaeoproterozoic paired metamorphic belts around the Congo Craton, which include subduction-related eclogites. (e) Interrelated *P-T*-deformation paths for three tectonic units of the Usagaran nappe stack. The mylonitic recrystallization of the low T/P rocks (Opx-eclogites and felsic rocks of Lower Isimani Group) started during exhumation after the breakdown of omphacite, but prior to the mesoperthitic exsolution, in the Ky stability field; critical line of Afs solvus after Parsons (1978). Post-peak deformation of the high T/P granulites (protomylonites of Upper Isimani Group) occurred after antiperthitic exsolution and was subsequently affected by intense re-volatilization. The related nappe emplacement of the high T/P granulites (Upper Isimani Group) on top of the Lower Isimani Group occurred after peak-metamorphism. Isobaric cooling of the eclogites after exhumation to an intermediate crustal level is documented by re-growth of garnet at the expense of exhumation-related Opx-Pl symplectites (Pl+Opx ↔ Grt+Cpx+Qz). (f) *P-T* paths of the ca. 140 Ma younger paired metamorphic belts of the adjoining Ubendian belt (cf. Fig. 1a); data after Boniface et al. (2012) and Kazimoto et al. (2014). (g) *P-T* paths of the Nyong eclogites (Cameroon) and the associated granulites (after Loose and Schenk, 2018). (h, i) Tectonic sketches illustrating the deduced east-directed subduction of the Palaeoproterozoic Usagaran ocean below an Archaean block in the east ('Mozambique Belt Meta-Craton'). The meta-craton included a Palaeoproterozoic continental arc, which contained the high T/P granulites of the Upper Isimani Group.

Fig. 11c, e) is proposed.

We argue that during the subduction process the oceanic plate dragged accretionary wedge sediments to significant depths (ca. 45 km), where they experienced a high-P amphibolite-facies metamorphism. After slab breakoff and continental collision, the rising slab became tectonically imbricated with the buried accretionary wedge sediments. This scenario can explain the coeval short-lived similar clockwise *P-T* paths of the two units (Fig. 15e). Our model of an accretionary wedge metamorphism for the Lower Isimani Group does not exclude the possibility that some metasediments may have reached subduction depths and temperatures similar to those of the eclogites, as proposed by Herms et al. (2023).

The metamorphism of the Upper Isimani Group contrasts in many respects to those of the eclogites and of the Lower Isimani Group metasediments. The metamorphism is 50–60 Ma older and the *P-T* path is counter-clockwise with prograde garnet growth in the sillimanite stability field. The very high temperature of ca. 820 °C at a shallow depth of ca. 25 km (7.2 kbar) points to an area of high heat flow. The grade of metamorphism is very uniform over its known outcrop area and the high-grade minerals garnet and cordierite did not preserve a prograde growth zoning but instead were homogenized during a prolonged stage of peak metamorphism (Fig. 14a,b). There was no rapid hot exhumation. Instead, the Upper Isimani granulites cooled near-isobarically, which points to a slowly vanishing heat source. During this near-isobaric cooling, the granulites were affected (likely some tens of million years after peak) by an intense and penetrative tectonic event, which resulted in the characteristic protomylonitic textures of this group (Fig. 12). At the time of deformation, the granulites remained at a deep crustal level of about 20–25 km and the rocks were still in the stability field of sillimanite and cordierite (recrystallization of plagioclase and cordierite) but antiperthitic plagioclase was already exsolved. This constrains the deformation temperature to about 550 ± 50 °C. The tectonic event was followed by an intense rehydration/carbonation event, which affected all rocks including the rare 2-pyroxene granulites of the Upper Isimani Group. The relative timing of recrystallization and rehydration is constrained, as hydration also affected recrystallized plagioclase (replaced by Ms-Czo) and cordierite grains (replaced by Sil-Bt-Qz) (Figs. 12 and 13).

The petrological and age data clearly point to contrasting geodynamic settings for the Upper Isimani Group compared to the Lower Isimani Group and eclogites at the time of their metamorphism. Whereas eclogites and Lower Isimani Group metasediments were metamorphosed in a subduction zone environment, the setting of the high T/P granulite nappe of the Upper Isimani Group fits a continental arc environment. As the contrasting tectonic groups were metamorphosed at different times and different settings during the same orogeny (ca. 2055 vs. 2000 Ma), they must have been juxtaposed during the Usagaran collisional event (at 2000 Ma). At the time of nappe stacking, the older high T/P granulites had already isobarically cooled at a depth of about 20 km in the arc. They obtained their protomylonitic textures likely during nappe emplacement. We regard a continental collision event as the most likely scenario for the emplacement of the granulite nappe, which derives from a cooling arc and now rests on top of the subduction-related complexes. The depth of nappe formation (ca. 20 km) corresponds roughly to the depth estimated for the end of the near-isothermal exhumation of the subduction-related groups. This coincidence may indicate that at this depth the different groups came in tectonic contact and experienced a common interrelated near-isobaric cooling (Fig. 15e). The loading of the Upper Isimani Group nappe caused devolatilization in the underlying units (Lower Isimani group). The rising fluids induced the late-stage re-volatilization of the overlying granulite nappe. Petrographic observations of garnet re-growth after garnet resorption in Opx- and Ky-eclogites (Fig. 7b inset; Fig. S8) is in line with this model of a common isobaric cooling history of the nappe stack at elevated pressures.

The geological sketches (Fig. 15h, i) aim at illustrating the tectono-metamorphic evolution. As the high T/P metasediments were already incorporated in the arc region at the time of their metamorphism (ca. 2055 Ma), we assume that the subduction process below the arc was already in operation ca. 50–60 Ma prior to the metamorphism of the eclogites (at ca. 2000 Ma; Fig. 15h, i). Thus, our model includes a long-lived subduction (ca. 55 Myr, from 2055 to 2000 Ma) below the Mozambique Belt Metacraton in the east that led to the development of a continental arc. This arc contained metasediments, which were metamorphosed to granulite grade at 2055 Ma (Fig. 15c, h). During the Usagaran orogeny (at 2000 Ma), the metasediments formed a nappe, which was detached from the colliding continental arc. The nappe rests now on the subduction related complexes of this orogen and its orogenic foreland (Konse Group; Fig. 15h, i).

The maximum duration of the Wilson cycle in the Usagaran Belt is so far constrained by the depositional age of the passive margin sequence (Konse Group), which, according to the beginning of the Lomagundi carbon isotopic excursion at ca. 2.2 Ga, did not exceed 200 Myrs. More likely, the duration was much shorter, if the highest carbon isotope values of marbles from the Konse correspond to the peak of the LCIE at ca. 2.15 Gyr ago (<150 Myr; Schenk et al., 2025). The minimum duration of the Wilson cycle is so far constrained to about 50–60 Myrs by the age difference between the arc metamorphism (2055 Ma) and the Usagaran orogeny (2000 Ma). Comparable spatial variations in metamorphic ages that span a time of 50 Myrs and record long lasting tectonic underplating are known from Cretaceous to Cenozoic subduction complexes in southern California (Chapman, 2017). In the absence of crystallization ages of the magmatic precursors of the eclogites, we have no further constraints for the duration of the Wilson cycle in the Usagaran Orogen.

The Neoproterozoic orogenic reworking intensely affected the Palaeoproterozoic arc region on the eastern side of the Usagaran Ocean, which is now obscured in the Tanzanian Kuunga Orogen. However, the available age data for the region east of the eclogite belt in the Usagaran Orogen (Fig. 2b) suggest that orogenic activity continued for some tens of million years after the orogenic event at ca. 2.0 Ga. The nature of these orogenic processes in the overriding hinterland is not well understood due to lack of data.

8. Evidence for widespread ‘modern-style’ plate tectonics in the Palaeoproterozoic

The Usagaran orogeny is related to the Palaeoproterozoic assembly of the supercontinent Nuna/Columbia, which represents a tectonically very active time (Figs. 16 and 17; Zhao et al. 2011; Li et al., 2023). Most authors agree that at this time any possible pre-plate tectonic modes, such as the stagnant lid and the stagnant-deformable (squishy) lid modes, were no longer active and that the Earth was completely covered by rigid lithospheric plates, which got subducted at convergent margins (e. g., Windley et al., 2021; Kusky et al., 2021; Cawood et al., 2022; Brown and Johnson, 2018; Brown et al., 2024). This is in agreement with the presence of lithological components related to plate-tectonic Wilson cycles that developed at the margins of many Archaean cratons during the Palaeoproterozoic (e. g., Trans-Hudsonian Orogen, Hofmann, 1988; Wopmay Orogen, Hoffman, 1973). The Usagaran Orogen contains a great number of these lithological components: (i) a passive margin sequence (Konse Group) at a rifted continental margin (Tanzania Craton), (ii) subducted oceanic crust metamorphosed to eclogite grade

at mantle depths (60–70 km), (iii) boninites related to subduction-initiation, which were subsequently subducted and metamorphosed to eclogite grade, (iv) an accretionary wedge complex deposited in a foreland basin and metamorphosed at high-P amphibolite-facies conditions during the subduction of oceanic crust (Lower Isimani Group), and (v) a nappe of high T/P granulites (the 'paired belt') metamorphosed in an arc environment several tens of million years prior to tectonic emplacement during the continent–continent collision.

Further PMB containing eclogites, which formed from ocean-floor basalts, as well as timely and spatially associated low-P granulites are known from two other orogenic belts framing the Congo Craton: the Ubendian and the Eburnian-Transamazonian belts (Figs. 16 and 17a), which are both regarded as evidence for modern-style plate tectonics during the Palaeoproterozoic (Möller et al., 1995; Boniface et al., 2012; Loose and Schenk, 2018). The metamorphism of the subducted oceanic crust in these belts have some characteristics in common with that of the Usagaran eclogites: the peak pressures of 16–19 kbar were reached at relatively high temperatures (700–880 °C) indicating higher apparent geothermal gradients of 12–14 °C/km compared to most Phanerozoic analogs (Penniston-Dorland et al., 2015; Brown and Johnson, 2018). However, the preserved prograde path of the Usagaran eclogites with ca. 10 °C/km is comparable to that of cold subduction zones (Figs. 15, 16, 17). After peak conditions, these eclogites experienced rapid high-T isothermal exhumation from ca. 60–70 km depths resulting in a transient granulite-facies stage. In all three orogenic belts high T/P granulite belts are timely and spatially associated with the subduction-related eclogites (Fig. 15e, f, g; Loose and Schenk, 2018).

In addition to these 'warm' subduction zones, there is also evidence for cold subduction in the Palaeoproterozoic (Fig. 17a). High-P chloritoid-kyanite-garnet micaschists and a meter-scale lawsonite eclogite lens in a granitic gneiss of the northern Kongling Complex (Yangtze Craton, China) record cold subduction to mantle depths at ca. 2.0 Ga (Han et al., 2020; Yin et al., submitted). The micaschists are spatially associated with structurally overlying coeval granulites further east (Li et al., 2022; Yin et al., submitted) and may represent a further example of Palaeoproterozoic PMB in the sense of Miyashiro. However, the high-P belt is essentially made of micaschists and the regional extent of these belts is not yet documented. In addition, a recent publication describes a mélange zone in this part of the Kongling Complex rather than paired metamorphic belts (Deng et al., 2025). Cold subduction is also known from the Trans-North China Orogen, where carbonatites exhumed ca. 1.85 Ga eclogite xenoliths (ca. 7 °C/km; Xu et al. 2018) and from the Kasai block (Congo Craton), where an eclogite sample of MORB chemistry documents partially exhumed Palaeoproterozoic oceanic crust at ca. 2.09 Ga (Fig. 17a; François et al., 2018). Finally, in the Lapland-Kola Belt, pseudosection modeling of a Salma eclogite points to a cold prograde subduction path (ca. 9 °C/km; cf. Usagaran eclogites) at ca. 1.9 Ga (Li et al., 2023), although conflicting with a higher T-estimate using Zr-in-rutile thermometry (>50 °C) on rutile inclusions in garnet (Li et al., 2023). Moreover, all previous *P-T* estimates on these Belomorian eclogites point to a 'warmer' subduction with intermediate *T/P* ratios (e. g., Mints et al., 2007, 2010; Imayama et al., 2017; Li et al., 2017; Liu et al., 2017).

The above listed Palaeoproterozoic subduction-related eclogites indicate that cold (< 11 °C/km) and warmer (12–14 °C/km) oceanic subduction zones were operating at the same time during the formation of the supercontinent Nuna/Columbia (Fig. 17a). The message from the cold subduction zones is that cold subduction (often equated with 'modern-style' plate tectonics) was already possible in the warmer Palaeoproterozoic Earth. The message from the 'warm' subduction zones (often equated with 'non-modern-style' plate tectonics) is that even warmer slabs were rigid and stable enough to build up a slab-pull force and that they were partially exhumed after slab breakoff during continental collision. In addition, the formation of eclogites in the Usagaran Orogen is related to a plate-tectonic Wilson cycle and the formation of a paired high-T metamorphic belt. This indicates that the 'modern-style' plate tectonic processes are not necessarily restricted to the 'cold' subduction zones (ca. < 11 °C/km), as commonly argued (e. g., Stern, 2005; Brown, 2006; Brown and Johnson, 2018; Li et al., 2023; Brown et al., 2024).

Modern-style plate tectonics during the formation of Nuna/Columbia are also inferred from several other Palaeoproterozoic orogenic belts, for which eclogite-facies and even UHP conditions in deep crustal roots have been reported (Fig. 16a, b), e.g. from the Trans-North China (Gao et al., 2001), the Lapland-Kola (Skublov et al., 2010; Tuisku et al., 1998; Mints et al., 2010; Li et al., 2023), the Trans-Hudsonian (Weller and St-Onge, 2017) and the Nagssugtoqidian (Nutman et al., 2008; Müller et al., 2018) orogens. However, these eclogites do not represent exhumed fragments of subducted oceanic crust, are not related to paired high-T belts, and some lack an associated passive margin sequence. These eclogites formed from mafic dykes in tectonically thickened or subducted continental crust (Fig. 16b). For some of these eclogites an Archaean age was originally assumed (Snow Bird zone, Snoeyenbos et al., 1995; Belomorian, Volodichev et al., 2004; Mints et al., 2010), but later revised to the timing of respective Palaeoproterozoic orogenies (Baldwin et al., 2003; Skublov et al., 2010; Herwartz et al., 2012; Li et al., 2023).

In addition, many other Palaeoproterozoic belts, which developed at the margins of Archaean cratons lack deeply subducted eclogites, but contain Wilson cycle related lithological components, such as passive margin successions, foreland basin sediments and metabasalts of MORB chemistry. Well known examples include the Trans-Hudsonian Orogen at the Hearne and the Superior cratons (e. g., Hofmann, 1988; Corrigan et al. 2007), the Wopmay Orogen (Slave province NW Canada; Hoffman, 1973; Hoffman and Bowring, 1984), the Minas Supergroup at the Sao Francisco Craton (Alkmim and Teixeira, 2017), the Magondi Fold Belt with the Lomagundi Group (northwestern Zimbabwe Craton; Master et al., 2010) and the Ruwenzori Fold Belt with the Buganda Group (northern Tanzania Craton; Barth and Meinhold, 1974; Master et al. 2013).

In summary, the Palaeoproterozoic orogenic belts that developed around Archaean cratons during the Nuna/Columbia supercontinent assembly were associated with widespread modern-style plate tectonic processes, including subduction of oceanic crust to mantle depths and its partial exhumation after slab breakoff.

9. Is the period of 'modern-style' plate tectonics at 2.1–1.8 Ga of peculiar significance for the pre-Neoproterozoic Earth?

The formation of Palaeoproterozoic PMB and deeply subducted oceanic eclogites that are related to plate-tectonic Wilson cycles only occur during the relatively short time interval 2.1–1.8 Ga (Figs. 16, 17a). This period is preceded by a period of 'tectono-magmatic lull' (Spencer et al., 2018; Condie et al., 2022; Fig. 17a) and succeeded by the Mesoproterozoic 'boring billion' (with relative 'orogenic quiescence': Tang et al., 2021; Zhu et al., 2022). During the latter period the Grenville and Kibaran orogens were formed, but eclogites representing subducted oceanic crust have not been reported so far (Fig. 16b). Only some Neoproterozoic orogens related to Gondwana formation contain eclogites that formed from ocean floor basalts (Fig. 16b; Zambesi Belt, John and Schenk, 2003; Ubendian Belt, Boniface and Schenk, 2012; Boniface et al., 2012).

In contrast with the widespread 'modern-style' plate tectonics during the Palaeoproterozoic period of 2.1–1.8 Ga, both early Palaeoproterozoic and Archaean terrains lack subduction-related eclogites (Fig. 16b, Fig. 17a). In the Archaean, the lack of subduction-related eclogites was, and still is, one of the main arguments against 'modern-style' plate tectonics (e. g., Stern, 2005; Brown, 2006; Huang et al., 2020; Ning et al., 2022a, b; Brown et al., 2024). To the best of our knowledge, the only report about eclogite-facies conditions in Archaean terrains is that of Ning et al. (2022a) for a ca. 2.5 Ga old lens of garnet-clinopyroxenite within a mélange block of garnet metagabbro in the North China Craton

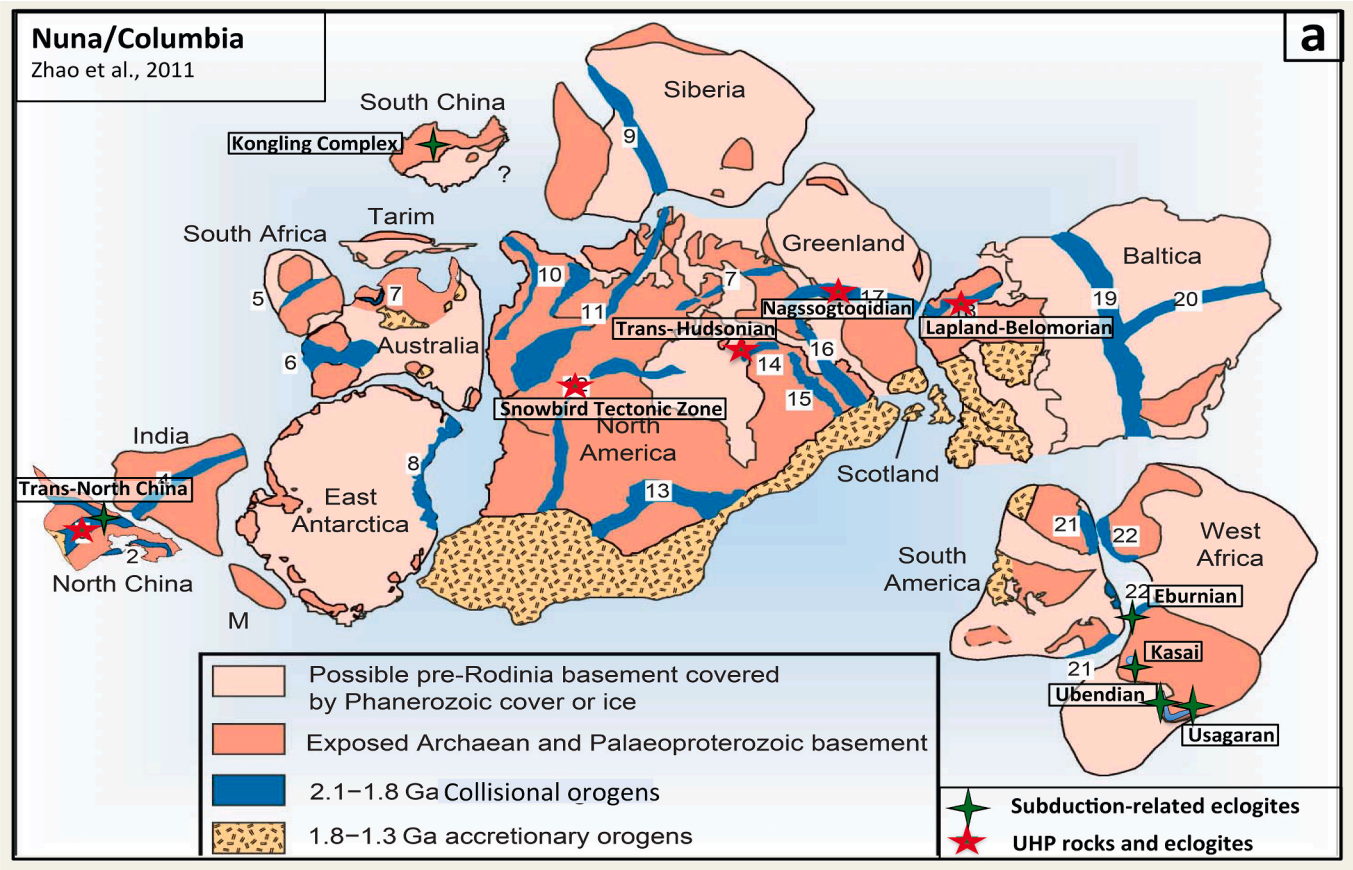

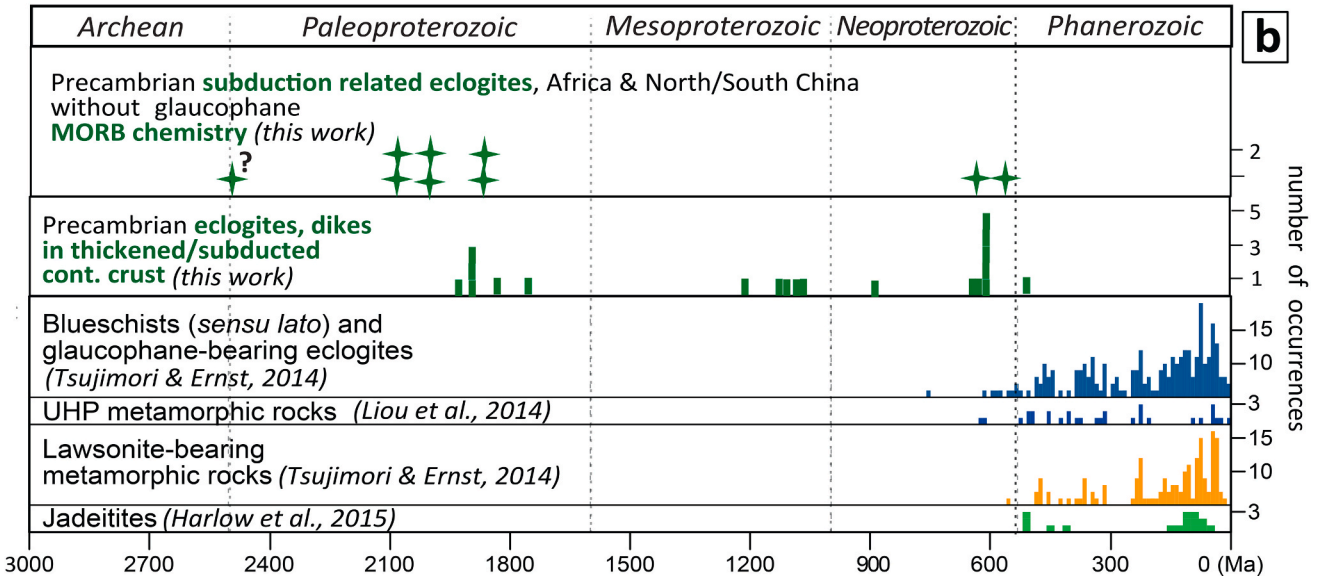

Fig. 16. (a) Reconstruction of the supercontinent Nuna/Columbia by Zhao et al. (2011). This older version of the supercontinent reconstruction is preferred here over the updated version by Li et al. (2023), as it shows the Palaeoproterozoic orogenic belts that host the eclogites discussed in our study. Marked are the five orogens with Palaeoproterozoic subduction related eclogites, which formed from ocean-floor basalts and the five orogens with eclogites that formed from mafic dikes in thickened or subducted continental crust. Some of the latter experienced UHP conditions. Following references deal with the first recognition of the Palaeoproterozoic eclogites: Usagaran (Möller et al., 1995); Ubendian (Boniface et al., 2012); Eburnian-Transamazonian (Loose and Schenk, 2018); Kasai Block (François et al., 2018); Kola-Lapland (Skublov et al., 2011; Tuisku & Huhma, 1998); Nagssugtoqidian (Nutman et al., 2008; Glassley, 2014); Trans-Hudson (Weller and St-Onge, 2017); Snow Bird Tectonic Zone (Baldwin et al., 2003); Trans-North China Orogen (Zhao et al., 2001; Xu et al., 2018); Yangtze Craton (Yin et al., submitted). The Neoarchaean eclogite-facies metamorphism in the North China Craton (Ning et al., 2022a) has been questioned by Zou et al. (2022). (b) Indicators for the operation of plate tectonics (modified from Stern, 2020; Harlow et al., 2015; Liou et al., 2014, Tsujimori and Ernst, 2014). The diagram is complemented by Precambrian eclogites, which are either subduction related (formed from ocean-floor basalts) or formed from mafic dikes in thickened/subducted continental crust. Further Precambrian subduction-related eclogites occur in Neoproterozoic orogens (Boniface and Schenk, 2012; John and Schenk, 2003; John et al., 2003).

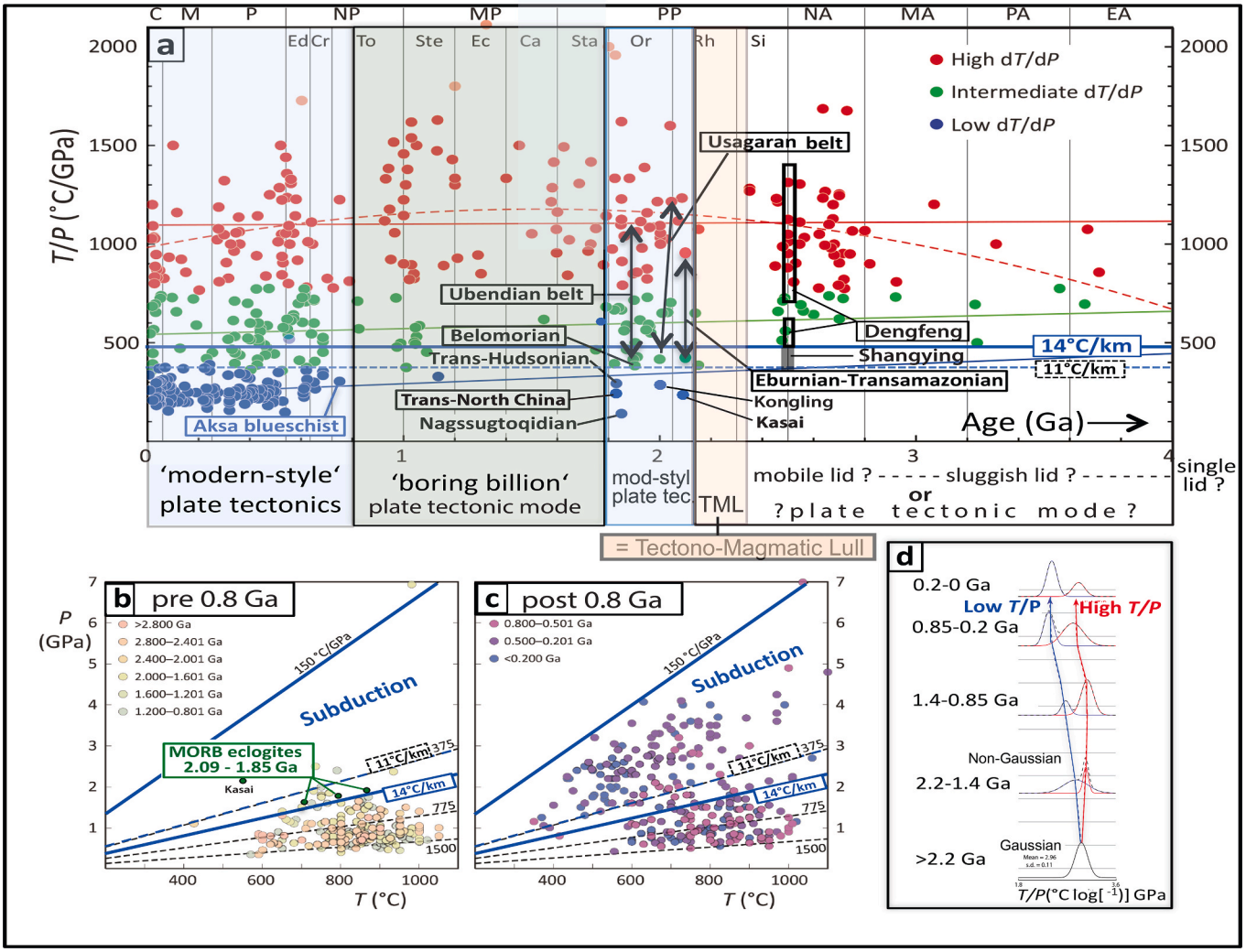

Fig. 17. (a) Apparent metamorphic gradients for 456 localities plotted against their age. (b) *P-T* conditions of metamorphism >0.8 Ga and (c) <0.8 Ga; (a)(b)(c) modified after Brown and Johnson (2018). (d) The gradual development of the duality of thermal regimes in metamorphic crustal rocks (as a proxy for subduction processes on Earth) emerged only after ca. 2.2 Ga (modified after Holder et al., 2019; Brown et al., 2024). This is in accordance with the Palaeoproterozoic age of the paired metamorphic belts and of the exhumed fragments of subducted oceanic slabs around the Congo Craton, described in the present study. The coloured time intervals in (a) emphasize the probability that the Earth experienced multiple tectonic regimes (plate tectonic vs. stagnant-deformable (sluggish) lid) and tectonically less active periods, such as the tectonic-magmatic lull and the 'boring billion'. The Palaeoproterozoic 'cold' and 'warm' subduction zones discussed here fall into the period 2.1–1.8 Ga. Brown and Johnson (2018) proposed a critical boundary for cold subduction at 11 °C/km or 375 °C/GPa (cf. a, b, c). It has been shifted here to 14 °C/km, in agreement with the calculation of Holder et al. (2019) and the *P-T* data of subduction-related eclogites of Palaeoproterozoic age around the Congo Craton (cf. a and b). In three orogens around the Congo Craton subduction-related eclogites are associated in space and time with high T/P belts (connecting black arrows in (a)). The Neoarchaean paired metamorphism of the Dengfeng Complex (North China Craton; Huang et al., 2020) and the eclogite-facies metamorphism in the Shangying mélange Ning et al. (2022b) are discussed in section 9.

(Shangying ophiolitic mélange; Fig. 17a). However, pseudosection modeling of this rock by Zou et al. (2022) instead pointed to UHT granulite-facies conditions (with P < 12 kbar), which seems to be in agreement with the mineral assemblage of the enclosing plagioclase-bearing garnet-metagabbro. In return, Ning et al. (2022b) criticized the pseudosection modeling by Zou et al. and justified their applied methods and results. Only further analysis can resolve the controversy regarding the metamorphic history of this unique and unusual rock of Archaean oceanic crust.

Admittedly, paired metamorphism with diverse apparent geothermal gradients has been known for a long time from early Archaean granite-greenstone terrains. However, greenstone belts are not part of paired belts in the sense of Miyashiro, because neither their apparent geothermal gradients nor the recorded pressures point to cold subduction zones to mantle depths. Instead, other models have been proposed for their formation, including delamination of the lower crust and sagduction tectonics (e.g., Van Kranendonk et al., 2002; Smithies et al., 2009; Johnson et al., 2014, 2017; François et al., 2014; Chowdhury et al., 2020; Dasgupta et al., 2023). These Early Archaean crustal fragments represent a distinct granite-dome/greenstone-keel crust, which has been interpreted as the result of a gravitationally unstable stratification of felsic proto-crust overlain by denser mafic volcanic rocks that became subject to reorganization by Rayleigh–Taylor flow (Sharp, 1984; Van Kranendonk et al., 2002; Smithies et al., 2009; van

Kranendonk et al., 2014; Johnson et al., 2014; François et al., 2014; Wiemer et al., 2018). The greenstone-keels are interpreted as cold drips during crustal overturn of the granite-dome. However, other authors have related the paired metamorphism of the granite-greenstone association to oceanic subduction zones, albeit evidence for cold subduction to mantle depths is lacking (e. g., Moyen et al., 2006; Pease et al., 2008; Roman and Arndt, 2020; Huang et al., 2020; Kusky et al., 2021; Windley et al., 2021).

Besides, the Neoarchaean paired metamorphism of the Dengfeng Complex (North China Craton; Fig. 17a) has been also regarded as subduction related (Huang et al., 2020). However, these belts are of amphibolite- and granulite-facies metamorphic grade and record neither subduction metamorphism at upper mantle depths nor apparent geothermal gradients typical of Phanerozoic cold subduction zones (Fig. 17a; <ca. 500 °C/GPa, as defined by Holder et al., 2019; Brown et al., 2024). The Dengfeng Complex shows a paired metamorphism in the modified sense of Brown and Johnson (2018). This type of paired metamorphism can also be represented by an intermediate T/P belt paired with a high T/P belt; such belts need not include (1) rocks of oceanic crust, (2) indicators of subduction to mantle depths and (3) evidence for metamorphism at cold apparent geothermal gradients typical for modern subduction zones. A specific pair of metamorphic belts in this sense is not unequivocally related to a deep subduction zone, but can also be explained by alternative tectonic models, such as sagduction, peel-off-tectonics or simply tectonic juxtaposition of different terrains, i.e. models that have been applied to several Archaean and Proterozoic terrains (e. g., Van Kranendonk et al., 2002; Smithies et al., 2009; van Kranendonk et al., 2014; Johnson et al., 2014; François et al., 2014; Wiemer et al., 2018; Bhowmik et al., 2018; Chowdhury et al., 2020; Dasgupta et al., 2023).

Brown (2006) and in a series of subsequent papers, e.g., Brown and Johnson, 2018, 2019; Brown et al., 2020a,b; Brown et al., 2024) proposed, like Stern (2005), that the first widespread occurrence of blueschists and UHP (coesite bearing) rocks in the Neoproterozoic (ca. 0.8 Ga) marks the onset of modern cold and deep subduction. These authors assumed that for the subduction of 'cold' oceanic lithosphere the geothermal gradient should not exceed 11 °C/km (Brown and Johnson, 2018; Fig. 17a, b). Yet, this view is contradicted by several reports of Palaeoproterozoic subduction related eclogites and of PMB at warm and cold deep subduction zones (Fig. 17a; cf. Möller et al., 1995; Boniface et al., 2012; Loose and Schenk, 2018; François et al., 2018; Xu et al., 2018; Li et al., 2023; Weller and St-Onge, 2017; Yin et al., submitted; present paper). On the other hand, the new observation of widespread cool and warm subduction zones and modern-style plate tectonics related to Wilson cycles in the Palaeoproterozoic (Fig. 17a), does not contradict the significant observation of the widespread emergence of blueschists and UHP rocks in the Neoproterozoic (e. g., Stern, 2005; Brown, 2006), which can be explained with lower Upper mantle temperatures related to the secular temperature evolution of the Earth (e.g., Labrosse and Jaupart, 2007; Herzberg et al., 2010; Ganne and Feng, 2019; Condie, 2018; Chen et al., 2022).

On the basis of 456 published *P-T* estimates of metamorphic rocks (updated to 728 localities, Brown et al., 2024), Brown and Johnson (2018) proposed the existence of a 'duality of thermal regimes' (intermediate and high T/P regimes; cf. Katz, 1974) as early as the Neoarchaean and concluded that some kind of plate tectonics (warm, shallow?) existed since the Archaean. Interestingly, Holder et al. (2019) and Brown et al. (2024) recalculated with their data set the gradual beginning of the duality of thermal regimes and obtained an age of <2.2 Ga (Fig. 17d). This age coincides remarkably well with the age of the Palaeoproterozoic paired metamorphic belts (in the sense of Miyashiro) discussed here. In contrast, the Archaean metamorphic data set records only intermediate and high T/P types of metamorphism and defines a unimodal thermal regime without cold subduction (Brown et al., 2024). In addition, Holder et al. (2019) recognized in the Phanerozoic metamorphic data set a frequency minimum for apparent geothermal gradients around 14 °C/km. This value is regarded as the borderline between the thermal regime of subducted rocks and that of other regional metamorphic rocks. In fact, an upper limit of 14 °C/km would better fit for the warm Palaeoproterozoic subduction zones (Fig. 17a, b) than the value of 11 °C/km originally assumed by Brown and Johnson (2018).

The warmer Palaeoproterozoic oceanic subduction zones documented for orogenic belts surrounding the Congo Craton differ from many Phanerozoic subduction zone rocks regarding their warmer isothermal exhumation (granulite-facies overprint). This peculiarity could be related to a slow subduction of a young and hot Palaeoproterozoic oceanic lithosphere and a fast exhumation rate after slab detachment.

In summary, all presently known Precambrian PMB (in the sense of Miyashiro) as well as pre-Neoproterozoic subduction related eclogites (exhumed oceanic crust subducted to mantle depth) only occur in the relatively short time interval 2.1–1.8 Ga. The formation of some PMB was related to plate-tectonic Wilson cycles, which developed immediately prior to and during the assembly of the supercontinent Nuna/Columbia.

CRediT authorship contribution statement

V. Schenk: Writing – review & editing, Visualization, Validation, Methodology, Investigation, Data curation, Conceptualization. **T. Sarkar:** Methodology, Review & editing. **D. Wiemer:** Methodology, Review & editing.

Declaration of competing interest

The authors declare that they have no known competing financial interests or personal relationships that could have appeared to influence the work reported in this paper.

Acknowledgements

VS thanks Dieter Meinhold (BGR Hannover) for sharing unpublished reports, maps, thin sections and valuable samples. He is also grateful to Alexander Varychev (Heidelberg University) for support with REM analyses and Jan Schmitt for Raman spectrometric determinations. Thomas Theye introduced TS to the U-Th-total Pb dating of monazite in the microprobe lab in Stuttgart and provided XRF analyses for the petrological modeling. The present paper includes analytical data from thesis work of Karen Rickers and Nadine Wittig at the University of Kiel. VS thanks Astrid Holzheid for useful discussions and Dominique Lattard for numerous suggestions, which greatly helped to improve the presentation of the results. We are grateful to Victoria Pease for editorial handling and to the anonymous reviewers for their critical comments. We particular thank the reviewer who constructively commented our manuscript twice and suggested precise improvements. Fieldwork for this study in 1990, 1991 and 1993 was financed by DFG project Sche/265-3, which at first led to the detection of the then oldest known orogenic eclogites from Yalumba Hill.

Appendix A. Supplementary material

Supplementary data to this article can be found online at https://doi.org/10.1016/j.precamres.2025.107891.

Data availability

All data are included in the published tables

References

Ackermand, D., Seifert, F., Schreyer, W., 1975. Instability of sapphirine at high pressures. Contrib. Miner. Petrol. 50 (2), 79–92.

Alkmim, F.F., Teixeira, W., 2017. The Paleoproterozoic Mineiro belt and the Quadrilátero Ferrífero. In: Heilbron, M., Alkmim, F.F., Cordani, U.G. (Eds.), The São Francisco Craton and Its Margins, Eastern Brazil. Springer-Verlag, Geology Review, pp. 71–94.

Ague, J.J., Eckert Jr, J.O., 2012. Precipitation of rutile and ilmenite needles in garnet: implications for extreme metamorphic conditions in the Acadian Orogen, USA. Am. Mineral. 97 (5–6), 840–855.

Appel, P., Möller, A., Schenk, V., 1998. High-pressure granulite facies metamorphism in the Pan-African belt of eastern Tanzania: P–T–t evidence against granulite formation by continent collision. J. Metam. Geol. 16, 491–509.

Arndt, N., 2023. How did the continental crust form: No basalt, no water, no granite. Precambr. Res. 397, 107196.

Baldwin, J.A., Bowring, S.A., Williams, M.L., 2003. Petrological and geochronological constraints on high pressure, high temperature metamorphism in the Snowbird tectonic zone. Canada. J. Metamorphic Geol. 21 (1), 81–98.

Barth, H., Meinhold, K.D., 1974. Note on the basic igneous activity in the Precambrian Buganda–Toro geosyncline. Uganda. Z. Deut. Geol. Ges. 125, 105–118.

Bédard, J.H., 2018. Stagnant lids and mantle overturns: Implications for Archaean tectonics, magmagenesis, crustal growth, mantle evolution, and the start of plate tectonics. Geosci. Front. 9, 19–49.

Bekker, A., Karhu, J.A., Kaufman, A.J., 2006. Carbon isotope record for the onset of the Lomagundi carbon isotope excursion in the Great Lakes area. Precambr. Res. 148, 145–180.

Berhe, S.M., 1990. Ophiolites in northeast and east Africa: implications for Pan-african crustalgrowth. J. Geol. Soc. London 147, 41–57.

Bhowmik, S.K., Dasgupta, S., Baruah, S., Kalita, D., 2018. Thermal history of a late Mesoproterozoic paired metamorphic belt (?) during Rodinia assembly: new insight from medium-pressure granulites from the Aravalli-Delhi Mobile Belt Northwestern India. Geosci. Front. 9 (2), 335–354.

Boniface, N., Schenk, V., Appel, P., 2012. Paleoproterozoic eclogites of MORB-type chemistry and three Proterozoic orogenic cycles in the Ubendian Belt (Tanzania): evidence from monazite and zircon geochronology, and geochemistry. Precambr. Res. 192, 16–33.

Boniface, N., Schenk, V., 2012. Neoproterozoic eclogites in the paleoproterozoic ubendian belt of Tanzania: evidence for a pan-african suture between the bangweulu block and the Tanzania Craton. Precambr. Res. 208, 72–89.

Boniface, N., Schenk, V., Appel, P., 2014. Mesoproterozoic high-grade metamorphism in pelitic rocks of the northwestern Ubendian Belt: implication for the extension of the Kibaran intra-continental basins to Tanzania. Precambr. Res. 249, 215–228.

Boniface, N., Tsujimori, T., 2021. New tectonic model and division of the Ubendian-Usagaran Belt, Tanzania: a review and in-situ dating of eclogites. Geol. Soc. Am. Special Paper 552, 133–175.

Brown, M., 2006. Duality of thermal regimes is the distinctive characteristic of plate tectonics since the Neoarchean. Geology 34, 961–964.

Brown, M., Johnson, T., 2018. Secular change in metamorphism and the onset of global plate tectonics. Am. Mineral. 103, 181–196.

Brown, M., Johnson, T., 2019. Metamorphism and the evolution of subduction on Earth. Am. Mineral. 104 (8), 1065–1082.

Brown, M., Johnson, T., Gardiner, N.J., 2020a. Plate tectonics and the Archean Earth. Annu. Rev. Earth Planet. Sci. 48, 291–320.

Brown, M., Pearce, J.A., Johnson, T.E., 2024. Is plate tectonics a post-Archean phenomenon? A petrological perspective. J. Geol. Soc. London 181 (6), jgs2024-091.

Brown, D.A., Tamblyn, R., Hand, M., Morrissey, L.J., 2020b. Thermobarometric constraints on burial and exhumation of 2-billion-year-old eclogites and their metapelitic hosts. Precambr. Res., 105833

Buick, I.S., Williams, I.S., Gibson, R.L., Cartwright, I., Miller, J.A., 2003. Carbon and U-Pb evidence for a Palaeoproterozoic crustal component in the Central Zone of the Limpopo Belt, South Africa. J. Geol. Soc. London 160, 601–612.

Cartwright, I., Barnicoat, A.C., 1987. Petrology of Scourian supracrustal rocks and orthogneisses from Stoer, NW Scotland: implications for the geological evolution of the Lewisian complex. In: Park, R.G., Tarney, J. (Eds.), Evolution of the Lewisian and Comparable High-Grade Terrains. *Geological Society*. Special Publications, London, pp. 93–107.

Cawood, P.A., Chowdhury, P., Mulder, J.A., Hawkesworth, C.J., Capitanio, F.A., Gunawardana, P.M., Nebel, O., 2022. Secular evolution of continents and the Earth system. Rev. Geophys. 60 (4), e2022RG000789.

Chapman, A.D., 2017. The pelona–orocopia–rand and related schists of southern California: a review of the best-known archive of shallow subduction on the planet. Int. Geol. Rev. 59, 664–701.

Chen, Q., Liu, H., Johnson, T., Hartnady, M., Kirkland, C.L., Lu, Y., Sun, W.D., 2022. Intraplate continental basalts over the past billion years track cooling of the mantle and the onset of modern plate tectonics. Earth Planet. Sci. Lett. 597, 117804.

Collins, A.S., Reddy, S.M., Buchan, C., Mruma, A., 2004. Temporal constraints on Palaeoproterozoic eclogite formation and exhumation (Usagaran Orogen, Tanzania). Earth Planet. Sci. Lett. 224, 175–192.

Condie, K.C., 2015. Changing tectonic settings through time: indiscriminate use of geochemical discriminant diagrams. Precambr. Res. 266, 587–591.

Condie, K.C., 2018. A planet in transition: the onset of plate tectonics on Earth between 3 and 2 Ga? Geosci. Front. 9, 51–60.

Condie, K.C., Pisarevsky, S.A., Puetz, S.J., Spencer, C.J., Teixeira, W., Faleiros, F.M., 2022. A reappraisal of the global tectono-magmatic lull at ~2.3 Ga. Precambr. Res. 376, 106690.

Condie, K.C., Stern, R.J., 2023. Ophiolites: identification and tectonic significance in space and time. Geosci. Front. 14 (6), 101680.

Connolly, J.A.D., 2009. The geodynamic equation of state: what and how. Geochem. Geophys. Geosyst. 10 (1–19), Q10014.

Coolen, J.J.M.M.M., Priem, H.N.A., Verdurmen, E.T., Verschure, R.H., 1982. Possible zircon U-Pb evidence for Pan-african granulite-facies metamorphism in the Mozambique belt of southern Tanzania. Precambr. Res. 17, 31–40.

Chowdhury, P., Chakraborty, S., Gerya, T.V., Cawood, P.A., Capitanio, F.A., 2020. Peel-back controlled lithospheric convergence explains the secular transitions in Archean metamorphism and magmatism. Earth Planet. Sci. Lett. 538, 116224.

Cutten, H., Johnson, S.P., Waele, B.D., 2006. Protolith ages and timing of metasomatism related to the formation of whiteschists at Mautia Hill, Tanzania: implications for the assembly of Gondwana. J. Geol. 114, 683–698.

Davies, G.F., 1992. On the emergence of plate tectonics. Geology 20, 963–966.

Dasgupta, A., Bhowmik, S.K., Das, A., Bhandari, A., Kumar, G.R., 2023. Paired metamorphism in peel back tectonics at the Archaean-Proterozoic boundary: New insights into Early Earth Plate tectonics from the Western Dharwar Craton, South India. Earth Planet. Sci. Lett. 622, 118414.

Deng, H., Chen, C., Wang, D., Peng, S., Lang, W., Zhang, H., Dong, Z., 2025. Magmatic tempo within the Paleoproterozoic ophiolitic mélange, Northern Kongling complex, Yangtze Craton: dynamics of a Paleoproterozoic subduction zone. *Chem. Geol.*, 122666

Eckert, J.O., Newton, R.C., Kleppa, O.J., 1991. The Δ H of reaction and recalibration of garnet-pyroxene-plagioclase-quartz geobarometers in the CMAS system by solution calorimetry. Am. Mineral. 76 (1–2), 148–160.

Ernst, W.G., 2010. Subduction-zone metamorphism, calc-alkaline magmatism, and convergent-margin crustal evolution. Gondw. Res. 18, 8–16.

François, C., Debaille, V., Paquette, J.-L., Baudet, D., Javaux, E.J., 2018. The earliest evidence for modern-style plate tectonics recorded by HP–LT metamorphism in the Paleoproterozoic of the Democratic Republic of the Congo. Sci. Rep. 8, 1–10.

François, C., Philippot, P., Rey, P., Rubatto, D., 2014. Burial and exhumation during Archean sagduction in the East Pilbara granite-greenstone terrane. Earth Planet. Sci. Lett. 396, 235–251.

Fritz, H., Tenczer, V., Hauzenberger, C.A., Wallbrecher, E., Hoinkes, G., Muhongo, S., Mogessie, A., 2005. Central Tanzanian tectonic map: a step forward to decipher Proterozoic structural events in the East African Orogen. Tectonics 24, TC6013.

Fritz, H., Abdelsalam, M., Ali, K., Bingen, B., Collins, A., Fowler, A., Ghebreab, W., Hauzenberger, C., Johnson, P., Kusky, T., 2013. Orogen styles in the East African Orogen: a review of the Neoproterozoic to Cambrian tectonic evolution. J. Afr. Earth Sc. 86, 65–106.

Gabert, G., Wendt, I., 1974. Datierung von granitischen Gesteinen im Dodoman- und Usagaran- System und in der Ndembera-Serie (Tanzania). Geol. Jahrbuch, Reihe B 11, 3–55.

Ganne, F., Feng, X.J., 2019. Primary magmas and mantle temperatures through time. Geochem. Geophys. Geosyst. 18, 872–888.

Geological Survey of Tanganyika (1959). Summary of the geology of Tanganyika. Part II: Geological map 1:2000 000. *Mem. Geol. Surv. Tanganyika* **1**, II, 6; 1 map, Dar-es-Salaam 1960.

Gerya, T.V., Connolly, J.A., Yuen, D.A., 2008. Why is terrestrial subduction one-sided? Geology 36, 43–46.

Gerya, T.V., Bercovici, D., Becker, T.W., 2021. Dynamic slab segmentation due to brittle–ductile damage in the outer rise. Nature 599 (7884), 245–250.

Glassley, W.E., Korstgård, J.A., Sørensen, K., Platou, S.W., 2014. A new UHP metamorphic complex in the ~1.8 Ga Nagssugtoqidian Orogen of West Greenland. Am. Mineral. 99, 1315–1334.

Grantham, D.R., 1927. Geology of the Dodoma-Iringa area. *Geological Survey Tanganyika, Dar-es-Salaam Tanzania.* Annual Report 1926, 18–25.

Green, D.H., Ringwood, A.E., 1967. An experimental investigation of the gabbro to eclogite transformation and its petrological applications. Geochim. Cosmochim. Acta 31 (5), 767–833.

Han, Q.S., Peng, S.B., Jiao, S.J., 2020. Discovery and tectonic implications of Paleoproterozoic cold subduction low-temperature/high-pressure eclogitic metapelites. Yangtze Craton. Earth Sci. 45 (6), 1986–1998.

Harley, S.L., Green, D.H., 1982. Garnet–orthopyroxene barometry for granulites and peridotites. Nature 300 (5894), 697–701.

Harlow, G.E., Tsujimori, T., Sorensen, S.S., 2015. Jadeitites and plate tectonics. Annu. Rev. Earth Planet. Sci. 43, 105–138.

Herms, P., Raase, P., Giehl, C., Aradi, L.E., Fußwinkel, T., Rohrbach, A., Möller, A., 2023. High-pressure melting in metapelites of a 2 Ga old subducted oceanic crust (Usagaran belt, Tanzania): implications from melt inclusions, fluid inclusions and thermodynamic modeling. Contrib. Miner. Petrol. 178 (11), 84.

Hepworth, J.V., 1972. The Mozambique Orogenic Belt and its foreland in northeast Tanzania, a photogeologically-based study. J. Geol. Soc. Lond. 128, 461–500.

Herwartz, D., Skublov, S.G., Berezin, A.V., Mel'nik, A.E., 2012. First Lu–Hf garnet ages of eclogites from the Belomorian mobile belt (Baltic Shield, Russia). Dokl. Earth Sci. 443, 377–380.

Herzberg, C., Condie, K., Korenaga, J., 2010. Thermal history of the Earth and its petrological expression. Earth Planet. Sci. Lett. 292, 79–88.

Hoffman, P.F. (1973). Evolution of an early Proterozoic continental margin: the Coronation geosyncline and associated aulacogens, northwest Canadian Shield, in Sutton, J., and Windley, B.F., eds., Evolution of the Precambrian crust: *Philosophical Transaction of the Royal Society, London, Series A* **273**, 547–581.

Hoffman, P.F., Bowring, S.A., 1984. Short-lived 1.9 Ga continental margin and its destruction, Wopmay orogen, northwest Canada. Geology 12 (2), 68–72.

Hofmann, A.W., 1988. Chemical differentiation of the Earth: the relationship between mantle, continental crust, and oceanic crust. Earth Planet. Sci. Lett. 90 (3), 297–314.

Holder, R.M., Viete, D.R., Brown, M., Johnson, T.E., 2019. Metamorphism and the evolution of plate tectonics. Nature 572 (7769), 378–381.
Holland, T.J., 1980. The reaction albite= jadeite+ quartz determined experimentally in the range 600–1200 °C. Am. Mineral. 65 (1–2), 129–134.
Holland, T.J.B., 1979. Experimental determination of the reaction paragonite= jadeite+ kyanite+ H_2O, and internally consistent thermodynamic data for part of the system Na_2O– Al_2O_3– SiO_2– H_2O, with applications to eclogites and blueschists. Contrib. Miner. Petrol. 68 (3), 293–301.
Holland, T.J.B., Powell, R., 2011. An improved and extended internally consistent thermodynamic dataset for phases of petrological interest, involving a new equation of state for solids. J. Metam. Geol. 29, 333–383.
Holmes, A. (1951). The sequence of Precambrian orogenic belts in south and central Africa. *Proceed. 18th Internat. Geol. Congr. London 1948* **14**, 254-269.
Hopkins, M.D., Harrison, T.M., Manning, C.E., 2010. Constraints on Hadean geodynamics from mineral inclusions in > 4 Ga zircons. Earth Planet. Sci. Lett. 298, 367–376.
Huang, B., Kusky, T.M., Johnson, T.E., Wilde, S.A., Wang, L., Poalt, A., Fu, D., 2020. Paired metamorphism in the Neoarchean: A record of accretionary-to-collisional orogenesis in the North China Craton. Earth Planet. Sci. Lett. 543, 116355.
Imayama, T., Oh, C.W., Baltybaev, S.K., Park, C.S., Yi, K., Jung, H., 2017. Paleoproterozoic high-pressure metamorphic history of the Salma eclogite on the Kola Peninsula. Russia. Lithosphere 9 (6), 855–873.
John, T., Schenk, V., Haase, K., Scherer, E., Tembo, F., 2003. Evidence for a Neoproterozoic ocean in south-central Africa from mid-oceanic-ridge–type geochemical signatures and pressure-temperature estimates of Zambian eclogites. Geology 31, 243–246.
John, T., Schenk, V., 2003. Partial eclogitisation of gabbroic rocks in a late Precambrian subduction zone (Zambia): prograde metamorphism triggered by fluid infiltration. Contrib. Miner. Petrol. 146, 174–191.
Johnson, S.P., Cutten, H.N.C., Muhongo, S., De Waele, B., 2003. Neoarchean magmatism and metamorphism of the western granulites in the central domain of the Mozambique belt, Tanzania: U-Pb SHRIMP geochronology and PT estimates. Tectonophysics 375, 125–145.
Johnson, T.E., Brown, M., Kaus, B.J., VanTongeren, J.A., 2014. Delamination and recycling of Archaean crust caused by gravitational instabilities. Nat. Geosci. 7 (1), 47–52.
Johnson, T.E., Brown, M., Gardiner, N.J., Kirkland, C.L., Smithies, R.H., 2017. Earth's first stable continents did not form by subduction. Nature 543 (7644), 239–242.
Jöns, N., Schenk, V., 2004. Petrology of whiteschists and associated rocks at Mautia Hill (Tanzania): fluid infiltration during high-grade metamorphism? J. Petrol. 45, 1959–1981.
Kabete, J.M., Groves, D.I., McNaughton, N.J., Mruma, A.H., 2012. A new tectonic and temporal framework for the Tanzanian Shield: implications for gold metallogeny and undiscovered endowment. Ore Geol. Rev. 48, 88–124.
Karhu, J.A., Holland, H.D., 1996. Carbon isotopes and the rise of atmospheric oxygen. Geology 24, 867–870.
Karmakar, S., Schenk, V., 2015. Neoarchean UHT metamorphism and Paleoproterozoic UHT reworking at Uweinat in the East Sahara ghost Craton, SW Egypt: evidence from petrology and texturally controlled in situ monazite dating. J. Petrol. 56 (9), 1703–1742.
Katz, M.B., 1974. Paired metamorphic belts in Precambrian granulite rocks in Gondwanaland. Geology 2, 237–241.
Kazimoto, E.O., Schenk, V., Berndt, J., 2014. Neoarchean and Paleoproterozoic crust formation in the Ubendian Belt of Tanzania: Insights from zircon geochronology and geochemistry. Precambr. Res. 252, 119–144.
Kazimoto, E.O., Schenk, V., Appel, P., 2015. Granulite-facies metamorphic events in the northwestern Ubendian Belt of Tanzania: Implications for the Neoarchean to Paleoproterozoic crustal evolution. Precambr. Res. 256, 31–47.
Kusky, T., Windley, B.F., Polat, A., Wang, L., Ning, W., Zhong, Y., 2021. Archean dome-and-basin style structures form during growth and death of intraoceanic and continental margin arcs in accretionary orogens. Earth Sci. Rev. 220, 103725.
Labrosse, S., Jaupart, C., 2007. Thermal evolution of the Earth: secular changes and fluctuations of plate characteristics. Earth Planet. Sci. Lett. 260 (3–4), 465–481.
Lenardic, A., 2018. The diversity of tectonic modes and thoughts about transitions between them. Philos. Trans. R. Soc. A Math. Phys. Eng. Sci. 376 (2132), 20170416.
Li, X., Zhang, L., Wei, C., Slabunov, A.I., Bader, T., 2017. Neoarchean-Paleoproterozoic granulite-facies metamorphism in Uzkaya Salma eclogite-bearing mélange, Belomorian Province (Russia). Precambr. Res. 294, 257–283.
Li, L.S., Wang, X.L., Yakymchuk, C., Schorn, S., Yu, J.H., Wang, D., Huang, Y., 2022. A refined study of Paleoproterozoic high-pressure granulite-facies metamorphism in the Kongling complex of northern Yangtze block. Precambr. Res. 378, 106741.
Li, X., Zhang, L., Wei, C., Bader, T., Guo, J., 2023. Cold subduction recorded by the 1.9 Ga Salma eclogite in Belomorian Province (Russia). Earth Planet. Sci. Lett. 602, 117930.
Liati, A., Seidel, E., 1994. Sapphirine and hogbomite in overprinted kyanite-eclogites of central Rhodope, N. Greece: first evidence of granulite-facies metamorphism. Eur. J. Mineral. 6 (5), 733–738.
Liou, J.G., Tsujimori, T., Yang, J., Zhang, R.Y., Ernst, W.G., 2014. Recycling of crustal materials through study of ultrahigh-pressure minerals in collisional orogens, ophiolites, and mantle xenoliths: a review. J. Asian Earth Sci. 96, 386–420.
Liu, F., Zhang, L., Li, X., Slabunov, A.I., Wei, C., Bader, T., 2017. The metamorphic evolution of Paleoproterozoic eclogites in Kuru-Vaara, northern Belomorian Province, Russia: Constraints from PT pseudosections and zircon dating. Precambr. Res. 289, 31–47.
Loose, D., Schenk, V., 2018. 2.09 Ga old eclogites in the Eburnian-Transamazonian orogen of southern Cameroon: significance for Palaeoproterozoic plate tectonics. Precambr. Res. 304, 1–11.
Master, S., Bekker, A., Hofmann, A., 2010. A review of the stratigraphy and geological setting of the Palaeoproterozoic Magondi Supergroup, Zimbabwe–Type locality for the Lomagundi carbon isotope excursion. Precambr. Res. 182, 254–273.
Master, S., Bekker, A., Karhu, J.A., 2013. Paleoproterozoic high δ13Ccarb marbles from the Ruwenzori Mountains, Uganda: Implications for the age of the Buganda Group. Chem. Geol. 362, 157–164.
Meinhold, K.D., 1968. Petrographie, Metamorphose und Tektonik der Konse-Serie in Zentral-Tanzania (Ostafrika). Dissertation Technische Hochschule München.
Meinhold, K.D., 1970. Petrographie, Metamorphose, Tektonik und stratigraphische Stellung der Konse-Serie in Zentral-Tanzania (Ostafrika). *Beihefte*. Geol. Jahrb. 91, 137 p., 3 maps, Hannover.
Meinhold, K.D., Frisch, T., 1970. Manganese-silicate-bearing metamorphic rocks from central Tanzania. Schweiz. Mineral. Petrogr. Mitt. 50, 493–507.
Meinhold, K. D. & Ott, G. (1993). Methods of Regional Geological Mapping in Africa. Explanatory Notes on the 1:50000 Geological map of the Rudi area. Unpublished report. BGR-Archive-No.: 111 011.
Mints, M.V., Belousova, E.A., Konilov, A.N., Natapov, L.M., Shchipansky, A.A., Griffin, W.L., O'Reilly, S.Y., Dokukina, K.A., Kaulina, T.V., 2010. Mesoarchean subduction processes: 2.87 Ga eclogites from the Kola Peninsula Russia. Geology 38, 739–742.
Mints, M.V., Kaulina, T.V., Konilov, A.N., Krotov, A.V., Stupak, V.M., 2007. The thermal and geodynamic evolution of the Lapland granulite belt: Implications for thermal structure of the lower crust during granulite-facies metamorphism. Gondw. Res. 12 (3), 252–267.
Miyashiro, A., 1961. Evolution of metamorphic belts. J. Petrol. 2, 277–311.
Miyashiro, A., 1973. Paired and unpaired metamorphic belts. Tectonophysics 17 (3), 241–254.
Moyen, J.F., Stevens, G., Kisters, A., 2006. Record of mid-Archaean subduction from metamorphism in the Barberton terrain South Africa. Nature 442 (7102), 559–562.
Möller, A., Appel, P., Mezger, K., Schenk, V., 1995. Evidence for a 2 Ga subduction zone: eclogites in the Usagaran belt of Tanzania. Geology 23, 1067–1070.
Möller, A., Mezger, K., Schenk, V., 1998. Crustal age domains and the evolution of the continental crust in the Mozambique Belt of Tanzania: combined Sm–Nd, Rb–Sr, and Pb–Pb isotopic evidence. J. Petrol. 39, 749–783.
Möller, A., Mezger, K., Schenk, V., 2000. U–Pb dating of metamorphic minerals: Pan-african metamorphism and prolonged slow cooling of high-pressure granulites in Tanzania, East Africa. Precambr. Res. 104, 123–146.
Möller, C., 1999. Sapphirine in SW Sweden: a record of Sveconorwegian (–Grenvillian) late-orogenic tectonic exhumation. J. Metam. Geol. 17 (1), 127–141.
Mruma, A.H., 1995. Stratigraphy and palaeodepositional environment of the Palaeoproterozoic volcano-sedimentary Konse Group in Tanzania. African Earth Sci. 21, 281–290.
Mruma, A.H., 1989. Stratigraphy, metamorphism and tectonic evolution of the early Proterozoic Usagaran Belt, Tanzania. *Res Terrae, Ser*. Publications of the Department of Geology. University of Oulu, Oulu.
Müller, S., Dziggel, A., Sindern, S., Kokfelt, T.F., Gerdes, A., Kolb, J., 2018. Age and temperature-time evolution of retrogressed eclogite-facies rocks in the Paleoproterozoic Nagssugtoqidian Orogen, South East Greenland: constrained from U-Pb dating of zircon, monazite, titanite and rutile. Precambr. Res. 314, 468–486.
Ning, W., Kusky, T., Wang, L., Huang, B., 2022a. Archean eclogite-facies oceanic crust indicates modern-style plate tectonics. Proc. Natl. Acad. Sci. 119 (15), e2117529119.
Ning, W., Kusky, T., Wang, L., Huang, B., 2022b. Reply to Zou et al.: Neoarchean eclogite-facies oceanic crust in the North China Craton. Proc. Natl. Acad. Sci. 119 (39), e2210169119.
Nutman, A.P., Kalsbeek, F., Friend, C.R.L., 2008. The Nagssugtoqidian Orogen in southeast Greenland: evidence for Paleoproterozoic collision and plate assembly. Am. J. Sci. 308, 529–572.
Parsons, I., 1978. Alkali-feldspars: which solvus? Phys. Chem. Miner. 2 (3), 199–213.
Pearce, J.A., 2008. Geochemical fingerprinting of oceanic basalts with applications to ophiolite classification and the search for Archean oceanic crust. Lithos 100, 14–48.
Pearce, J.A., Reagan, M.K., 2019. Identification, classification, and interpretation of boninites from Anthropocene to Eoarchean using Si-Mg-Ti systematics. Geosphere 15, 1008–1037.
Pease, V., Percival, J., Smithies, H., Stevens, G., Van Kranendonk, M.J., 2008. When did plate tectonics begin? Evidence from the orogenic record. Special Paper Geol. Soc. Am. 440, 281–294.
Penniston-Dorland, S.C., Kohn, M.J., Manning, C.E., 2015. The global range of subduction zone thermal structures from exhumed blueschists and eclogites: rocks are hotter than models. Earth Planet. Sci. Lett. 428, 243–254.
Reddy, S.M., Collins, A.S., Mruma, A., 2003. Complex high-strain deformation in the Usagaran Orogen, Tanzania: structural setting of Palaeoproterozoic eclogites. Tectonophysics 375, 101–123.
Reddy, S.M., Collins, A.S., Buchan, C., Mruma, A.H., 2004. Heterogeneous excess argon and Neoproterozoic heating in the Usagaran Orogen, Tanzania, revealed by single grain 40Ar/39Ar thermochronology. J. Afr. Earth Sc. 39 (3–5), 165–176.
Roman, A., Arndt, N., 2020. Differentiated Archean oceanic crust: its thermal structure, mechanical stability and a test of the sagduction hypothesis. Geochim. Cosmochim. Acta 278, 65–77.
Schenk, V., 1984. Petrology of felsic granulites, metapelites, metabasics, ultramafics, and metacarbonates from Southern Calabria (Italy): prograde metamorphism, uplift and cooling of a former lower crust. J. Petrol. 25, 255–296.
Schenk, V., Schumann, A., Jöns, N., Loose, D., Tiberindwa, J.V., Wegner, H., Wittig, N., 2002. Petrological evidence for crustal thickening, ultra-high temperatures and

isobaric cooling in Archean granulite-facies gneisses from the West Nile area (Uganda). In: *19th Colloquium of African Geology*. El Jadida, Morocco Abstracts Volume, pp. 165–166.
Schenk, V., Bekker, A., Schmitt, A.K., 2025. The Konse Group on the SE margin of the Tanzania Craton– a Paleoproterozoic passive margin succession of the Usagaran Orogen: constraints from metamorphic monazite ages and isotopically heavy carbon in marbles. Precambr. Res. 427, 107874.
Schidlowski, M., Eichmann, R., Junge, C.E., 1976. Carbon isotope geochemistry of the Precambrian Lomagundi carbonate province. Geochim. Cosmochim. Acta 40, 449–455.
Seifert, F.T., Schreyer, W., 1970. Lower temperature stability limit of Mg cordierite in the range 1–7 kb water pressure: a redetermination. Contrib. Miner. Petrol. 27, 225–238.
Shackleton, R.M., 1986. Precambrian collision tectonics in Africa. Geol. Soc. Lond. Spec. Publ. 19 (1), 329–349.
Sharp, D.H., 1984. An overview of Rayleigh-Taylor instability. Phys. D 12, 3–18.
Simon, G., Chopin, C., 2001. Enstatite–sapphirine crack-related assemblages in ultrahigh-pressure pyrope megablasts, Dora-Maira massif, western Alps. Contrib. Miner. Petrol. 140 (4), 422–440.
Sizova, E., Gerya, T., Brown, M., Perchuk, L.L., 2010. Subduction styles in the Precambrian: insight from numerical experiments. Lithos 116, 209–229.
Skublov, S.G., Berezin, A.V., Marin, Y.B., Rizvanova, N.G., Bogomolov, E.S., Sergeeva, N. A., Guseva, V.F., 2010. Complex isotopic-geochemical (Sm-Nd, U-Pb) study of Salma eclogites. Dokl. Earth Sci. 434 (2), 1396–1400.
Smithies, R.H., Champion, D.C., Van Kranendonk, M.J., 2009. Formation of Paleoarchean continental crust through infracrustal melting of enriched basalt. Earth Planet. Sci. Lett. 281, 298–306.
Snoeyenbos, D.R., Williams, M.L., Hanmer, S., 1995. Archean high-pressure metamorphism in the western Canadian Shield. Eur. J. Mineral. 7, 1251–1272.
Sommer, H., Kröner, A., Muhongo, S., Hauzenberger, C., 2005. SHRIMP zircon ages for post-Usagaran granitoid and rhyolitic rocks from the Palaeoproterozoic terrain of southwestern Tanzania. S. Afr. J. Geol. 108, 247–256.
Sommer, H., Kröner, A., 2019. Igneous petrology, zircon geochronology and geochemistry of multiply emplaced granitoid bodies from the Palaeoproterozoic Usagaran domain in central Tanzania. J. Afr. Earth Sc. 150, 626–656.
Spencer, C.J., Murphy, J.B., Kirkland, C.L., Liu, Y., Mitchell, R.N., 2018. A Paleoproterozoic tectonic-magmatic lull as a potential trigger for the Supercontinent Cycle. Nat. Geosci. 11, 97–101.
Stern, R.J., 1994. Arc assembly and continental collision in the Neoproterozoic East African Orogen: implications for the consolidation of Gondwanaland. Annu. Rev. Earth Planet. Sci. 22, 319–351.
Stern, R.J., 2005. Evidence from ophiolites, blueschists, and ultrahigh-pressure metamorphic terranes that the modern episode of subduction tectonics began in Neoproterozoic time. Geology 33, 557–560.
Stern, R.J., 2018. The evolution of plate tectonics. Philos. Trans. R. Soc. A Math. Phys. Eng. Sci. 376 (2132), 20170406.
Stern, R.J., 2020. The Mesoproterozoic single-lid tectonic episode: Prelude to modern plate tectonics. GSA Today 30, 4–10.
Tamblyn, R., Brown, D., Hand, M., Morrissey, L., Clark, C., Anczkiewicz, R., 2021. The 2 Ga eclogites of Central Tanzania: directly linking age and metamorphism. Lithos 380, 105890.
Tang, M., Chu, X., Hao, J., Shen, B., 2021. Orogenic quiescence in Earth's middle age. Science 371 (6530), 728–731.
Temperley, B.N., Reeve, W.H. & King, A.J. (1953). Degree Sheet 53, Mpwapwa-South (B37/M1), 1:125 000 Series Geological Maps, *Tanganyika Series*. Geological Survey Department, Dodoma.
Tenczer, V., Hauzenberger, C., Fritz, H., Hoinkes, G., Muhongo, S., Klötzli, U., 2013. Crustal age domains and metamorphic reworking of the deep crust in Northern-Central Tanzania: a U/Pb zircon and monazite age study. Mineral. Petrol. 107, 679–707.
Thomas, R.J., Roberts, N.M., Jacobs, J., Bushi, A.M., Horstwood, M.S., Mruma, A., 2013. Structural and geochronological constraints on the evolution of the eastern margin of the Tanzania Craton in the Mpwapwa area, central Tanzania. Precambr. Res. 224, 671–689.
Thomas, R.J., Spencer, C., Bushi, A.M., Baglow, N., Boniface, N., de Kock, G., Horstwood, M.S.A., Hollick, L., Jacobs, J., Kajara, S., Kamihanda, G., Key, R.M., Maganga, Z., Mbawala, F., McCourt, W., Momburi, P., Moses, F., Mruma, A., Myambilwa, Y., Roberts, N.M.W., Saidi, H., Nyanda, P., Nyoka, K., Millar, I., 2016. Geochronology of the central Tanzania Craton and its southern and eastern orogenic margins. Precambr. Res. 277, 47–67.
Tsujimori, T., Ernst, W.G., 2014. Lawsonite blueschists and lawsonite eclogites as proxies for paleo-subduction zone processes: a review. J. Metam. Geol. 32, 437–454.
Tuisku, P., Huhma, H., 1998. Eclogite from the SW-marginal zone of the Lapland Granulite belt: evidence from the 1.90–1.88 Ga subduction zone. In: Hanski, E., Vuollo, J. (Eds.), International Ophiolite Symposium and Field Excursion: Generation and Emplacement of Ophiolites through Time. Geological Survey of Finland, Oulu, Finland, p. 61.
Tulibonywa, T., Manya, S., Maboko, M.A., 2015. Palaeoproterozoic volcanism and granitic magmatism in the Ngualla area of the Ubendian Belt, SW Tanzania: Constraints from SHRIMP U-Pb zircon ages, and Sm–Nd isotope systematics. Precambr. Res. 256, 120–130.
van Hunen, J., van den Berg, A.P., 2008. Plate tectonics on the early Earth: limitations imposed by strength and buoyancy of subducted lithosphere. Lithos 103, 217–235.
Van Kranendonk, M.J.V., Hickman, A.H., Smithies, R.H., Nelson, D.R., Pike, G., 2002. Geology and tectonic evolution of the Archean North Pilbara terrain, Pilbara Craton Western Australia. Econ. Geol. 97 (4), 695–732.
Van Kranendonk, M.J., Kröner, A., Hoffmann, J.E., Nagel, T., Anhaeusser, C.R., 2014. Just another drip: Re-analysis of a proposed Mesoarchean suture from the Barberton Mountain Land, South Africa. Precambr. Res. 254, 19–35.
Voll, G. (1976). Recrystallisation of quartz, biotite and feldspars from Erstfeld to the Leventina Nappe, Swiss Alps, and its geological significance. *Schweizerische mineralogische und petrographische Mitteilungen* **56**, 641-647.
Volodichev, O.I., Slabunov, A.I., Bibikova, E.V., Konilov, A.N., Kuzenko, T.I., 2004. Archean eclogites in the Belomorian mobile belt, Baltic shield. Petrology 12, 609–631.
Weller, O.M., St-Onge, M.R., 2017. Record of modern-style plate tectonics in the Palaeoproterozoic Trans-Hudson orogen. Nat. Geosci. 10, 305–311.
Wendt, I., Besang, C., Harre, W., Kreuzer, H., Lenz, H. & Müller, P. (1972). Age determinations of granitic intrusions and metamorphic events in the Early Precambrian of Tanzania. *International Geological Congress, 24th, Montreal, 1972, Proceedings*, 295–314.
Whitney, D.L., Evans, B.W., 2010. Abbreviations for names of rock-forming minerals. Am. Mineral. 95 (1), 185–187.
Whittingham, J.K. (1959). Geological map and a brief explanation of the geology of QDS 215, *Geological map, Geological Survey Division, Dodoma.*.
Wiemer, D., Schrank, C.E., Murphy, D.T., Wenham, L., Allen, C.M., 2018. Earth's oldest stable crust in the Pilbara Craton formed by cyclic gravitational overturns. Nat. Geosci. 11, 357–361.
Windley, B.F., Kusky, T., Polat, A., 2021. Onset of plate tectonics by the Eoarchean. Precambr. Res. 352, 105980.
Xu, C., Kynický, J., Song, W., Tao, R., Lü, Z., Li, Y., Fei, Y., 2018. Cold deep subduction recorded by remnants of a Paleoproterozoic carbonated slab. Nat. Commun. 9 (1), 2790.
Yin, C., Xia, Y., Cawood, P., Zhao, G., Xiao, W., Lin, S., ... & Wu, S. (submitted). Modern-style plate tectonics preserved in the Paleoproterozoic paired metamorphic belts driven by cold deep subduction. Manuscript.
Zou, Y., Chu, X., Wu, J., Zhao, L., 2022. No evidence for Archean eclogite-facies metamorphism. Proc. Natl. Acad. Sci. 119 (39), e2208090119.
Zhang, R.Y., Zhai, S.M., Fei, Y.W., Liou, J.G., 2003. Titanium solubility in coexisting garnet and clinopyroxene at very high pressure: the significance of exsolved rutile in garnet. Earth Planet. Sci. Lett. 216 (4), 591–601.
Zhao, G.C., Cawood, P.A., Wilde, S.A., Lu, L.Z., 2001. High-pressure granulites (retrograded eclogites) from the Hengshan complex, North China Craton: Petrology and tectonic implications. J. Petrol. 42, 1141–1170.
Zhao, G., Li, S., Sun, M., Wilde, S.A., 2011. Assembly, accretion, and break-up of the Palaeo-Mesoproterozoic Columbia supercontinent: record in the North China Craton revisited. Int. Geol. Rev. 53, 1331–1356.
Zhu, Z., Campbell, I.H., Allen, C.M., Brocks, J.J., Chen, B., 2022. The temporal distribution of Earth's supermountains and their potential link to the rise of atmospheric oxygen and biological evolution. Earth Planet. Sci. Lett. 580, 117391.